NAVAL POSTGRADUATE SCHOOL

MONTEREY, CALIFORNIA

THESIS

DESIGN AND QUALIFICATION OF A HIGH-PRESSURE COMBUSTION CHAMBER FOR IGNITION DELAY TESTING OF DIESEL FUELS

by

Warren P. Fischer

June 2013

Thesis Co-Advisors: Christopher M. Brophy
Patrick A. Caton

THIS PAGE INTENTIONALLY LEFT BLANK

REPORT DOCUMENTATION PAGE			Form Approved OMB No. 0704-0188
Public reporting burden for this collection of information is estimated to average 1 hour per response, including the time for reviewing instruction, searching existing data sources, gathering and maintaining the data needed, and completing and reviewing the collection of information. Send comments regarding this burden estimate or any other aspect of this collection of information, including suggestions for reducing this burden, to Washington headquarters Services, Directorate for Information Operations and Reports, 1215 Jefferson Davis Highway, Suite 1204, Arlington, VA 22202-4302, and to the Office of Management and Budget, Paperwork Reduction Project (0704-0188) Washington DC 20503.			
1. AGENCY USE ONLY ***(Leave blank)***	**2. REPORT DATE** June 2013	**3. REPORT TYPE AND DATES COVERED** Master's Thesis	
4. TITLE AND SUBTITLE DESIGN AND QUALIFICATION OF A HIGH-PRESSURE COMBUSTION CHAMBER FOR IGNITION DELAY TESTING OF DIESEL FUELS		**5. FUNDING NUMBERS** **N0001413WX20922**	
6. AUTHOR(S) Warren P. Fischer			
7. PERFORMING ORGANIZATION NAME(S) AND ADDRESS(ES) Naval Postgraduate School Monterey, CA 93943-5000		**8. PERFORMING ORGANIZATION REPORT NUMBER**	
9. SPONSORING /MONITORING AGENCY NAME(S) AND ADDRESS(ES) N/A		**10. SPONSORING/MONITORING AGENCY REPORT NUMBER**	
11. SUPPLEMENTARY NOTES The views expressed in this thesis are those of the author and do not reflect the official policy or position of the Department of Defense or the U.S. government. IRB Protocol number ____N/A____.			
12a. DISTRIBUTION / AVAILABILITY STATEMENT Approved for public release; distribution is unlimited		**12b. DISTRIBUTION CODE** A	

13. ABSTRACT (maximum 200 words)

A high pressure and temperature combustion chamber was designed to compare the ignition properties of different fuels, including conventional F76 diesel and hydrotreated renewable diesel (HRD), derived from algae. Conditions were selected to capture the operating conditions within a large number of Navy systems, testing at a range of temperatures from 800–1340 °F and pressures as high as 20 atm. Three Navy-relevant injectors were procured for the testing as well as a commercial injector made by Sturman Industries. The Sturman diesel injector was characterized up to a fuel tip pressure of 9600 psi and produced Sauter Mean Diameters of approximately 90 microns, generally showing improved atomization for F-76 when compared to HRD at similar conditions. The combustion chamber utilized dynamic air injection with increased turbulence and the ability to alter the amounts of combustion products including CO, CO_2 and H_2O that typically exist in real engines from the previous combustion event. Qualification testing of the combustion chamber evaluated final pressures of up to 15 atmospheres and temperatures of 472 °F, but revealed heat losses during the dynamic air injection events, resulting in temperatures below expected values and auto-ignition conditions for fuels under consideration. A fluidized bed heat exchanger will be implemented to supplement the existing design and reach the desired temperatures.

14. SUBJECT TERMS F-76; HRD; High-pressure; Ignition delay; Diesel injectors; Alternative fuels			**15. NUMBER OF PAGES** 101
			16. PRICE CODE
17. SECURITY CLASSIFICATION OF REPORT Unclassified	**18. SECURITY CLASSIFICATION OF THIS PAGE** Unclassified	**19. SECURITY CLASSIFICATION OF ABSTRACT** Unclassified	**20. LIMITATION OF ABSTRACT** UU

NSN 7540-01-280-5500 Standard Form 298 (Rev. 2-89)
Prescribed by ANSI Std. 239-18

THIS PAGE INTENTIONALLY LEFT BLANK

Approved for public release; distribution is unlimited

DESIGN AND QUALIFICATION OF A HIGH-PRESSURE COMBUSTION CHAMBER FOR IGNITION DELAY TESTING OF DIESEL FUELS

Warren P. Fischer
Ensign, United States Navy
B.S., United States Naval Academy, 2012

Submitted in partial fulfillment of the
requirements for the degree of

MASTER OF SCIENCE IN MECHANICAL ENGINEERING

from the

NAVAL POSTGRADUATE SCHOOL
June 2013

Author: Warren P. Fischer

Approved by: Christopher M. Brophy
Thesis Co-Advisor

Patrick A. Caton
Thesis Co-Advisor

Knox T Millsaps
Chair, Department of Mechanical and Aerospace Engineering

THIS PAGE INTENTIONALLY LEFT BLANK

ABSTRACT

A high pressure and temperature combustion chamber was designed to compare the ignition properties of different fuels, including conventional F76 diesel and hydrotreated renewable diesel (HRD), derived from algae. Conditions were selected to capture the operating conditions within a large number of Navy systems, testing at a range of temperatures from 800–1340 °F and pressures as high as 20 atm. Three Navy-relevant injectors were procured for the testing as well as a commercial injector made by Sturman Industries. The Sturman diesel injector was characterized up to a fuel tip pressure of 9600 psi and produced Sauter Mean Diameters of approximately 90 microns, generally showing improved atomization for F-76 when compared to HRD at similar conditions. The combustion chamber utilized dynamic air injection with increased turbulence and the ability to alter the amounts of combustion products including CO, CO2 and H2O that typically exist in real engines from the previous combustion event. Qualification testing of the combustion chamber evaluated final pressures of up to 15 atmospheres and temperatures of 472 °F, but revealed heat losses during the dynamic air injection events, resulting in temperatures below expected values and auto-ignition conditions for fuels under consideration. A fluidized bed heat exchanger will be implemented to supplement the existing design and reach the desired temperatures.

THIS PAGE INTENTIONALLY LEFT BLANK

TABLE OF CONTENTS

LIST OF FIGURES

LIST OF TABLES

THIS PAGE INTENTIONALLY LEFT BLANK

LIST OF ACRONYMS AND ABBREVIATIONS

ABE	Acetone, n-Butanol, and Ethanol
BD	Biodiesel
CAT	Caterpillar Inc.
DoD	Department of Defense
DSH	Direct Sugar to Hydrocarbon
EMD	Electo Motive Diesel
FT	Fischer-Tropsch
FWH	Full Width at Half Maximum
HRD	Hydrotreated Renewable Diesel
LHV	Lower Heating Value
NPS	Naval Postgraduate School
PAH	Polycyclic Aromatic Hydrocarbon
PDPA	Phase Doppler Anemometry
SMD	Sauter Mean Diameter
SPK	Synthetic Paraffinic Kerosene

THIS PAGE INTENTIONALLY LEFT BLANK

ACKNOWLEDGMENTS

I would like to thank Dr. Chris Brophy, who made it possible to conduct this research. Your experience and knowledge were incredible resources without which I would not have succeeded.

I would also like to thank Dave Dausen for his patience and helpful input throughout this research and especially for always being happy to share advice during the design phase of this thesis. Your positive attitude and willingness to answer any questions I had were invaluable to me and my research.

Thank you to Bobby Wright and Lee Van Houtte for doing an incredible job ensuring the experimental setup was assembled with expert precision. Without your hard work this thesis would never have been completed on time.

Thanks to the Office of Naval Research and Dr. Sharon Beermann Curtin for funding this research.

Finally, I would like to extend a special thank you to Dr. Patrick Caton, who has been an incredible mentor and advisor for this research and my entire academic career. Your enthusiasm and expertise have been a major source of inspiration throughout my studies.

THIS PAGE INTENTIONALLY LEFT BLANK

I. INTRODUCTION

A. BACKGROUND AND HISTORY

Petroleum-based fuel is a widely used source of energy around the world. The United States Navy relies heavily on petroleum-based fuels to conduct defense operations and power many of its ships, aircraft and weapons. In fiscal year 2008, the Navy consumed approximately 46,000 barrels per day (bpd) of F-76 diesel fuel to power its ships and other combat vehicles and 47,000 bpd of JP-5 jet fuel to fly its aircraft [1]. In the past decade the U.S. Department of Defense (DoD) has shown increased interest in exploring alternative fuels for use in engines that may have been in service for decades. The use of alternative fuels in such systems presents challenges in terms of seal compatibility, combustion efficiency, and general operability. This interest has been sparked by environmental issues, concerns about future supply and cost of petroleum-based products and the need to decrease the military's dependence on foreign suppliers.

In October of 2009, Secretary of the Navy Ray Mabus announced that by the year 2020 he intended for the U.S. fleet to fulfill half of its energy needs through alternative sources of energy. This would mean cutting the approximately 100,000 bpd of petroleum-based fuels used by the Navy down to 50,000 bpd. In addition, Secretary Mabus discussed a "Green Strike Group," which will consist of nuclear-powered platforms as well as ships and aircraft powered entirely by alternatives to petroleum-based fuels. This fleet would be deployable by the year 2016 [2].

Since Secretary Mabus' announcement the Navy has begun to test alternative fuels in its existing engines. On April 22, 2010, the Navy showcased a supersonic test of an F/A-18 Super Hornet fighter aircraft, nicknamed the "Green Hornet," using a 50/50 blend of JP-5 petroleum-based jet fuel and an alternative fuel derived from the *Camelina sativa* plant [3]. In October of 2010 the first full test of a naval vessel was conducted using a 50/50 blend of F-76 petroleum-based diesel fuel and hydrotreated renewable diesel (HRD), derived from algae [4].

The Navy's tests of alternative fuel blends have been extremely successful, but more extensive study of alternative fuel is needed before they can be permanently implemented in combat systems. Many of the tests have been conducted for short durations and have only used samples of 50% conventional fuel and 50% alternative fuel. Further testing of pure blends of the new fuels can provide insight into physical and chemical differences between the fuels that could provide information on the potential performance of alternative fuels in legacy engines if other material compatibility issues can be overcome.

The atomization characteristics of alternative fuels when they are injected into a diesel engine directly affect the behavior of the fuel in the chamber of the engine. A fuel that breaks up into small particles and mixes with the air quickly will show more complete combustion than one which breaks up more slowly. Comparing the resulting particle size for the various fuels generated during the injection process can show how completely alternative fuels will combust in comparison with well-known fuels such as F-76.

Differences in chemical properties between fuels also have a large impact on the ignition delay time, which characterizes the amount of time between fuel injection and auto-ignition of the fuel due to the high temperature and pressure in the cylinder. This information is used to define the cetane number, which is a relative measure of the auto-ignition tendency. If a fuel injected into a diesel engine does not auto-ignite rapidly enough it can cause "knock," potentially causing damage to the components of the engine [5]. Diesel knock is an explosion, not a deflagration, caused by excessive premixing of fuel with air prior to ignition, leading to a large amount of energy release in a short time after ignition. The need to determine the ignition delay time of alternative diesel fuels at peak pressures and temperatures inspired the design of a high-pressure and temperature combustion chamber. Optical techniques were considered and implemented from the design stage to more accurately determine how long the fuel takes to auto-ignite.

In the past, alternative fuels have been studied in laboratory research using research-specific injectors. However, for this project several Navy-specific injectors were considered in order to study the effects of alternative fuels in real military applications. Table 1 shows the Navy platforms and engine information for each of the injectors that was considered. These injectors vary in size and flow rate depending on the engines they

are used in. Three of the injectors in Table 1 were selected for this research to provide a wide range of engine size and Navy application. The three injectors chosen were the Yanmar, the CAT, and the EMD.

Ship Class or Vehicle Designation	Use	Engine and Size	Cyl. Vol. (L) Bore (in)	Injector Type
Special Warfare boats	Propulsion	Yanmar 6LPA-STP DI, I-6, 4.16 L	0.694 L 3.70 in	Nozzle
HMMWV	Propulsion	AM General IDI, V-8, 6.5 L	0.813 L 4.06 in	Nozzle
FFG-7 Frigate	Ship service generator	CAT 3512 DI, V-12, 51.8 L	4.32 L 6.70 in	Electronically controlled, mechanically actuated unit injector
SSN-774 Virginia-Class Submarine	Emergency generator			
CVN-68 Nimitz-Class Aircraft Carrier	Emergency generator	EMD 645-E5 DI, V-16, 169 L	10.6 L 9.06 in	Mechanical unit injector
SSBN 726 Ohio-Class Submarine	Emergency generator	Fairbanks-Morse 38D 8-1/8 Opposed Piston	17.0 L 8.13 in	Nozzle
SSN-688 Los Angeles-Class Submarine				
SSN-21 Seawolf-Class Submarine				
LSD-41 Whidbey Island-Class Dock Landing Ship	Ship service generator			
LPD-17 San Antonio-Class Amphibious Transport Dock	Propulsion	Colt-Pielstick PC 2.5 V-16, 1250 L (est.)	78 L (est.) 16 in	Nozzle

Table 1. Injectors for Research Consideration

B. TYPES OF ALTERNATIVE DIESEL FUEL

There are many different types of possible alternative diesel fuels currently under consideration. Among the different categories considered here are biodiesel, Fischer-Tropsch (FT), hydrotreated, and direct sugar to hydrocarbon (DSH). These different biofuels will be discussed in the following paragraphs.

Biodiesel is a type of biofuel that is being increasingly used in the United States. It is produced by reacting raw oil such as soybean oil with an alcohol, commonly methanol or ethanol, which produces glycerol and a monoalkyl-ester molecule [6]. The glycerol is a byproduct that can be sold commercially and the monoalkyl-ester is "biodiesel," which can be used as-is or in combination with other diesel fuel. This process used to produce biodiesel fuel is called transesterification. Biodiesel performs much like conventional diesel fuel, but there are also issues with its use. Some conventional sealing materials will not seal correctly with high concentrations of biodiesel, meaning that the fuel must either be used in small percentages in mixtures or the sealing material must be replaced in existing engines. Biodiesel also absorbs water, which allows organisms to grow in the fuels, potentially building up enough to clog filters if left standing too long. Finally, at colder temperatures the fuel thickens and stops flowing well, meaning that it must be heated in cold climates [5]. Because of these problems the U.S. military has moved away from using biodiesel.

Fischer-Tropsch fuel is liquid fuel typically derived from coal. The process used to produce this fuel has been used since the 1920s and 1930s in Germany. Fischer-Tropsch fuels accounted for 90 percent of the fuel used by the Luftwaffe in World War II. This fuel is produced in a three-step process. The first step is gasification, in which a feedstock fuel, such as a coal, is heated with steam to produce CO_2, H_2, and CO as well as a small amount of methane. The second step, when steam is reacted with CO in order to produce more H_2, is called the synthesis gas shift. Finally, reaction over a catalyst bed allows the formation of higher carbon-number molecules from the synthesis gas with water as a side product. These molecules are very similar to those that are found in conventional diesel fuel and are known to have high cetane numbers [7].

Hydrotreated diesel fuels can be made using various hydrocarbon feedstocks particularly of biological origin, such as vegetable oils and animal fats. Some of the common oils that are used are rapeseed, sunflower, soybean, and palm oil [8]. The hydrotreating process produces high quality fuel with similar properties to Fischer-Tropsch fuels. In this process, the oils are pretreated to remove solid impurities. Hydrogen is used to convert the fatty acids in these oils into fuels. The hydrotreatment produces synthetic versions of diesel fuel as well as gasoline and liquefied petroleum gas, which can be used for energy purposes [9]. Hydrotreated vegetable oil fuels have high cetane numbers, which means that autoignition is more rapid, implying easier cold-starting and fewer particulates in the combustion products than most other diesel fuels. Hydrotreated fuels work in existing engines and can be used in high concentrations. An advantage of these fuels is that they can reduce emissions, including nitrogen oxides, particle emissions, aldehydes, benzene, and polycyclic aromatic hydrocarbons (PAHs) [8].

Synthetic Paraffinic Kerosene (SPK) is a type of fuel that has a similar production process to hydrotreated fuels but is used in the aviation industry. The same bio-derived oils used for the hydrotreatment process are purified by removing solid impurities. Oxygen molecules are removed from the oils and hydrogen is used to convert the molecules to paraffins, single-bonded carbon chains bonded with hydrogens. Finally, the long-chain paraffins that represent the types of molecules in diesel fuel are broken up into shorter carbon chains that are commonly found in jet fuel [10]. Figure 1 shows the molecules through the process of producing SPK. This fuel is being looked into by Boeing and other large commercial airlines as a potential alternative fuel that will help lower emissions and perform well in existing engines. Boeing's June 2009 report states that in all the tests that have been conducted SPK has "either met or exceeded the performance specifications for jet fuel" [10].

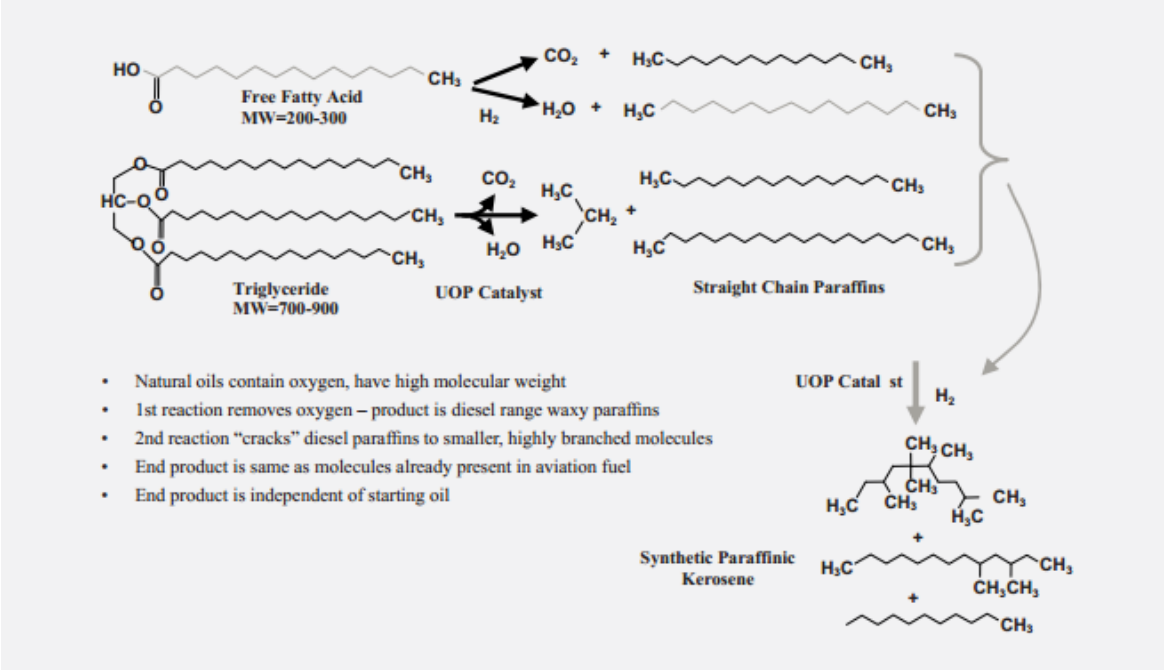

Figure 1. Chemical process used to produce SPK. From [10]

Direct sugar to hydrocarbon (DSH) fuel is another type of biofuel described in a 2012 article by Anbarasan et al. It is created by using bacteria to convert sugar to products that can be used to make fuel. The bacteria *Clostridium acetobutylicum* produces a mixture of acetone, n-butanol, and ethanol (ABE). In this paper the ABE is reacted using different catalysts and at different temperatures to produce longer carbon chains more representative of the size of molecules in diesel fuel. Oxygen is removed from the products of this process to produce C_7 to C_{15} paraffins which can be used as fuel. Anbarasan et al.'s team was able to complete this process converting 38 percent of the carbon in the initial sugars to carbon in the product fuel [11].

Table 2 compares the properties of the types of fuels that have been discussed in this section. Each of these fuels will have varying properties based on the small differences in their production process or in the feedstock. Table 2 is intended to give a basic idea of the ranges of values that will be found for these properties. In Table 2 T_x is the temperature at which "x" percent of a fuel has vaporized, and LHV stands for lower heating value.

Fuel / Properties	F-76	BD	FT	HRD	SPK	DSH
ρ [kg/m^3]	844.2 [a]	885.1	753.9 [a]	778.1 [a]	740	766 [a]
σ [mN/m]	25.8 [b]	24.0	25.3	24.9 [b]	26.8	26
μ (cSt)	2.955 [c]	6.489	4.503	2.748 [c]	1.088 [c]	4.1 [a]
T_{10} -T_{90} [°C]	-	-	173-244	-	-	244-245
T_{50} [°C]	-	-	207.5	-	-	245
LHV [MJ/kg]	42.75	37.6	43.94	43.96	44.05	43.9
Cetane No.	52	56	75	~75	24.7	60
Composition						
Wt% C	86.4	-	96.78	85	84.8	85.1
Wt% H	13.32	-	3.22	15	15.2	14.9
Wt% O	0	10.9	0	0	0	0
% paraffin	70.7	-	95.3	98.5	94.3	99.9
% olefin	2.3	-	1.1	0.9	4.7	0
% aromatic	27	-	3.6	0.6	1.0	0

Table 2. Properties of biodiesel fuels at STP (20°C) After [6], [12]–[18]

[a] Property found at 15° C

[b] Property found at 24.2° C

[c] Property found at 40° C

C. SPRAY STRUCTURE

The discussion of diesel fuel spray properties requires understanding the basic structure of a diesel spray. Before optical techniques were developed, limited information was available regarding the breakup and structure of diesel sprays. Flynn et al. describe many different hypotheses for spray structure [19]. An initial model proposed by researchers in the 1970s was that the diesel spray was composed of a very fuel-rich center which became leaner radially. The fuel would react at a distance from the core where there was enough oxygen mixed in with the fuel to generate a combustible mixture. In more recent models the fuel is in liquid form when it is injected and breaks up into tiny droplets. Hot air from the cylinder surrounding the spray is entrained into the jet, which causes the fuel around the outside regions of the spray to vaporize. Once there is enough oxygen entrained in the spray combustion begins as a diffusion flame where the fuel vapor and hot air meet. The core of the jet is mostly fuel, either in liquid or vapor form. Figure 2 shows schematics of the early and more recent spray models, respectively [19].

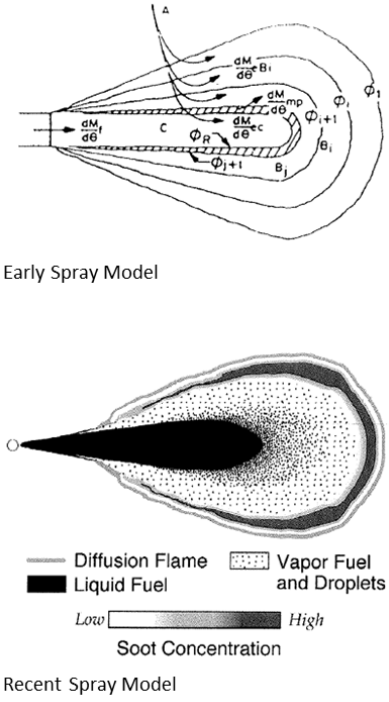

Figure 2. Schematics of early and more recent spray models. After [19]

Atomization is the process by which the spray breaks up into small droplets, which directly affects the initial combustion behavior. Even with current techniques for visualizing sprays it is difficult to observe the detailed breakup of the fuel because of the dense sprays and small length scales. Therefore, computer modeling of spray behavior is important. Reitz [20] developed a method of modeling atomization in which "parcels" or "blobs" of fuel leave the injector. These parcels experience small perturbations in the flow, causing surface waves to form. Eventually the instability due to these surface waves causes the larger drops to break up into smaller drops and the wavelengths associated with the surface disturbances determine the size of the new drops. The fuel properties that most heavily govern atomization of the spray are density (ρ), viscosity (μ), and surface tension (σ).

Reitz identifies four different breakup regimes for diesel spray, depending on the Weber number of the spray. The first regime is the Rayleigh breakup regime, which occurs at very low Weber numbers [20]. The Weber number is defined by the equation:

$$We = \frac{\rho U^2 L}{\sigma} \tag{1}$$

where ρ is the density, U is velocity, L is a reference length, and σ is surface tension. The Weber number represents the ratio of inertial forces (numerator) to surface tension (denominator) [21]. In the Raleigh regime (We≈4.5), the jet does not break up until many nozzle diameters from the injector and the drop sizes are comparable to the diameter of the jet. The second regime is the first wind-induced regime (We≈18), and is very similar to the Raleigh regime in that the break-up occurs well downstream of the nozzle and the droplet sizes are on the order of the spray diameter. The second wind-induced regime (We≈45) is characterized by much smaller droplets with breakup still occurring downstream. The fourth regime is the atomization regime (We≈226), which has the highest Weber numbers, shows much smaller droplets than the nozzle diameter and breakup begins as soon as the fuel leaves the nozzle. The last regime is very characteristic of diesel sprays [22].

Experiments have been conducted to determine what properties of fuels cause changes in the characteristics of the injection sprays. Ochoterena et al. used several different fuels and measured the liquid phase penetration depth and spray cone angle. The differences in penetration seemed to be caused by the variation in surface tension, viscosity, and density between the different fuels. In addition the authors concluded that the penetration depth was longer for fuels with low volatility [23]. This makes sense because one should expect that a fuel that more readily vaporizes will remain in the liquid phase in the spray for a shorter duration, shortening the liquid penetration depth.

Ochoterena et al. also found that the spray cone angle was heavily influenced by the fuels' viscosity. In those experiments the fuels with the higher viscosity showed wider cone angles than those with lower viscosity [23].

Although there is little explanation in technical papers on exactly how fuels sprays are affected by the properties of the fuels, the work of Ochoterena et al. shows that different fuels will certainly produce differences in the injection spray due to their properties. This means that when a new fuel is being considered testing it to see how it will behave in a diesel injection environment can be extremely valuable.

D. IMAGING DIESEL FUEL SPRAYS

Optical methods have been developed to image diesel sprays and learn more about diesel injection. Two of the common methods used to image the spray are shadowgraph and schlieren imaging. Both methods involve passing a collimated beam of light through the spray, which is then focused and a camera is located just after the focal point. For the shadowgraph technique the camera sees what looks like a shadow image of the spray. What the camera actually sees is the difference in the refractive index between the fuel and the surrounding gases [24]. A shadowgraph image becomes a schlieren image when a "cutoff," usually a knife edge is used to obscure part of the light at the focal point just before the camera. This increases the system's sensitivity to differences in the refractive index [24]. These techniques are particularly useful because they show combustion locations where high temperatures result in low density. Since these density gradients can be seen with these imaging methods, they are useful in showing relative

temperatures at different locations in the injection [24]. Pickett et al. demonstrated that the shadowgraph and schlieren techniques are useful in obtaining information about what parts of the spray do not burn completely and about the lift-off length of the flame.

Another commonly used method of imaging diesel sprays is Mie-scattering, in which a laser is used to illuminate the spray and a high-speed camera is used to image the light scattered off of the fuel droplets. As discussed in [24] this technique can be used with shadowgraph and schlieren imaging in order to determine the locations of vapor and liquid zones.

Liquid fuel locations can be imaged by seeding the fuel with fluorescent dyes and using a laser to excite the dye which then fluoresces at a longer wavelength. If the wavelength of the emitted light is known, a narrow bandpass filter can be used to image this light and eliminate contributions from the excitation surface, providing information on the location of the liquid spray [25].

Chemiluminescence imaging is another method widely used to characterize the ignition process and visualize the combustion zones of the resulting flames. CH* and other radicals emit light at certain wavelengths which can be captured using a high-speed camera. This can be combined with the shadowgraph technique to distinguish the high temperature combustion from unburned areas in the spray, helping to find the sources of incomplete burning [24]. OH* and CH* chemiluminescence can also be used combined with shadowgraph imaging to determine the lift-off length.

E. GOALS AND OBJECTIVES

This research had three main goals. The first was to design, build, and calibrate a high-pressure and high-temperature combustion chamber for conditions of up to 3000 psi and bulk temeratures up to 500 degrees Fahrenheit. The second objective was to characterize spray patterns and droplet distributions of several different diesel injectors operating on conventional F-76 fuel as well as HRD and F-76 and HRD blends. The last goal was to begin analyzing ignition delay properties of alternative fuels using different Navy-specific injectors at initial pressures of 18 atmospheres and temperatures between 800 and 1340 degrees Fahrenheit.

THIS PAGE INTENTIONALLY LEFT BLANK

II. EXPERIMENTAL SETUP

Two different experimental setups were utilized in this research. The first was an experimental combustion chamber used to image the injection and combustion of the diesel spray. The second was a rectangular test chamber with optical access designed to characterize the particle velocity and size distribution of the sprays produced. Engineering drawing for all the components discussed and utilized in this research are shown in Appendix A and Appendix B.

A. COMBUSTION CHAMBER SETUP

The combustion chamber was made up of several different parts: a) combustion chamber, b) fuel supply system, c) air supply system, d) exhaust system, e) high-speed imaging system and f) control system. Figure 3 shows the complete experimental setup used during the combustion experiments. This combustion chamber was designed to visualize the spray and combustion of diesel fuels from different injectors, including Navy-specific injectors, using both laser-induced fluorescence and CH* chemiluminescence.

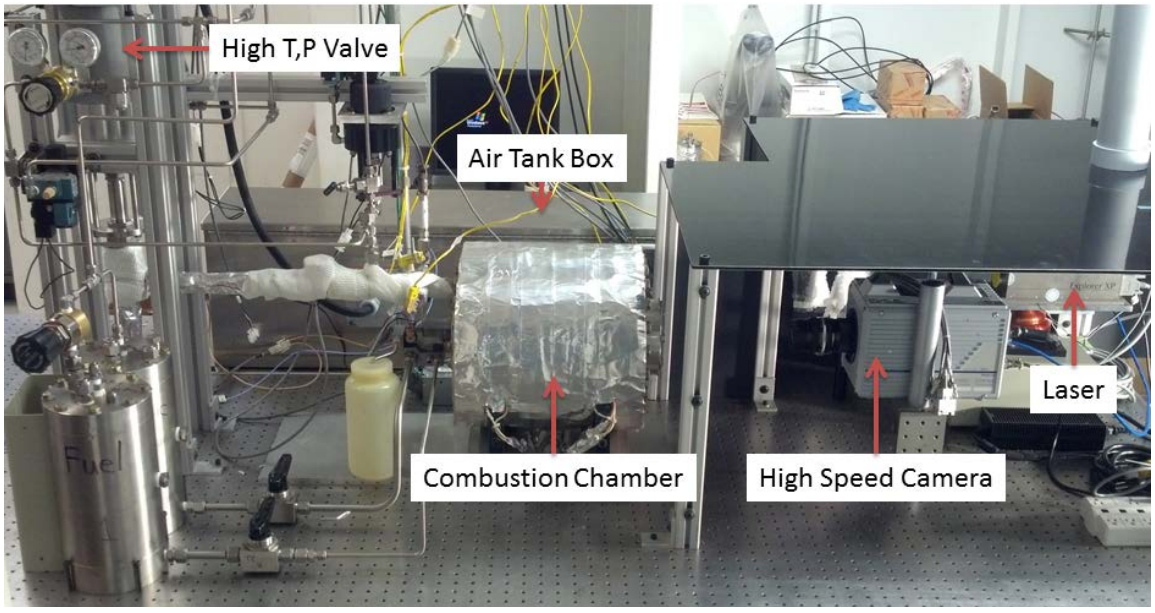

Figure 3. Layout of Combustion Chamber Setup

1. Combustion Chamber

The combustion chamber was designed to withstand peak pressures of 3000 psi and nominal bulk temperatures of 400 degrees Fahrenheit. The main body was fabricated from a large piece of 17-4 stainless steel and was heat treated to increase its strength. The material was chosen because of its good corrosion resistance, thermal stability, and its high yield strength in order to allow high internal pressures. Two flanges fabricated from the same material are located at each end. An O-ring groove was machined on each end to seal the chamber and the flanges are each attached with 20 ½-20 grade-eight bolts. The body of the chamber does not have any ports to preserve the strength of the chamber due to the expected pressures. Figure 4 shows an exploded view of the combustion chamber assembly.

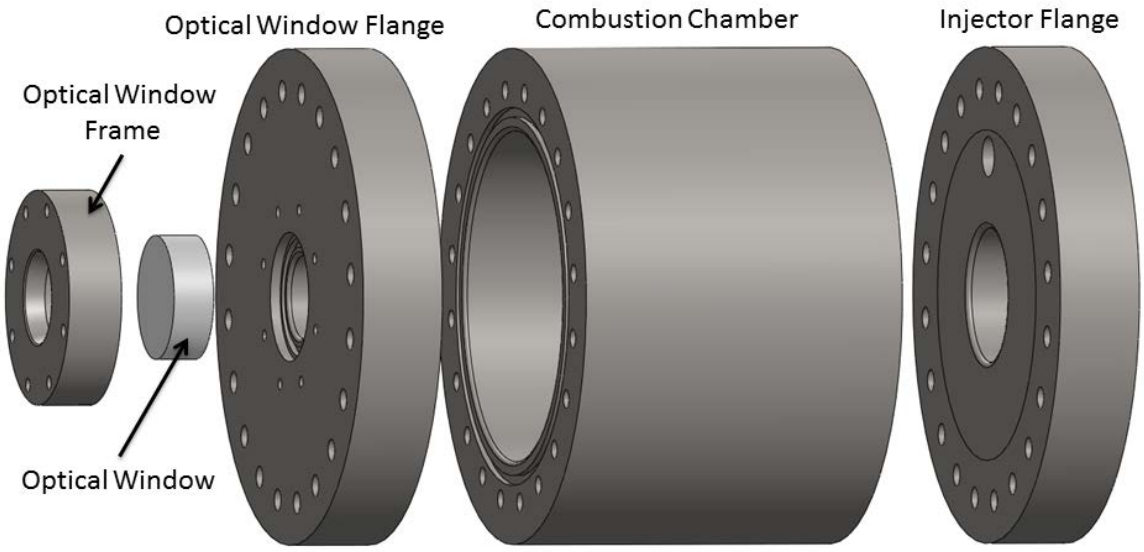

Figure 4. Exploded View of Combustion Chamber Assembly

Stress analysis for the chamber assembly was conducted in ANSYS using an internal pressure of 3,000 psi. The maximum Von Mises stress that was calculated was just under 20 ksi, which is well under the 180 ksi yield strength of 17-4 steel after heat treatment. This gives a factor of safety of over 9 for the main body of the chamber. Figure 5 shows the ANSYS Von Mises stress results.

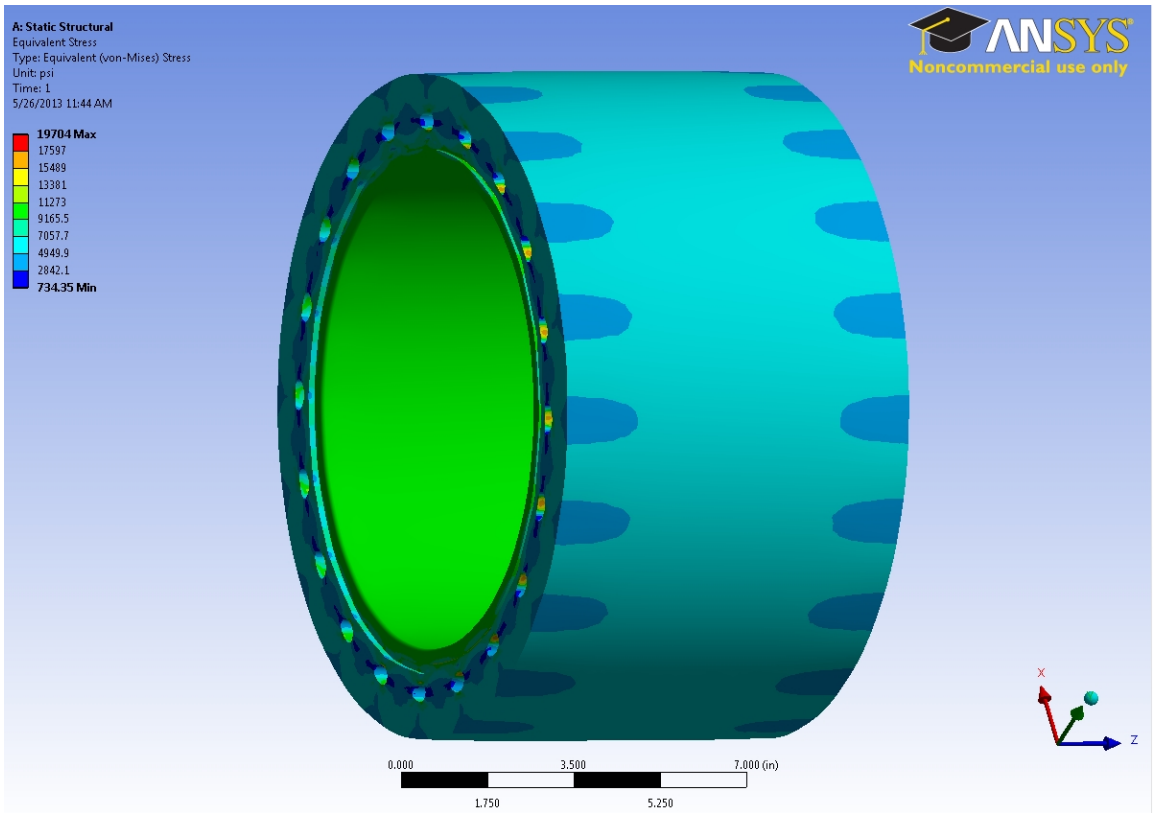

Figure 5. ANSYS Stress Analysis of Combustion Chamber

a. Injector Flange

One of the flanges bolted to the main chamber was designed to hold the fuel injector as well as to inject and exhaust the chamber products. This flange will be referred to as the "injector flange" throughout this thesis. The flange was machined out of 12 inch bar stock of the same material as the main chamber and heat treated for increased strength. Stress analysis was conducted using ANSYS, finding a maximum Von Mises stress of 29.4 ksi, thereby providing a minimum factor of safety of 6.1. Figure 6 shows the results of the Von Mises stress analysis conducted in ANSYS.

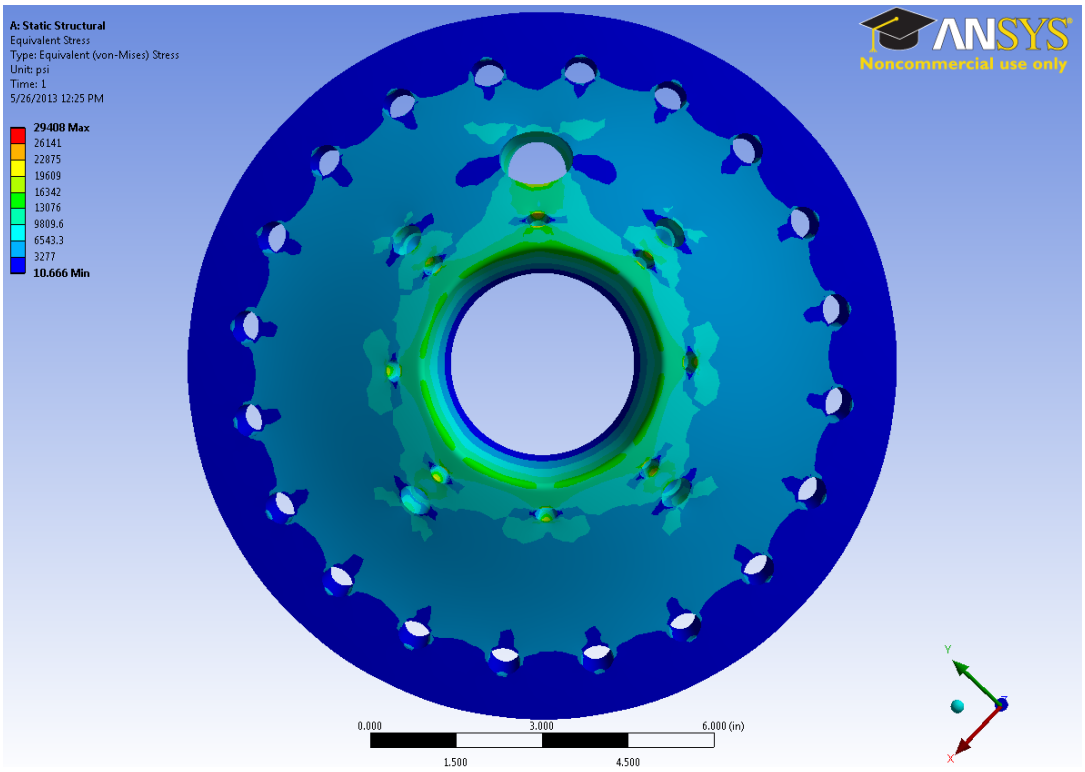

Figure 6. ANSYS Stress Analysis of Injector Flange

The injector flange has two ports. A 1-1/16 inch port allows for a ¾ inch tube to deliver high pressure and temperature air into the chamber. A large orifice in the center of the flange is where adapters for individual injectors were attached to the flange. Since several injectors were intended for use with this combustion chamber the flange was designed so that instead of needing a new flange for each injector, a smaller adapter could be machined, significantly reducing the cost of the chamber and machining time needed to finish the parts. The inner bolt pattern was used to fasten the adapters to the injector flange. The injector adapters are discussed in more detail later in this section.

b. Optical Window Flange

The flange on the side opposite of the injector is used to hold a sapphire window so that the spray and CH* emission can be imaged. The flange is also made from hardened 17-4 stainless steel and is fastened to the main chamber using high-strength grade-eight bolts. There is a small recess in the outer face of the flange where the window is seated. Stress analysis of the window flange was also conducted using ANSYS, which

gave a maximum Von Mises stress of 26 ksi, giving it a factor of safety of 6.9. Figure 7 shows the ANSYS stress analysis output for the optical window flange.

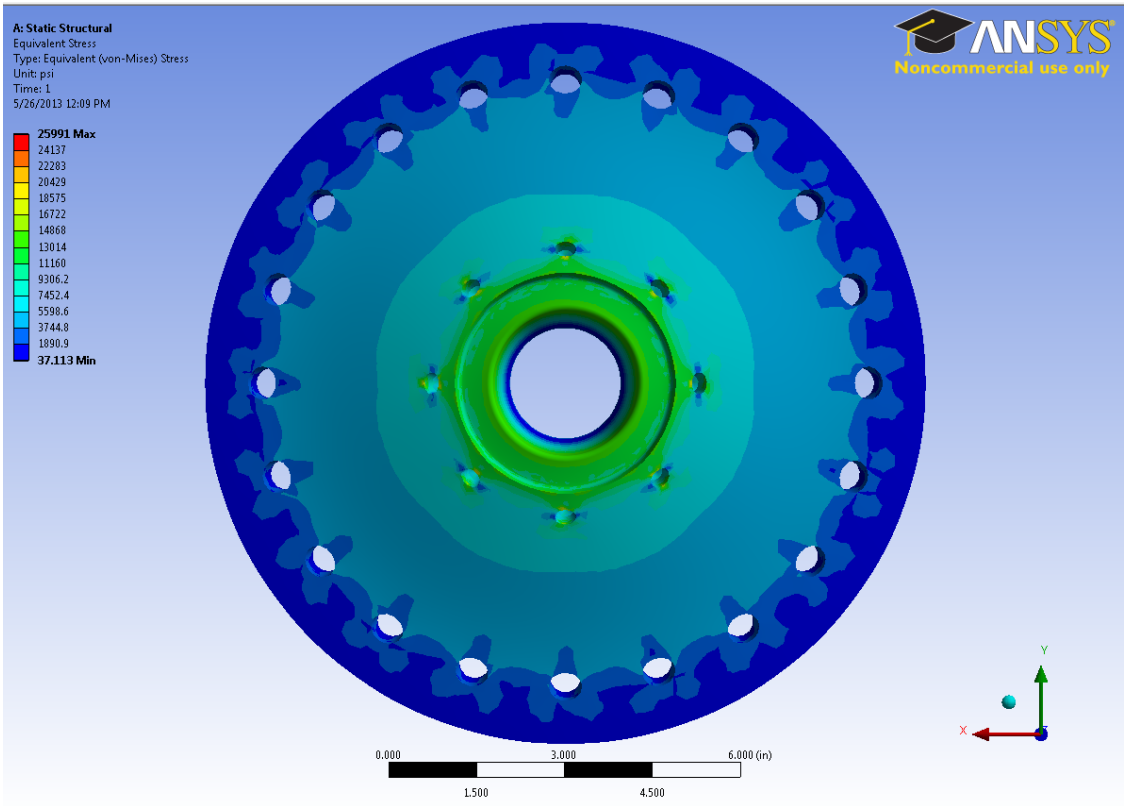

Figure 7. ANSYS Stress Analysis of Window Flange

c. Optical Window

The window has a diameter of three inches and a thickness of one inch and was designed for the chamber pressure of 3,000 psi. It was made out of sapphire because of its relatively high strength compared with other optical materials that were considered such as quartz. Stress analysis of the window was conducted in ANSYS. The outer half inch of the radius was fixed, with a pressure of 3,000 psi on the opposite side of the sapphire. This analysis provided a factor of safety greater than 10.

d. Optical Window Frame

The optical window frame is a metal adapter that holds the window in place and seals the leak paths of the air around the window. Figure 8 shows a section

view of the optical window frame. The orifice that is used to look through is two inches in diameter at the smallest point. This is the same size as the orifice in the optical window flange. The optical window frame has two O-ring grooves: one acts as a face seal against the sapphire window, and the other is installed in the corner of the face that connects to the optical window flange (see Figure 8.).

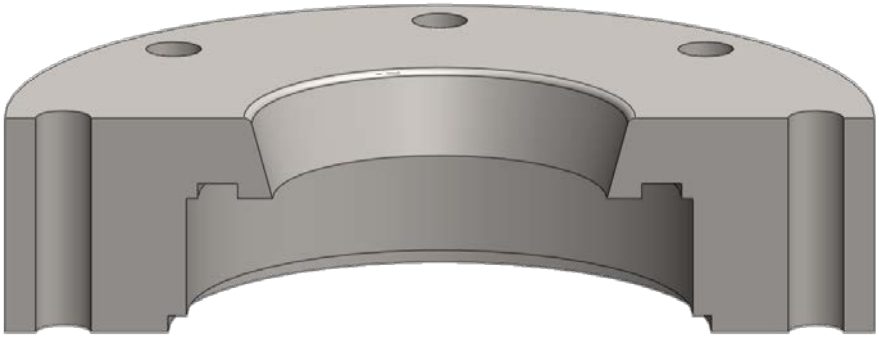

Figure 8. Optical Window Frame

One of the design challenges of the window frame was that there were two leak paths that needed to be sealed, one between the window frame and the window flange and the other between the outside of the window and the window frame. Both paths needed to be sealed without allowing the sapphire to touch metal, which would increase the possibility of fracture. Any interference of the window and metal, particularly asymmetric contact due to the window shifting under load, could lead to local chipping or cracking and subsequent window failure. To solve this problem O-rings are used on the top and bottom of the window with shallow O-ring grooves. The O-rings crush into the grooves but protrude far enough to prevent the window from reaching the metal face on top or bottom. An O-ring on the inner corner seals the leak path between the flange and the window frame.

2. Fuel Supply System

Several injectors were available for use with the combustion chamber. An adapter was designed for each of the injectors to interface with the same orifice in the injector flange to avoid creating a new flange for each injector. The three injectors that were

focused on in this thesis are a Sturman research injector, a Yanmar injector, and an Electro Motive Diesel (EMD) injector. The three injectors are shown in Figure 9.

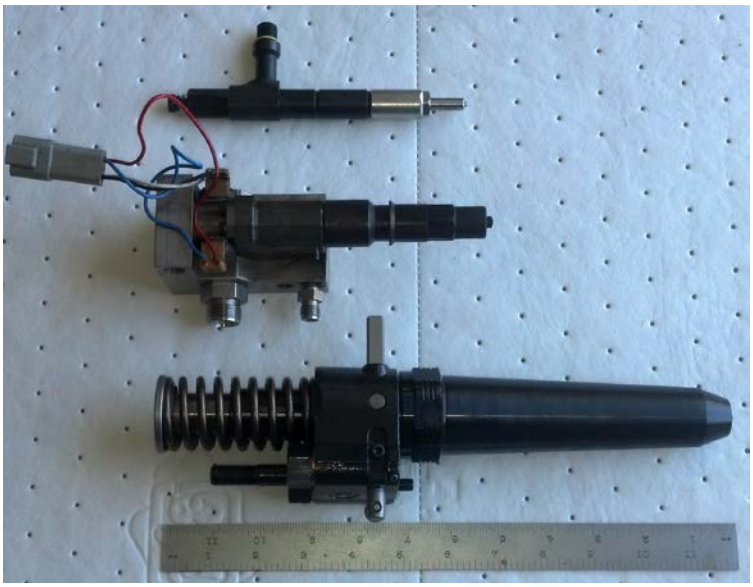

Figure 9. Injectors Used for Testing. From top to bottom: Yanmar injector, Sturman injector, EMD injector.

Because all the adapters were designed to fit in the same injector flange, the outer dimensions of the adapters were the same, with the inner dimensions designed to fit the individual injector. They were all made of the same 17-4 stainless steel as the main combustor and two flanges. In addition to each injector using its own adapter, the injectors were all actuated differently. In this section the design of each adapter and its method of actuation are described.

a. Sturman Injector

The Sturman injector was custom-made for the NPS Rocket Lab for a previous research program. Since then it has been used as a research injector for various fuels. Figure 10 shows an assembly cross section of the adapter that was made for this injector.

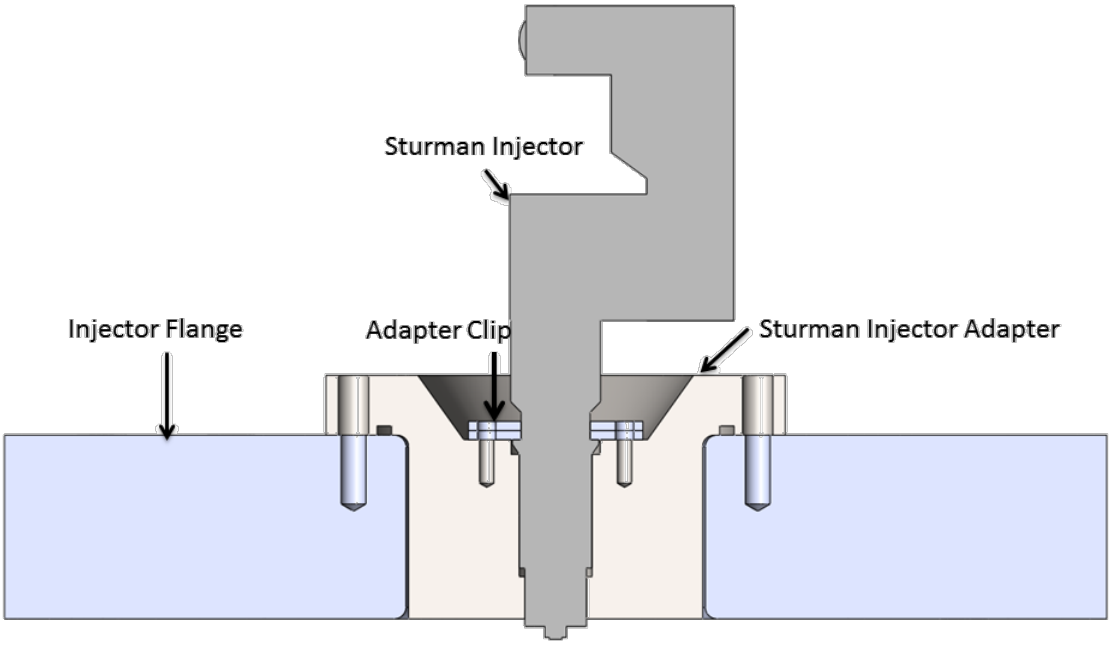

Figure 10. Cross-sectional View of Sturman Adapter Assembly

The adapter bolts onto the injector flange using eight high-strength grade-eight bolts. The injector was held in place by small adapter clips that were bolted to the adapter.

The Sturman injector is hydraulically powered using up to 3000 psi of hydraulic fluid with a fuel pressure of 100 to 200 psi. It is actuated electrically using a high-power driver to actuate a fast-acting spool valve that has a variable 1-5 millisecond pulse width. The internal design of the Sturman injector creates a 6:1 pressure amplification of the hydraulic supply pressure at the tip of the injector. Figure 11 shows the Sturman injector setup in the combustion chamber. Fuel and hydraulic fluid were stored in high-pressure tanks which are shown in Figure 11. These tanks were pressurized using Nitrogen gas.

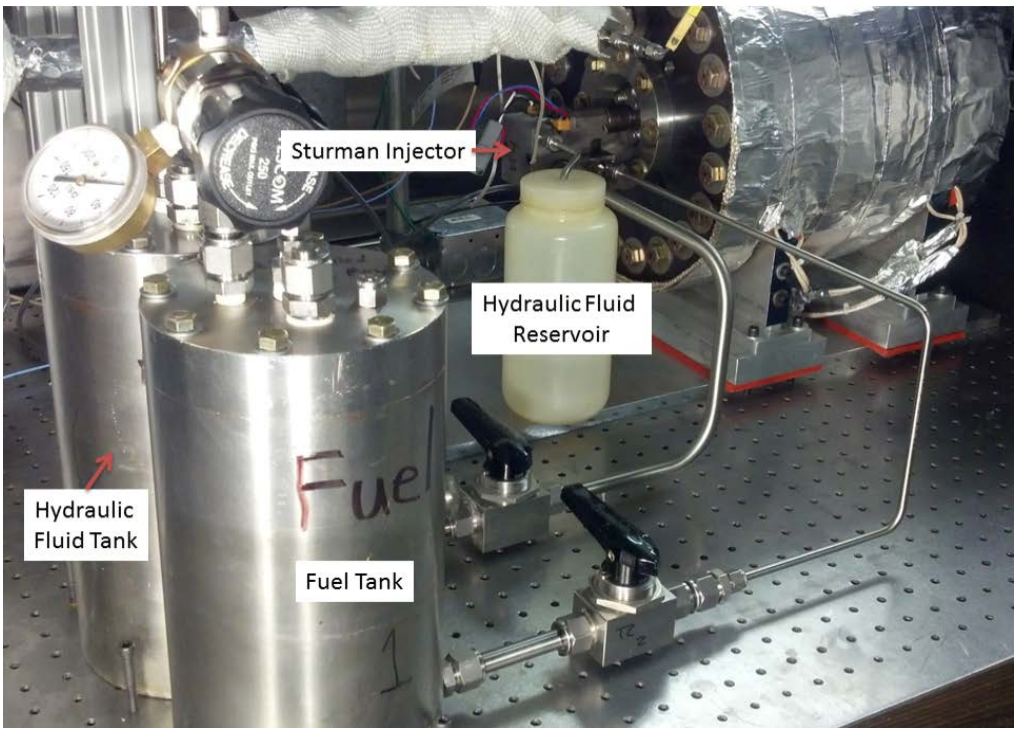

Figure 11. Sturman Injector Setup

b. Yanmar Injector

The Yanmar injector is the smallest of the injectors studied in this research. A cross section of the adapter mated to the flange is shown in Figure 12.

The outer dimensions of the Yanmar adapter were identical to those of the Sturman adapter. The rest of the adapter was designed for the dimensions of the Yanmar injector. The adapter collar shown in Figure 12 prevented the injector from sliding too far into the adapter in order to allow the fuel line to be attached to the injector. The adapter clip mated with a lip on the injector and bolted the injector to the adapter so that when the chamber was pressurized the injector was held in place.

The Yanmar injector is essentially a nozzle with a cracking pressure of about 250 bar (3,625 psi). The fuel was stored in a 5,000 psi tank and delivered to the injector by a fast-acting high-pressure solenoid valve

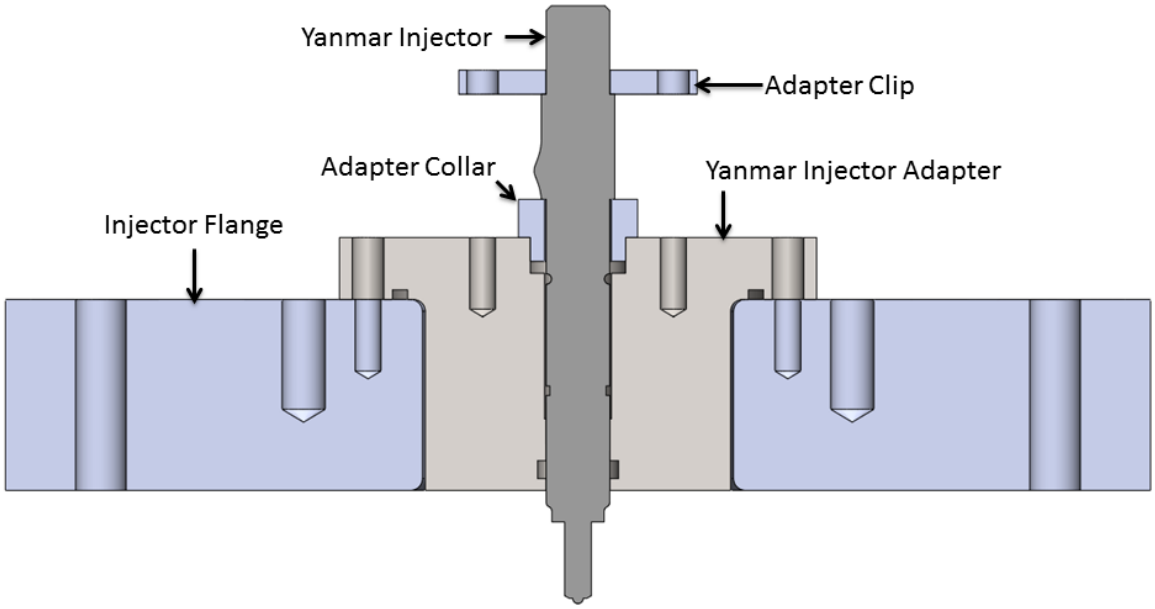

Figure 12. Cross-section of Yanmar Adapter Assembly

c. EMD Injector

The largest injector included in this thesis research is made by EMD. Figure 13 shows a cross-section of the adapter designed for this injector.

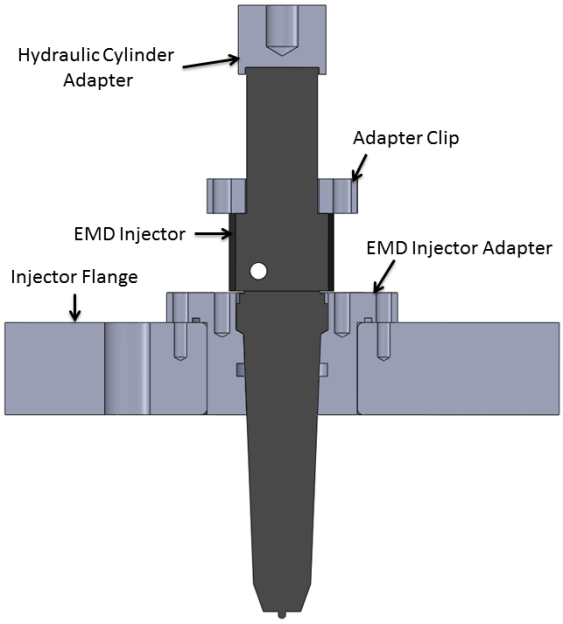

Figure 13. EMD Adapter Assembly

The EMD adapter held the injector down using an adapter clip with two high-strength grade-eight bolts. These bolted straight into the adapter and prevented the injector from moving with respect to the adapter, thereby creating a stacked assembly.

The EMD injector needed to be mechanically actuated by using a hydraulic cylinder to depress the plunger, which pressurized the fuel, causing the nozzle to inject once the pressure was high enough. The hydraulic cylinder adapter shown in Figure 13 was used to ensure that the hydraulic cylinder pushed evenly on the center of the plunger.

3. Air Supply System

The combustion chamber needed to be supplied with high pressure and temperature air to closely match the in-cylinder conditions of a diesel engine. Four high-pressure air tanks were used to supply this air. The tanks are rated for 5,000 psi at room temperature and over 3000 psi at a temperature of 1000° F. For this application the tanks were wrapped in heater tape and placed in an insulated box to heat them to approximately 1,000° F. These tanks were supplied with dry air with pressures up to 1,500 psi. A high-pressure and temperature valve was used to control when the air was allowed to rush into the chamber. Figure 14 shows a schematic of the air supply system. The high pressure delivery lines were also wrapped in heater tape (not shown) to minimize heat loss from this tubing.

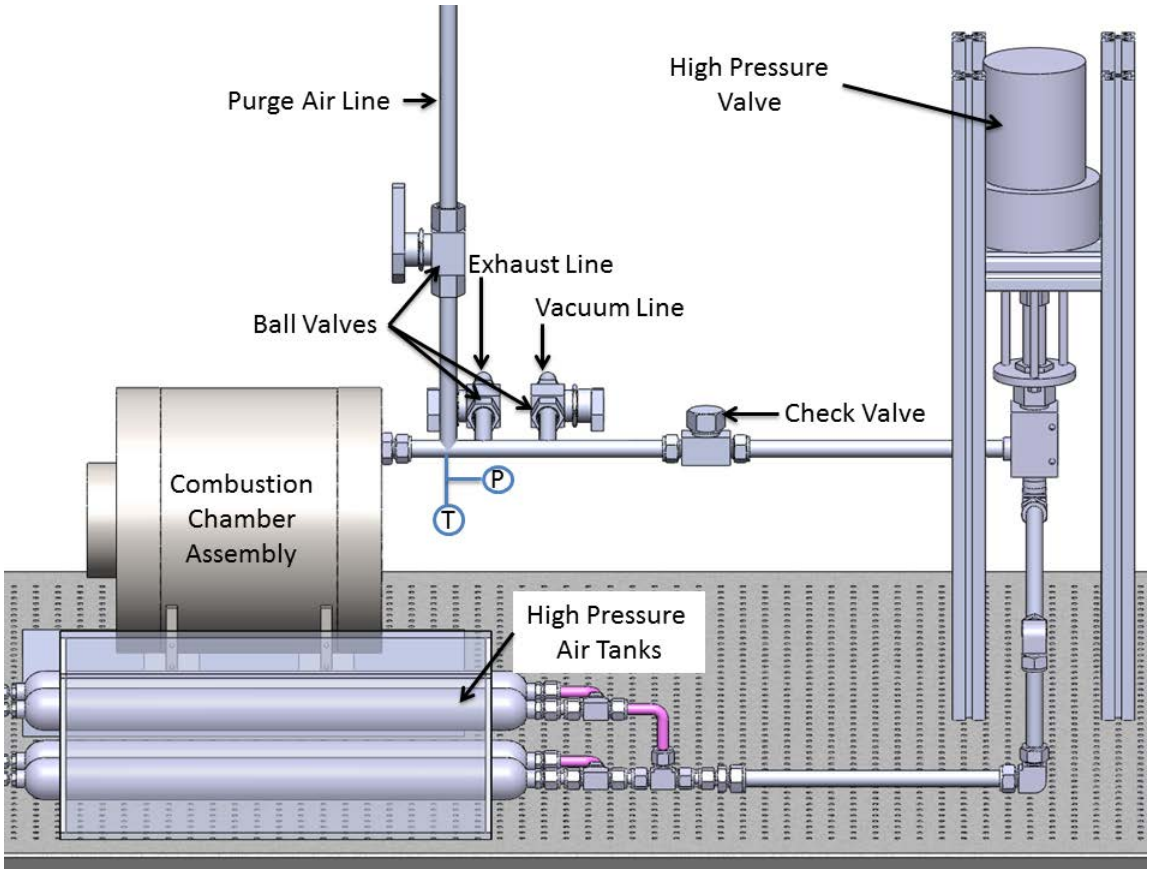

Figure 14. Air Supply System Schematic

Air enters the chamber through a large port in the injector flange which can be seen in the cross-sectional Figure 13 as a straight hole through the injector flange. When the air enters the chamber it is turbulent, mimicking the conditions that would be seen in the cylinder of a diesel engine, and the fuel injection event begins soon afterward.

4. Exhaust System

Once the injection and combustion were completed the chamber was purged of the exhaust. Since the chamber was at extremely high pressures and more ports in the flanges would create more stress concentrations, lowering the factor of safety for the system, the large port that was used to supply the air was also used to remove the exhaust. An exhaust valve was opened to allow most of the high pressure air and combustion products that were already in the chamber after combustion to leave the system. In order to remove the combustion products still remaining in the chamber, the

exhaust valve was closed and shop air at 100 psi was brought into the vessel. Once the chamber reached shop air pressure the exhaust valve was opened again to remove the excess air. This process was repeated twice to ensure that very little of the combustion products were left in the chamber after each run. After two purge cycles, a vacuum pump could also be used to completely evacuate the chamber if necessary.

5. High-Speed Imaging System

The fuel injection and combustion events imaged in this research lasted less than 10 milliseconds. A high speed camera was used to provide images of the fuel injection and subsequent combustion process. The camera used for this research was a Photron SA5. This camera was used in combination with a laser that illuminated a fluorescent dye (Pyrromethene 567A) in the fuel to capture the fuel injection event so that ignition delays could be referenced. The Explorer XP 532 nm laser was pulsed with a frequency varying from 100 to 300 kHz which correspond with 52.9 µJ per pulse and 15.5 µJ per pulse, respectively. Figure 15 contains a schematic of the setup of the optics system.

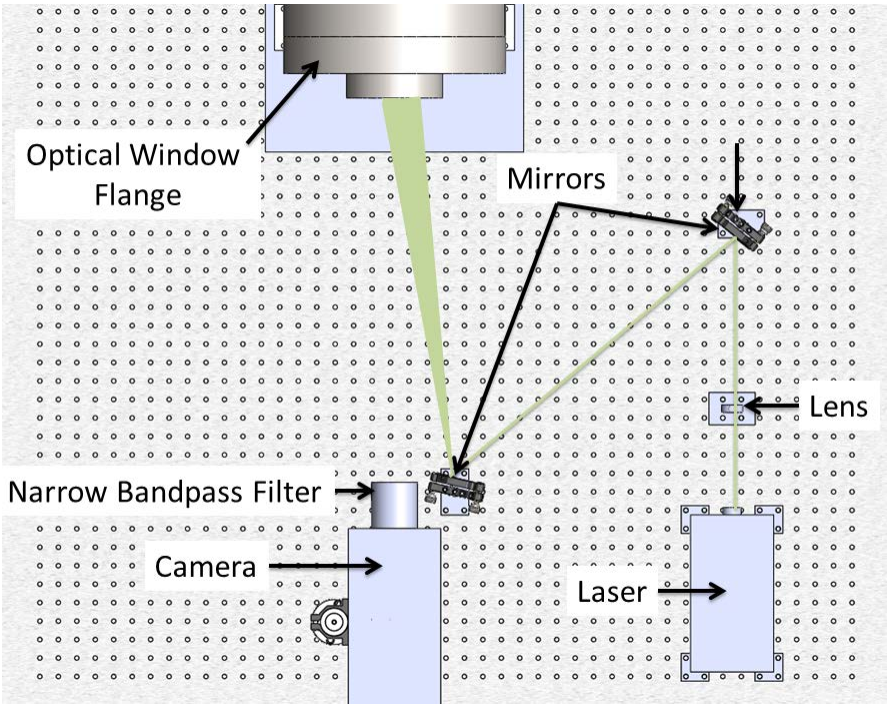

Figure 15. Schematic of Optics Setup

Although the laser emitted light at wavelength of 532 nm, the light given off of the dye in the fuel as a result of this excitation had a wavelength of 570 nm. A 570 nm narrow bandpass filter with a Full Width at Half Maximum (FWHM) of 10 nm was used to show only the light given off of the dye due to the laser illumination, providing a high-quality image of the fuel spray. The combustion event was individually imaged using CH* chemiluminescence located at 431.5 nm and also used a narrow band interference filter.

6. Control System

The control system for the combustion chamber filled the chamber to the desired initial pressure. The pressure in the air tanks was manually set and once the heater tape brought the air to the desired temperature, the control system opened the high pressure and temperature valve, allowing the high pressure, hot air from the tanks to flow into the combustion chamber. After a one second delay, the high-temperature valve was closed and the injector and camera were triggered at the same time. High speed pressure and temperature transducers located in the air delivery tubing just outside the chamber, which can be seen in Figure 14, recorded data for the air injection as well as the fuel injection and combustion events. The controller then opened the exhaust valve, allowing the hot, high-pressure air to leave the chamber. The valve for the purge air was opened, allowing the air to flow into the chamber, after which the exhaust valve was again opened. This purge cycle was repeated once more, ensuring that the combustion products were removed from the chamber.

B. PARTICLE SIZING CHAMBER SETUP

The particle sizing chamber was designed to analyze the particle sizes of injection sprays using a Phase Doppler Particle Anemometry (PDPA) laser system. The experimental setup was composed of four subsystems: a) spray chamber, b) fuel delivery system, c) PDPA laser system, and d) control system. Figure 16 shows the experimental setup of the chamber.

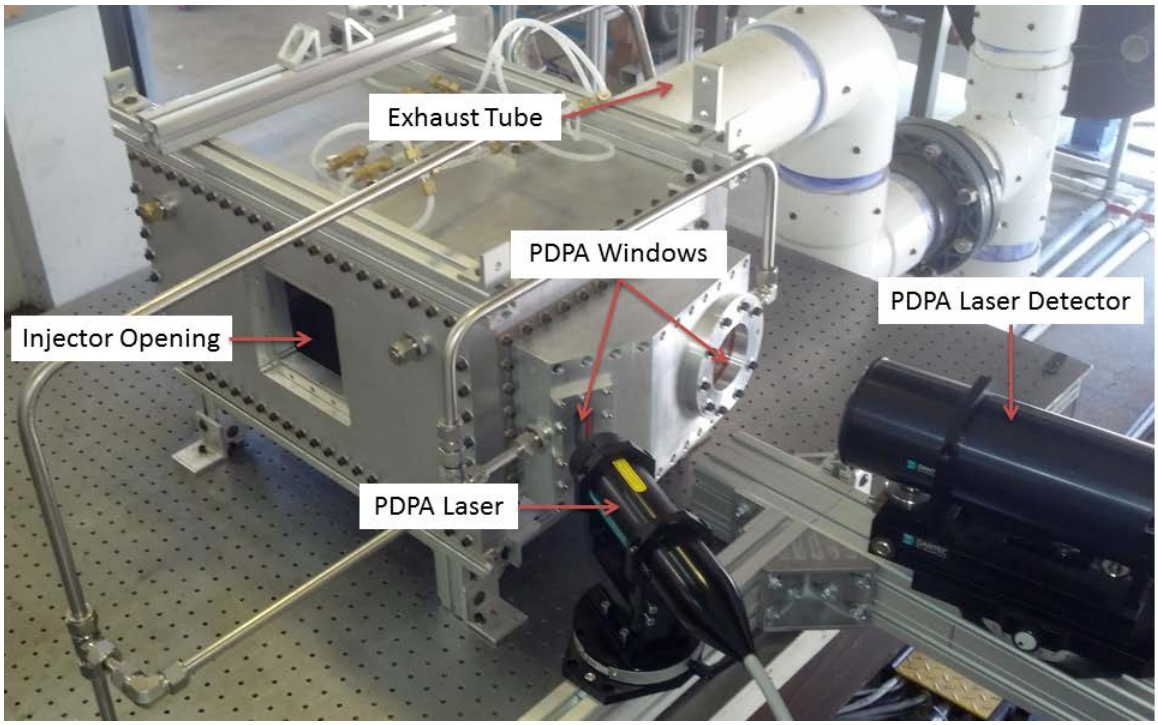

Figure 16. Particle Sizing Chamber Setup

1. Spray Chamber

The particle sizing chamber was a rectangular box designed to withstand pressures of up to 150 psi, but in this experiment the box was used at ambient pressure. One face of the box had an opening where an injector adapter flange was attached. The injector sprayed into the box and the laser system determined the size of the particles contained within the spray. The chamber is made of aluminum for manufacturing convenience because stronger materials, such as stainless steel, were not required to meet the strength requirements of the vessel.

2. Fuel Delivery System

As with the combustion chamber described earlier in this section, the spray chamber was designed to accept different injectors. The square part on the injector side of the box was used to attach the injectors to the chamber. In this section the method of attaching each of the injectors is discussed.

a. Sturman Injector

A mounting apparatus was created out of Aluminum bar stock for the Sturman injector. The bottom of the injector was bolted to the mount, which could translate further into the box so the injector position could be changed. The mount could also move up or down, allowing the tip of the injector to be moved in two dimensions, only being constrained in that it needed to be along the vertical plane bisecting the injector side of the box. The experimental setup of the Sturman injector is shown in Figure 17.

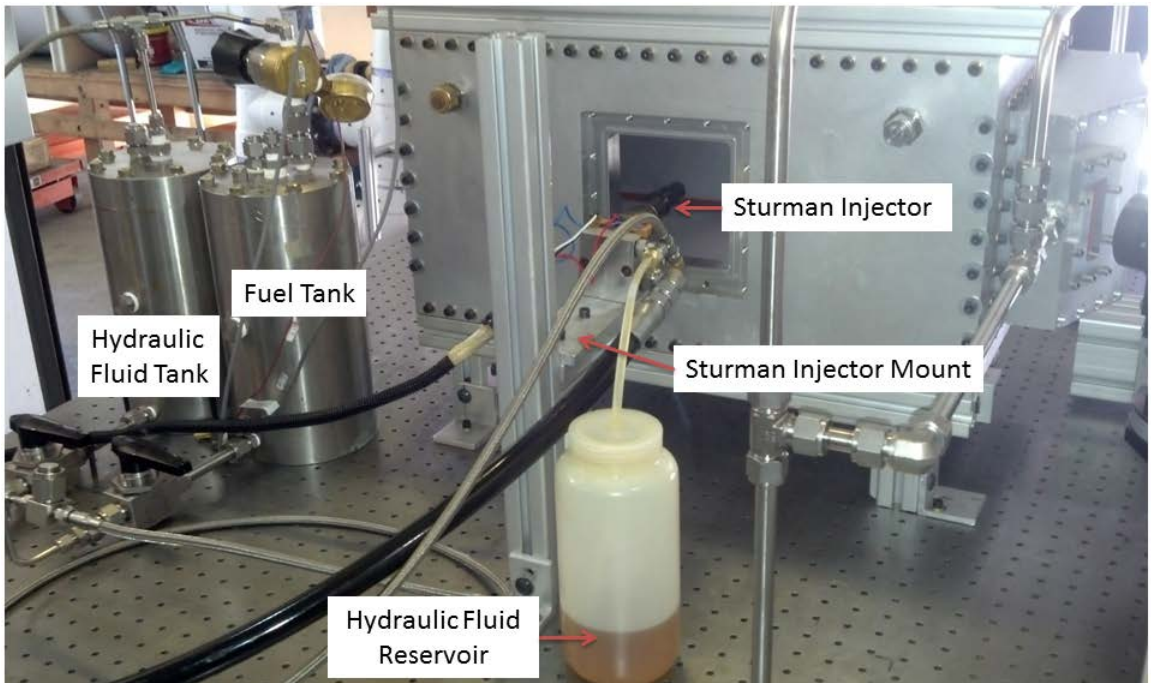

Figure 17. Sturman Injector Particle Sizing Setup

The Sturman injector was hydraulically controlled and electrically powered, using a 3000 psi nitrogen gas tank to pressurize the hydraulic fluid and regulated to 200 psig for the fuel. The hydraulic reservoir shown in Figure 17 collected the hydraulic fluid that was spilled out of the injector once it had been used.

b. Yanmar Injector

A separate square flange was designed to adapt the Yanmar injector to the particle sizing chamber. This was because most of the injector needed to be inside the chamber. The laser system only takes data at a very specific location and since the injector was small, most of it had to be inside the box in order for the spray to cross that point. This flange was designed so the back of the injector fit into a slot in the flange. A bolt that screwed into the back of the injector held it in place. An exploded view of the square flange adapter assembly is shown in Figure 18.

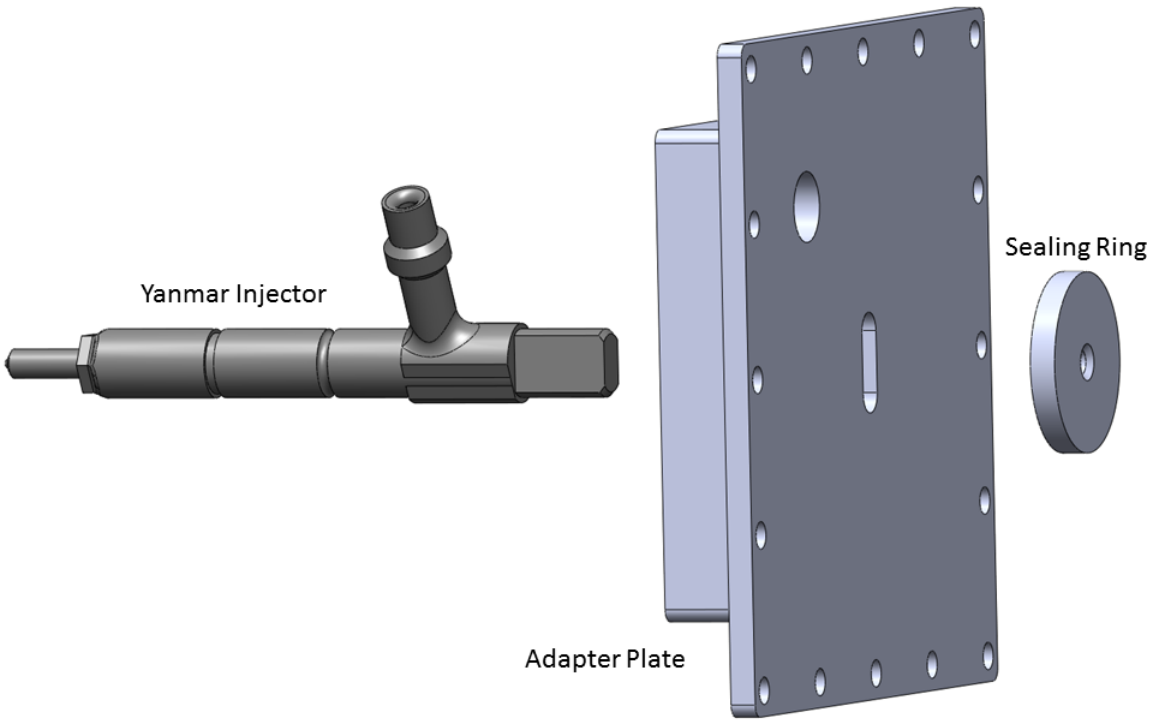

Figure 18. Yanmar Injector Particle Sizing Adapter

The sealing ring shown in Figure 18 was designed with an O-ring groove on the underside to seal the box if testing called for the chamber to be internally pressurized. The circular fitting in the flange was fabricated to bring fuel to the inlet of the injector, which was inside the chamber.

c. EMD Injector

The adapter piece for the EMD injector was designed to work in both the combustion chamber and the particle sizing chamber. This EMD adapter is shown in Figure 13. Since the injector is approximately 12 inches in length the original adapter was designed with both experimental setups in mind. The adapter was designed for the injector to penetrate five inches into the chamber, very close to the ideal position for the PDPA laser to capture the spray particle size. Beyond this only a small adjustment of the laser system would be required in order to collect useful data. The only difference between the EMD injector setup in this chamber and in the combustion chamber was that the flange the adapter was designed to mate with was square rather than circular.

3. PDPA Laser System

The PDPA laser system, made by Dantec Dynamics, is comprised of a laser and a laser detector, shown in Figure 16. The system uses two crossed laser beams to measure the size of the particles of the spray. There is a small volume where the two beams cross through which particles occasionally pass. Light from these two laser beams is scattered off of the particles that pass through this volume in all directions, including toward the detector. The box labeled “PDPA Laser Detector” in Figure 16 contains two light detectors that receive the scattered light from the spray particles that pass through the laser crossing. Both of these detectors receive light of the same frequency but of different phases because of the difference in location of the receivers. The magnitude of the difference between the two phases can be used to determine the size of the particle which scattered the Doppler burst [26]. In this experiment, a backward scattering angle of 148 degrees was used and the system was capable of giving particle sizes up to 332 micrometers.

4. Control System

The control system for the particle sizing chamber was used to actuate the injectors as well as to record the particle size data. Testing was only completed with the Sturman injector due to time restrictions. A pulse generator was used to create 10 ms injection pulses at a frequency of 10 Hz for 30 seconds. The extended time allowed the

PDPA system to find larger numbers of particles and increase the number of data points the experiments generated. The BSA Flow Software provided by Dantec Dynamics collected the particle size data as the test was conducted and output a text file with the data.

THIS PAGE INTENTIONALLY LEFT BLANK

III. RESULTS AND ANALYSIS

This section describes the particle sizing results along with the initial combustion chamber calibration.

A. PARTICLE SIZING CHAMBER

Three different injectors had adapters fabricated for use in the particle sizing chamber. However, due to fabrication delays and time restrictions, only the Sturman injector was able to be tested. The mount for the Sturman injector allowed its position to be adjusted with respect to the injector orifice. This flexibility was used to locate the position where the injection spray best intersected with the laser measurement volume, providing a large number of data points when testing. The optimal location determined for the Sturman injector was for the laser to be 1.25 inches radially from the centerline of the injector and 3.375 inches from the tip axially. Many injectors have several individual sprays generated from multiple small holes in the injector, but the Sturman injector had a conical spray pattern, thereby simplifying the positioning for the spray characterization.

Testing was done for three different fuels: conventional F76 diesel fuel used by the U.S. Navy, hydrotreated renewable diesel fuel (HRD) derived from algae, and a 50/50 blend of F76 and HRD. The injection event lasted for a maximum of 10 ms with a frequency of 10 Hz for 30 seconds. For each of the fuels the fuel pressure was held constant at 200 psi and the hydraulic fluid pressure was varied from 600 to 1600 psi in 200 psi increments. The Sturman injector has a six to one pressure ratio, resulting in a range of fuel pressures at the tip of the injector from 3600 to 9600 psi. Each test point was repeated until at least 450 validated data points were collected. Dantec Dynamics' BSA Flow Software output a list of the determined particle sizes as well as a histogram. The list was exported to a text file that was used in conjunction with a MATLAB code that processed the data for the calculation of characteristic diameters. This code can be found in Appendix C.

Multiple tests were performed at the same conditions and MATLAB was used to combine the data sets into one larger set. The code eliminated any data points above 332

micrometers which the aperture lens was incapable of detecting. “Mask A,” the aperture lens used in this testing, is discussed in Dantec Dynamics’ reference manual [26]. The resolved particle diameters were sorted into 50 diameter bins, and bins with only one or two data points were zeroed to remove outliers. The remaining bins were used to calculate the average diameter of the particles as well as the Sauter Mean Diameter (SMD).

Sauter Mean Diameter is a characteristic diameter that relates the ratio of the volume to surface area of the particles contained in a spray. SMD represents the diameter of a spray particle with the same ratio of volume to surface area as the spray as a whole and is calculated using the equation:

$$SMD = \frac{\sum_{i=1}^{\#bins} n_i D_i^3}{\sum_{i=1}^{\#bins} n_i D_i^2} \tag{2}$$

In the SMD equation n_i represents the number of data points for bin *i* of diameter D_i. A small SMD is ideal for combustion because there is more surface area available to support combustion for a given volume of fuel.

The code exports the average diameter of the particles, the SMD, and bin sizes and number of data points in each bin, normalizing the number of data points by dividing each by the maximum number of data points contained in a particular bin, meaning that the largest bin has a value of 1. These outputs were then plotted, comparing the three different fuels used. Figure 19 shows a typical histogram plot.

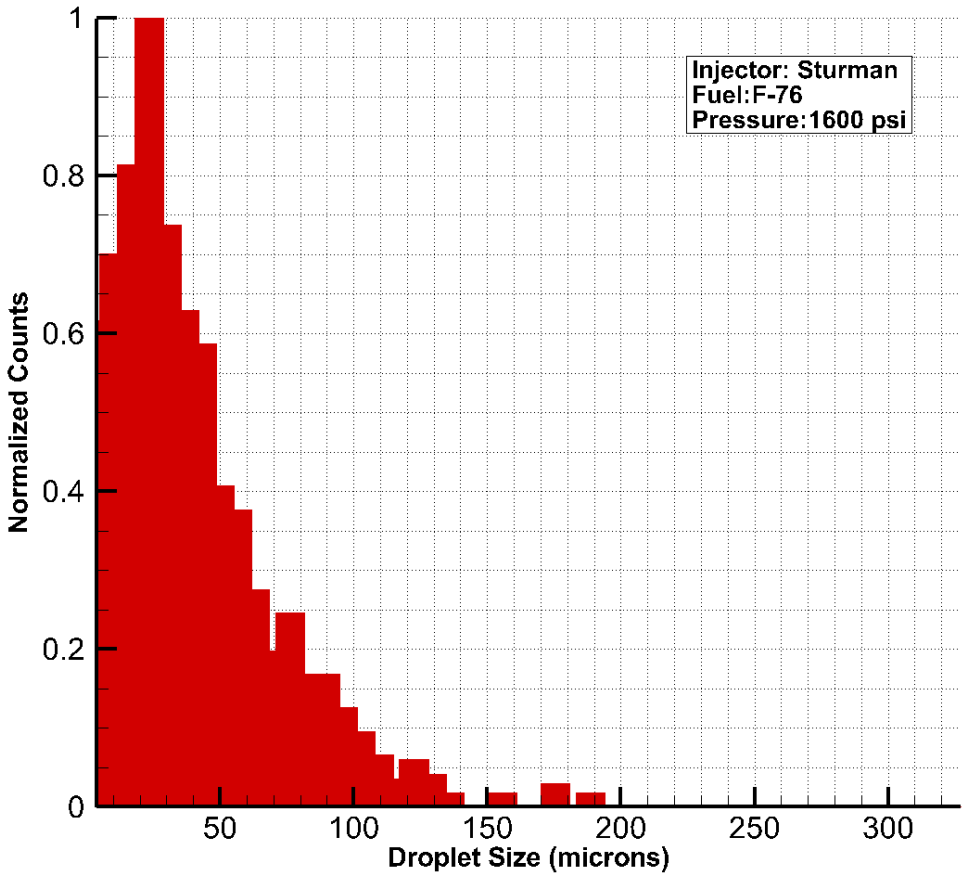

Figure 19. Typical Histogram. Taken from 1600 psi data point for F-76

A linear curve fit of the Sauter Mean Diameter was plotted as a function of hydraulic fluid pressure and can be seen in Figure 20. As expected, for all of the fuels the SMD decreases with increasing hydraulic pressure. This means that the average ratio of the surface area to the volume is increasing, which supports higher aggregate combustion rates. Figure 20 shows that as the amount of HRD in the fuel increases, the SMD also increases.

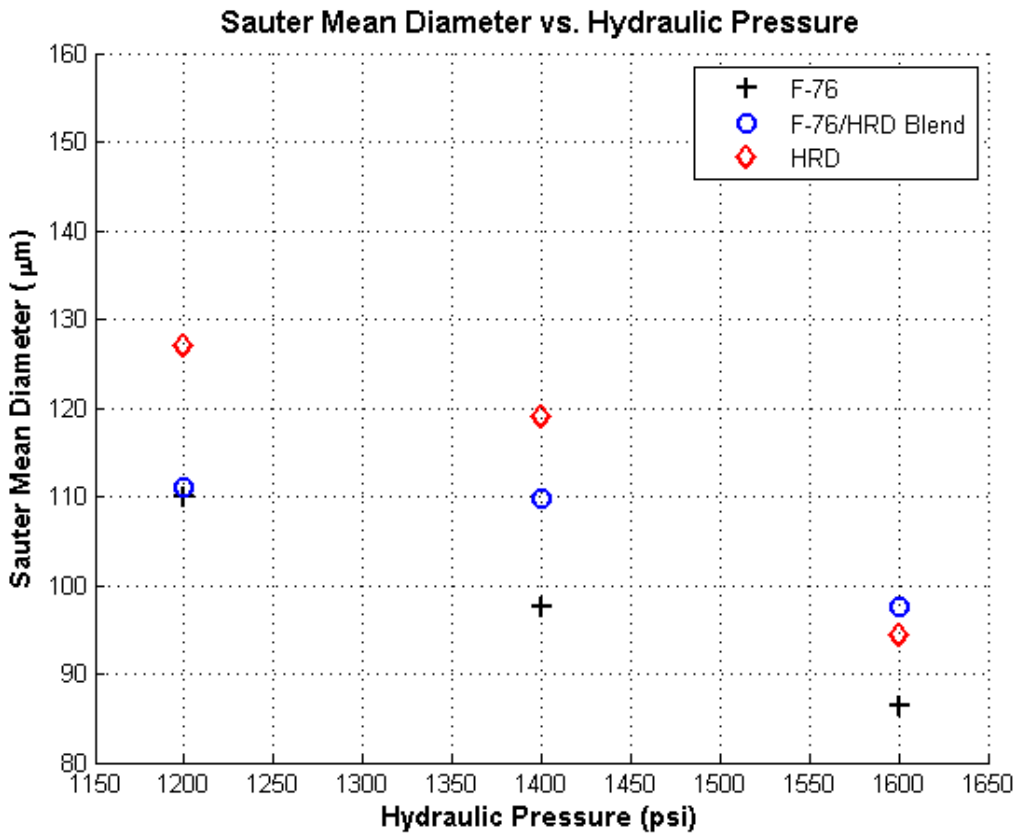

Figure 20. Sauter Mean Diameter as a Function of Hydraulic Pressure

B. COMBUSTION CHAMBER CALIBRATION

The combustion chamber was calibrated by injecting air into the system without injecting fuel to determine the final temperatures and pressures inside the combustion chamber milliseconds before fuel injection would occur. Figure 21 shows a typical pressure and temperature trace from the high speed and low speed transducers as well as an Omega type-K 1/16 inch thermocouple with an exposed junction located 1.5 inches inside the chamber. The high-speed Kistler transducer produced the pressure trace that spikes initially and then quickly trails off. This is due to the piezoelectric transducer response for a short time constant, which causes the charge (and associated voltage) to fall quickly under steady-state conditions. Although the initial overpressure read by both transducers was caused by transient gas dynamics, the lower frequency response pressure transducer eventually rises and captures the effective final pressures after a few tenths of

a second. The Kistler high-speed transducer will continue to be used to show the rate at which the mixing of the two gases occurs and to capture future pressure rises during combustion events.

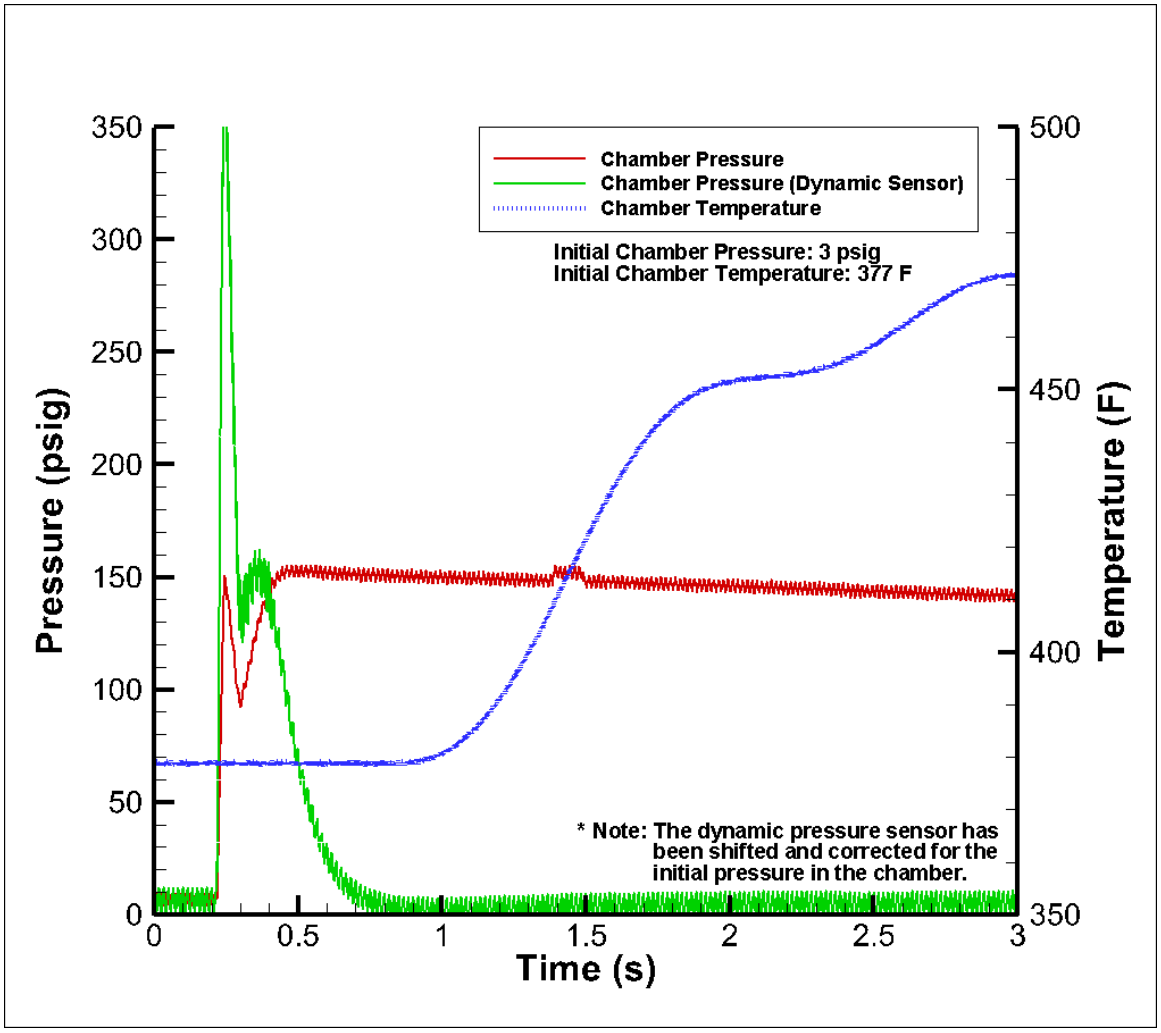

Figure 21. Pressure and Temperature Response in Combustion Chamber

The pressure traces in Figure 21 show that the fill process is complete in 200 ms. However, the temperature rise lags behind the pressure rise due to the low frequency response of conventional thermocouples. It was believed that the actual gas temperature rise was more similar to the pressure behavior.

An Excel spreadsheet was created that predicted the final chamber temperature and pressure for the given initial condition and assumed the constant-volume and adiabatic mixing of two gases. The calculations assumed constant internal energy and an average value for the specific heat at constant volume. The results of this code were compared to the measured temperature and pressure after mixing, knowing the initial pressures and temperatures in both the combustion chamber and the air tanks. Table 3 shows the different conditions that were tested and the resulting temperature and pressures after mixing, compared with the values predicted.

Initial Values				Measured Final Values		Expected Final Values	
Chamber P[psig]	Chamber T [°F]	Air Tank P [psig]	Air Tank T [°F]	P [psig]	T [°F]	P [psig]	T [°F]
58	307	858	900	194	382	250	710
17	309	880	902	151	407	224	803
0	314	900	901	141	418	216	852
4	353	835	992	127	448	204	920
1	377	944	899	157	472	228	858

Table 3. Combustor Calibration Data Points

Table 3 shows that the temperatures measured by the thermocouple fall well short of the expected temperatures calculated based on the adiabatic mixing assumption. A potential cause of this discrepancy was believed to be that not all of the tubing was well insulated and heated. Because of this, there would naturally be heat transfer into portions of the plumbing, thereby violating the adiabatic assumption. Additionally, the thermocouple location within the chamber could register temperatures lower than the bulk temperature in the chamber or, is simply too slow to respond.

In order to increase the temperature in the chamber, the ability to conduct an ethylene/air pre-burn with make-up oxygen was added. This system was designed to fill the chamber with ethylene gas and ignite it using a spark plug, raising the temperature and pressure in the chamber to desired values so fuel could be injected and would then auto-ignite due to the elevated temperatures and pressures in the chamber. In addition to adding a pre-burn capability, a pebble-bed heater would enable the chamber to reach the temperatures required for fuel autoignition. This would involve a tank full of ball bearings kept at high temperatures. Due to the large amount of surface area of the ball bearings, the air flowing over this pebble bed from the high pressure tanks would be heated further before entering the combustion chamber.

THIS PAGE INTENTIONALLY LEFT BLANK

IV. SUMMARY AND CONCLUSIONS

A combustion chamber capable of high-pressure and high-temperature testing was designed, built, and calibrated for the evaluation of conventional and alternative fuels under consideration for diesel engines. This chamber was created to withstand pressures of 3000 psi at temperatures up to 500 degrees Fahrenheit and provide the ability to dynamically inject clean heated air at temperatures up to 900 degrees Fahrenheit or perform an ethylene/air preburn with make-up oxygen to produce the desired initial conditions. By utilizing a dynamic fill option, varying levels of CO, CO_2, and H_2O can be prescribed during the ignition delay testing to simulate varying levels of residual exhaust products in actual engines.

Three Navy-relevant fuel injectors were acquired and interfacing hardware was manufactured for the characterization of the sprays from those injectors. Particle sizing data was acquired for a Sturman Industries research injector over a tip fuel pressure range of 3,600-9,600 psi providing average particle diameter and Sauter Mean Diameter values. Although only the Sturman injector was evaluated due to time constraints, the results showed decreasing Sauter Mean Diameters with increasing fuel pressure, producing values near 90 microns at the highest fuel pressure evaluated. Although F-76 produced generally smaller particle sizes (approximately 10-20%) than the HRD fuel, additional data is required before this trend could be conclusively validated.

During calibration and checkout testing of the combustion chamber, the temperatures reached inside the chamber were significantly lower than the values calculated assuming adiabatic mixing. This was believed to be due to excessive heat loss in the tubing between the heated, high pressure air tanks and the combustion chamber. These losses were evident across the entire span of operating range, but the discrepancy was greater at higher temperatures where greater temperature differences existed. Although conditions sufficient for ignition were not obtained for the dynamic clean air injection events, solutions were identified and are being implemented that will allow the chamber to reach the desired temperatures.

THIS PAGE INTENTIONALLY LEFT BLANK

V. FUTURE WORK

The particle size testing will be continued using the same fuels and different injectors, including those made by Yanmar and EMD, as well as a Caterpillar Inc. injector, listed in Table 1.

The calibration of the combustion chamber will be completed by improving the heat transfer of the dynamic air delivery system. One way this can be done is by using higher temperature heat tape on the tubing, preventing much of the unnecessary heat loss from the system. A second method that may increase the post-mixing temperature of the air in the combustion chamber just before injection is using a pebble bed heater using extremely high-temperature ball bearings, thereby providing a temperature boost immediately before entering the chamber.

With the calibration of the combustion chamber complete laser fluorescence will be used to determine the injection delay time so that CH* chemiluminescence and chamber pressure can be used to determine the ignition delay time of each of the fuels using the Sturman, Yanmar, and EMD injectors. Once an adapter is designed for the Caterpillar injector, injection and ignition delay times for the three fuels will be determined using that injector.

THIS PAGE INTENTIONALLY LEFT BLANK

APPENDIX A. FABRICATION DRAWINGS FOR COMBUSTION CHAMBER

A. HIGH PRESSURE CHAMBER

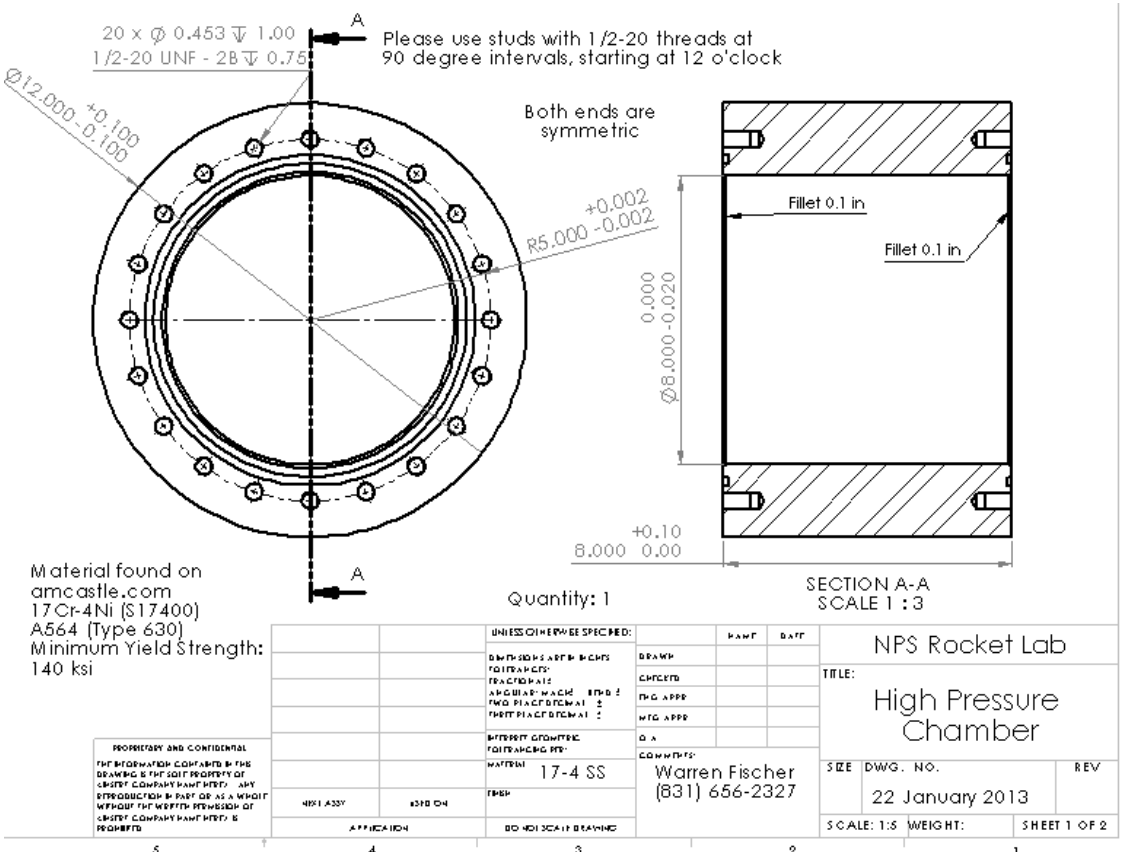

Figure 22. High Pressure Chamber Fabrication Drawing (View 1 of 2)

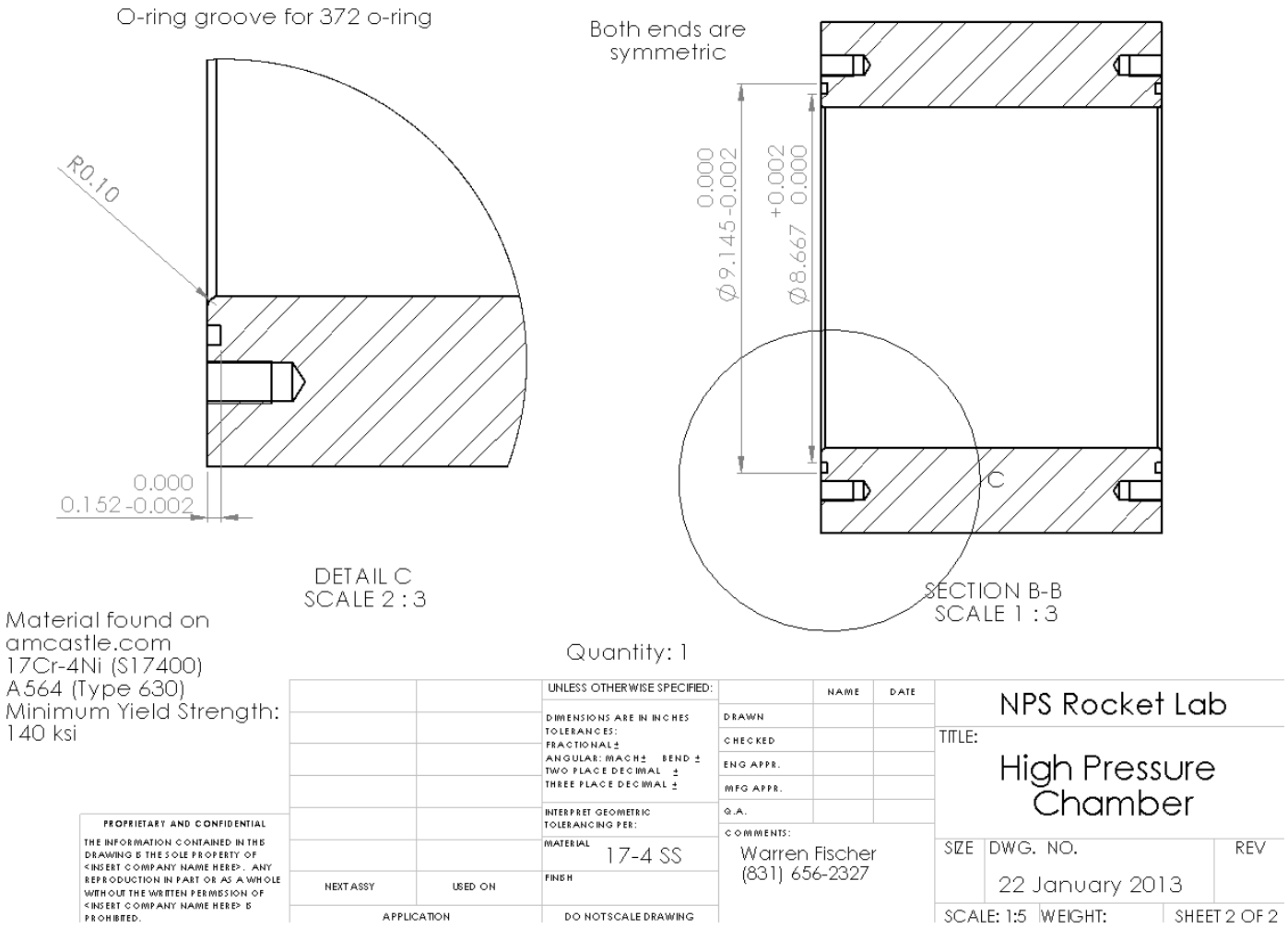

Figure 23. High Pressure Chamber Fabrication Drawing (View 2 of 2)

B. INJECTOR FLANGE

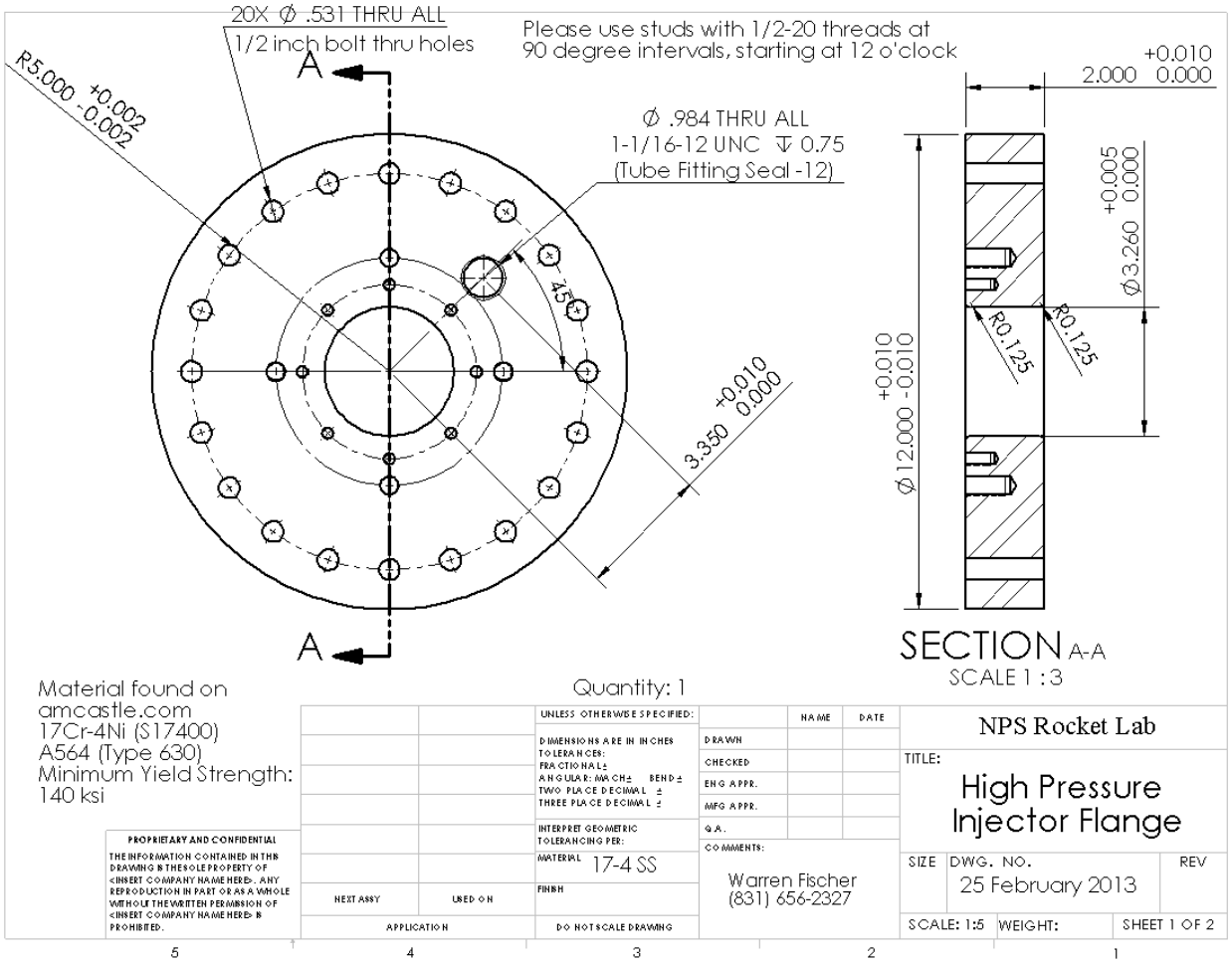

Figure 24. Injector Flange Fabrication Drawing (View 1 of 2)

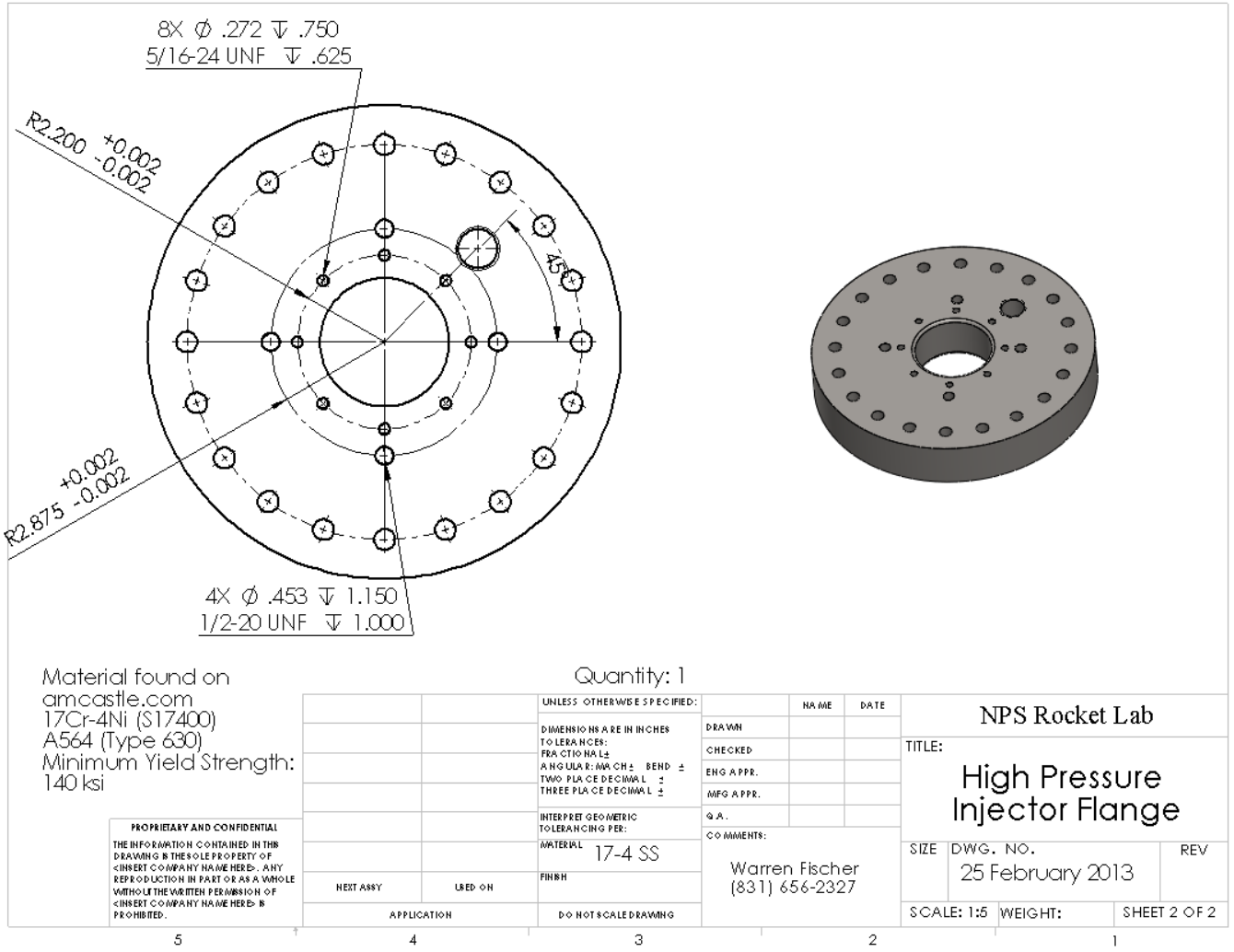

Figure 25. Injector Flange Fabrication Drawing (View 2 of 2)

C. OPTICAL WINDOW FLANGE

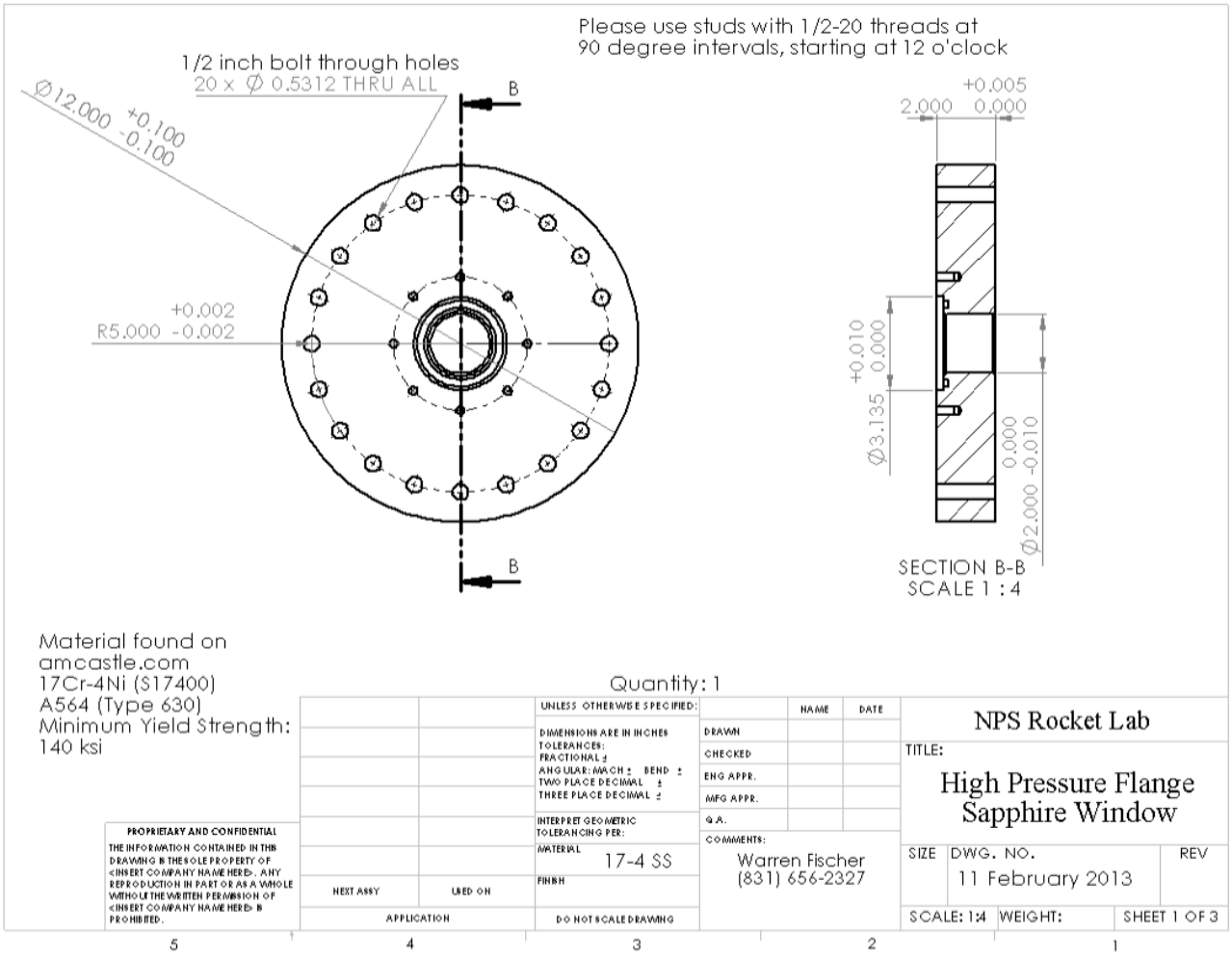

Figure 26. Optical Window Flange Fabrication Drawing (View 1 of 3)

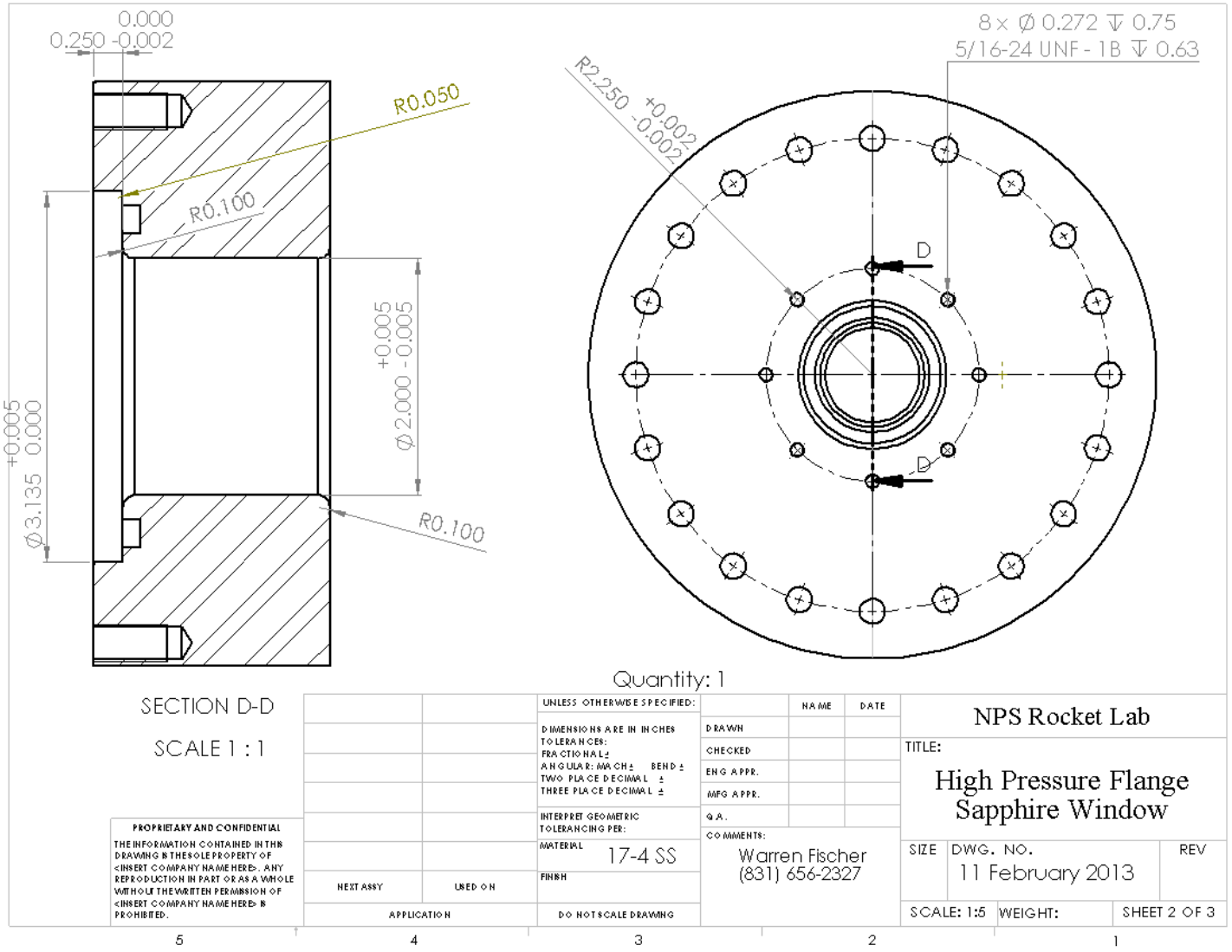

Figure 27. Optical Window Flange Fabrication Drawing (View 2 of 3)

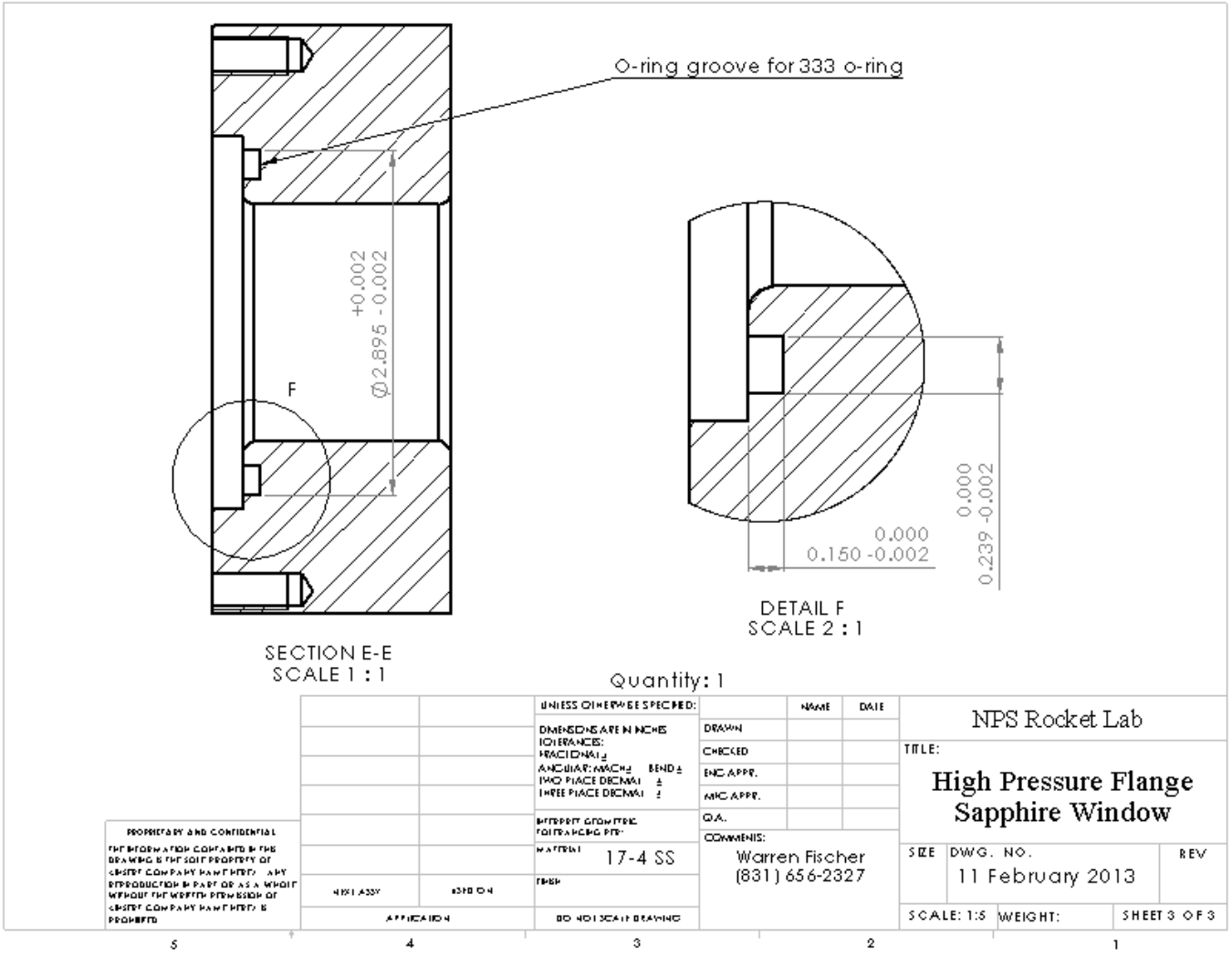

Figure 28. Optical Window Flange Fabrication Drawing (View 3 of 3)

D. OPTICAL WINDOW

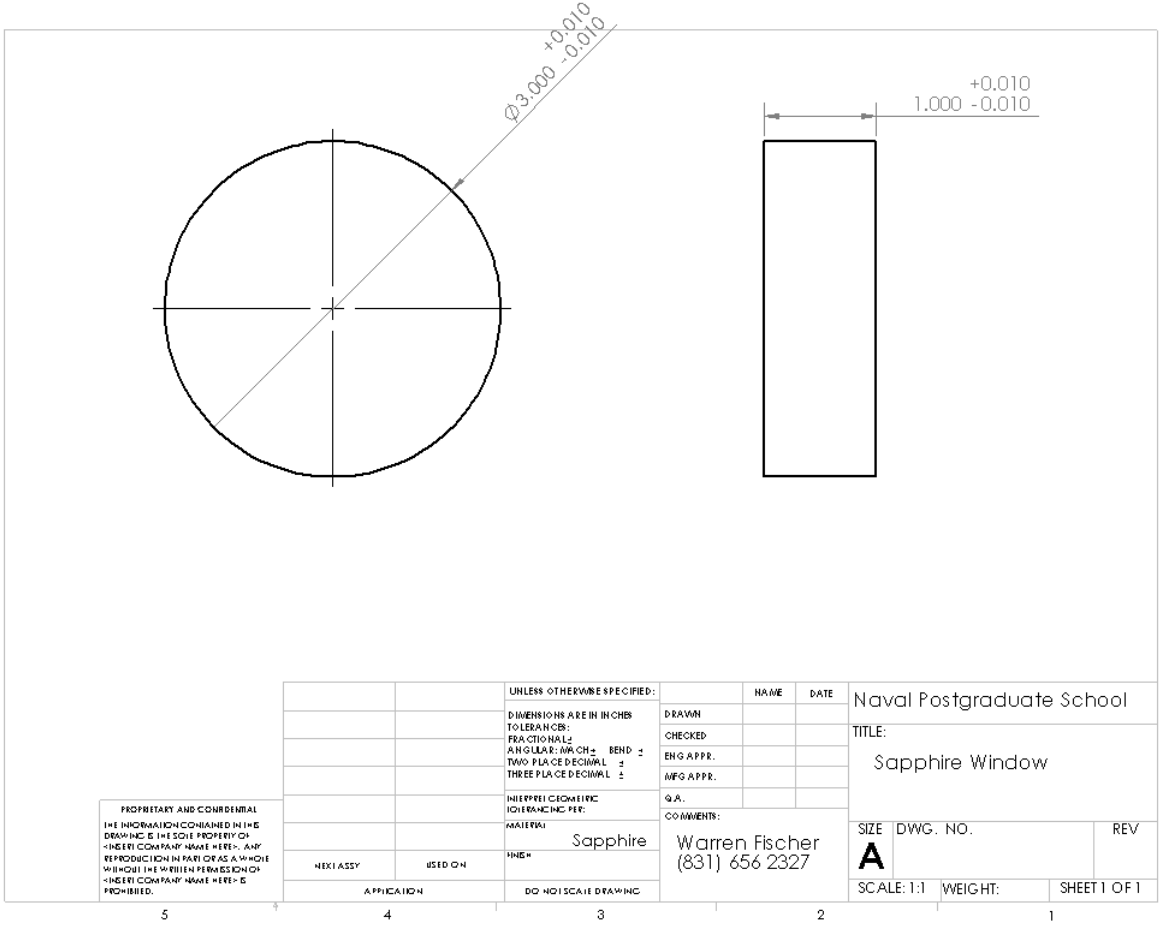

Figure 29. Optical Window Fabrication Drawing

E. OPTICAL WINDOW FRAME

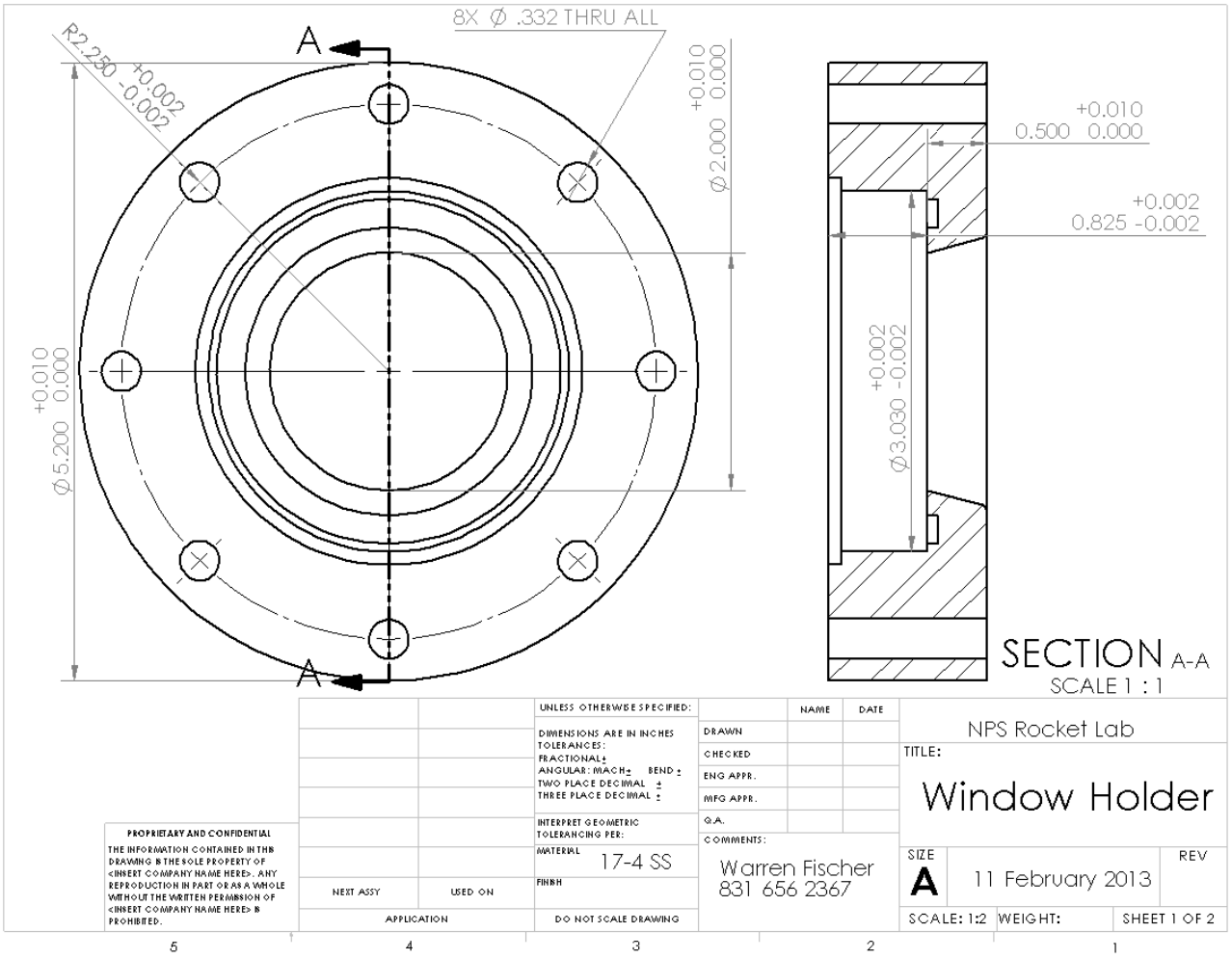

Figure 30. Optical Window Frame Fabrication Drawing (View 1 of 2)

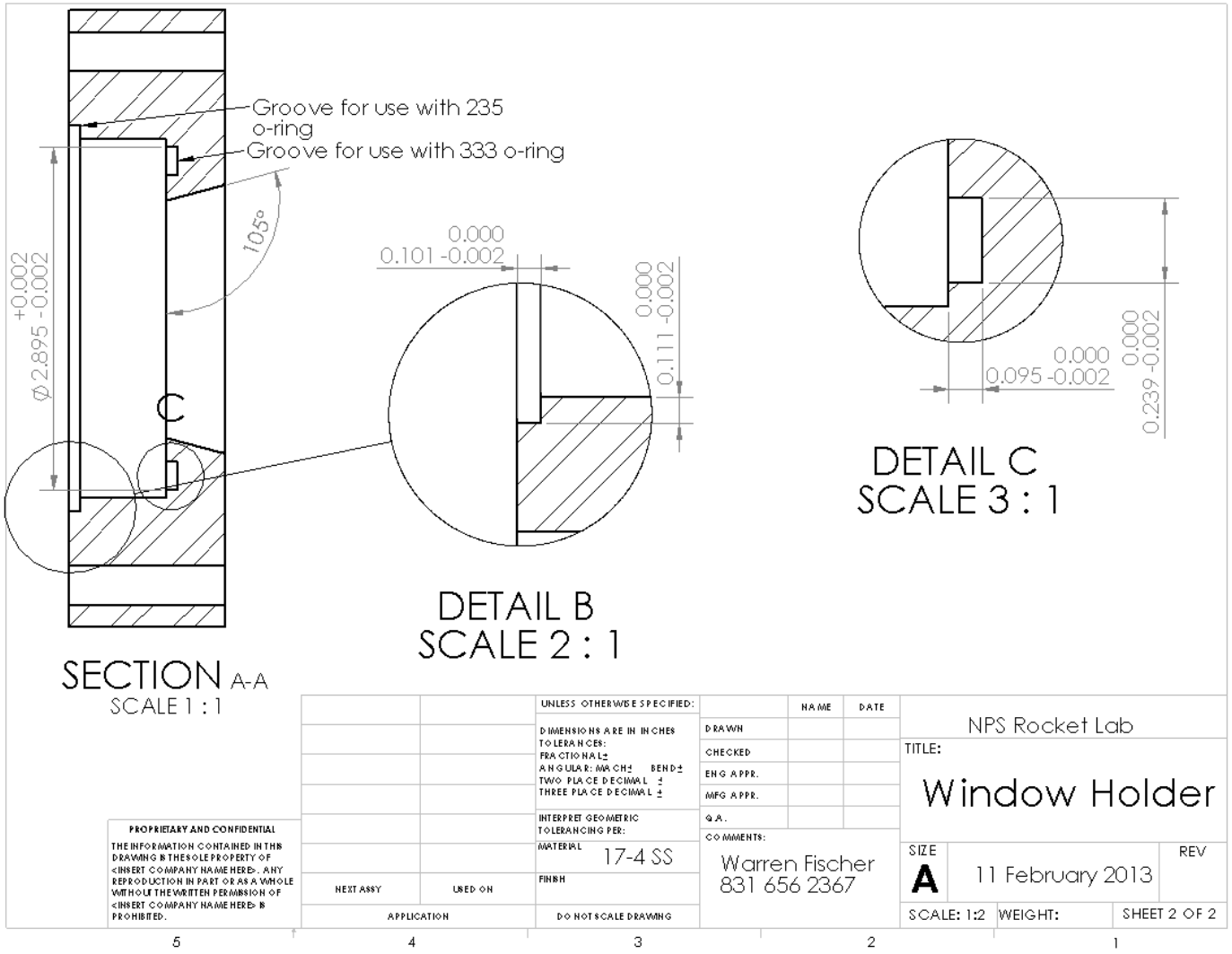

Figure 31. Optical Window Frame Fabrication Drawing (View 2 of 2)

F. STURMAN INJECTOR ADAPTER

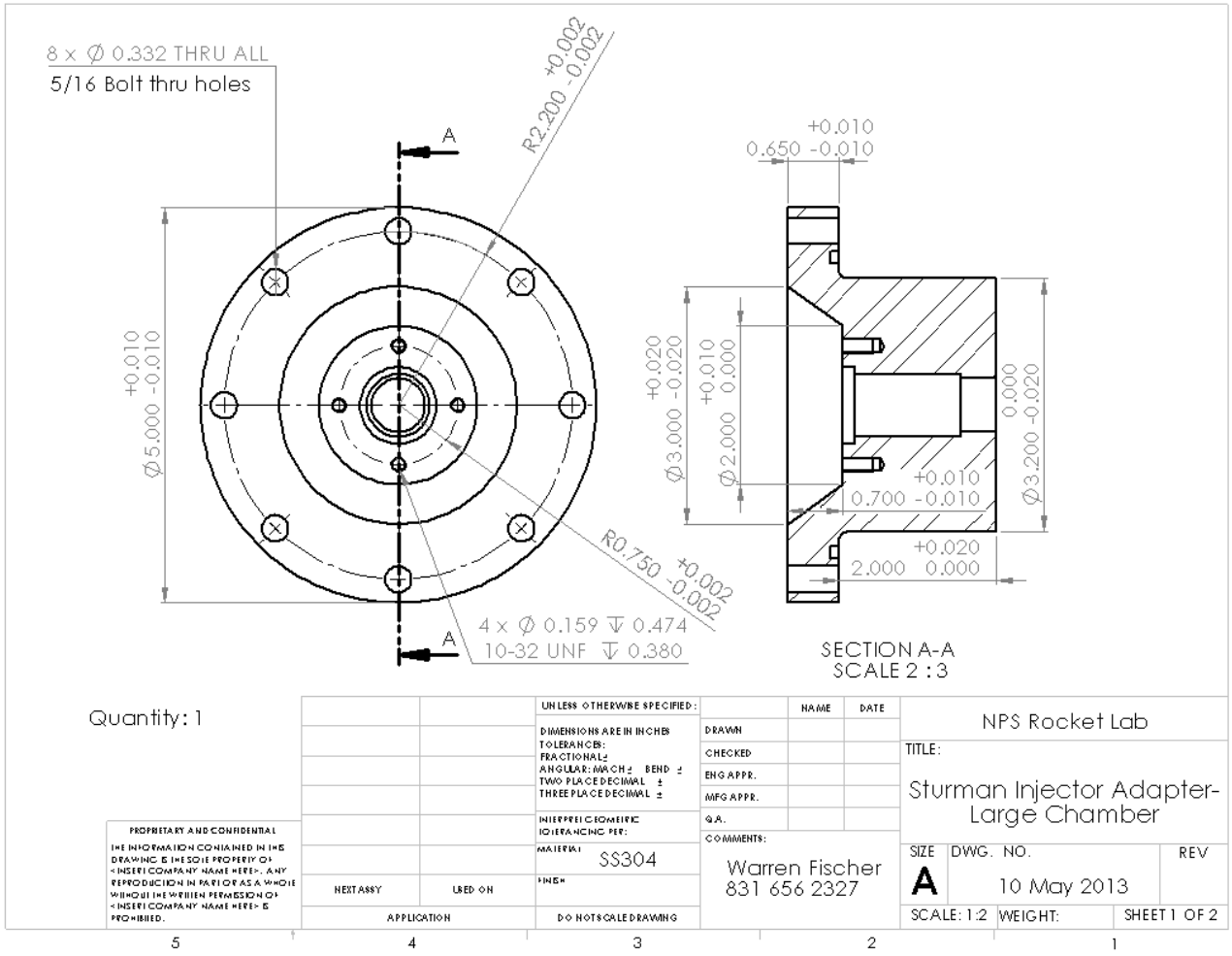

Figure 32. Sturman Injector Adapter Fabrication Drawing (Page 1 of 2)

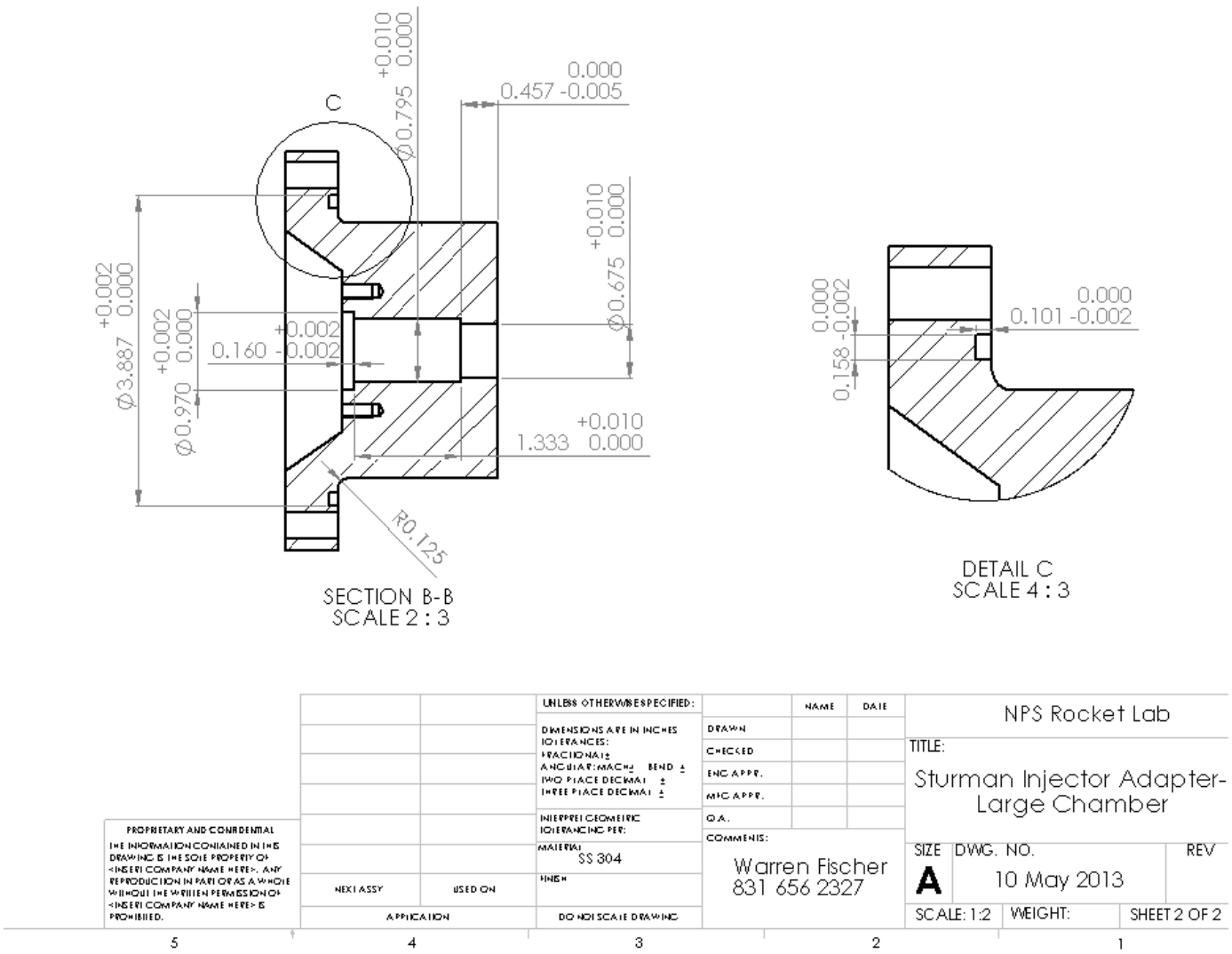

Figure 33. Sturman Injector Adapter Fabrication Drawing (Page 2 of 2)

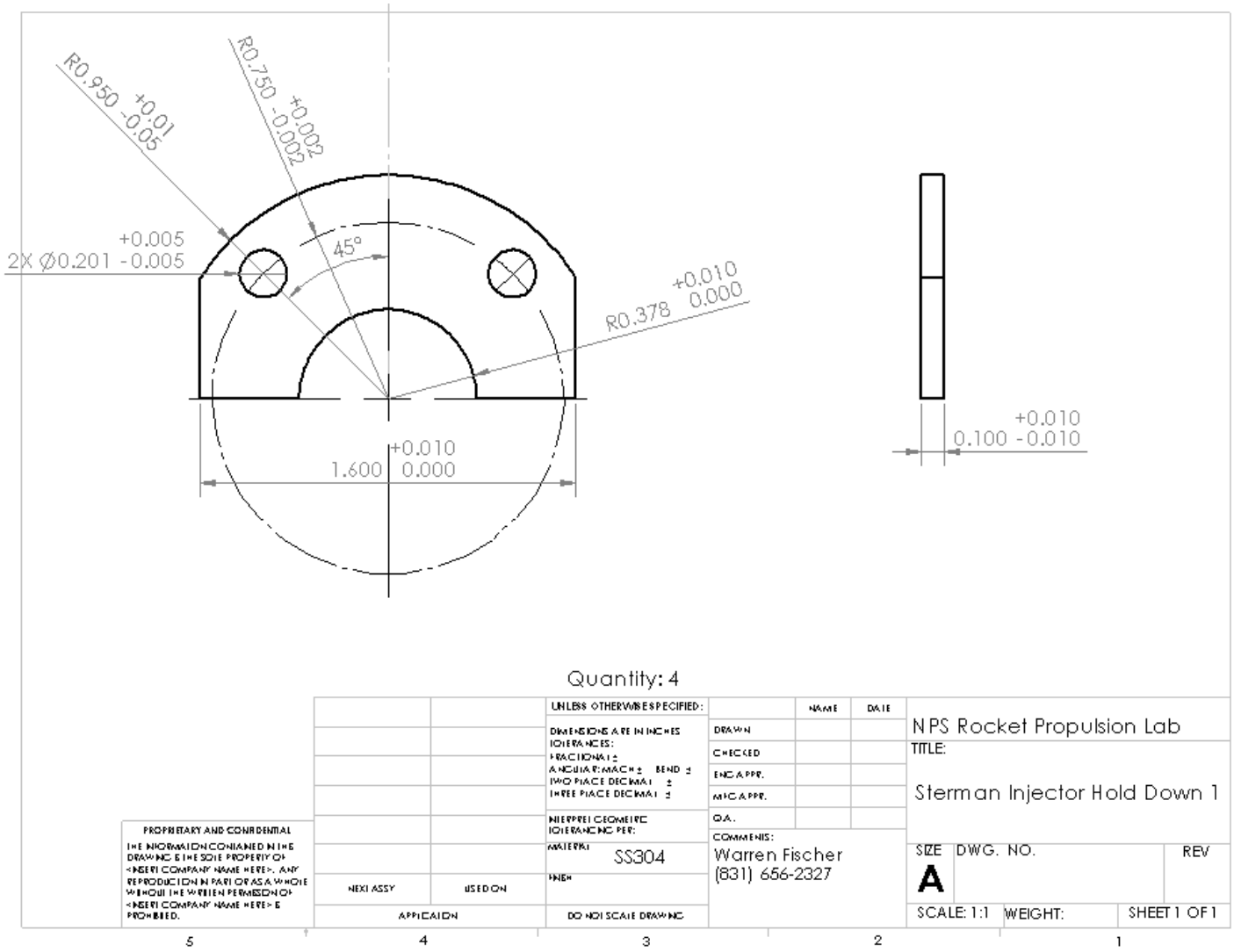

Figure 34. Sturman Injector Adapter Retainer Clip Fabrication Drawing

G. YANMAR INJECTOR ADAPTER

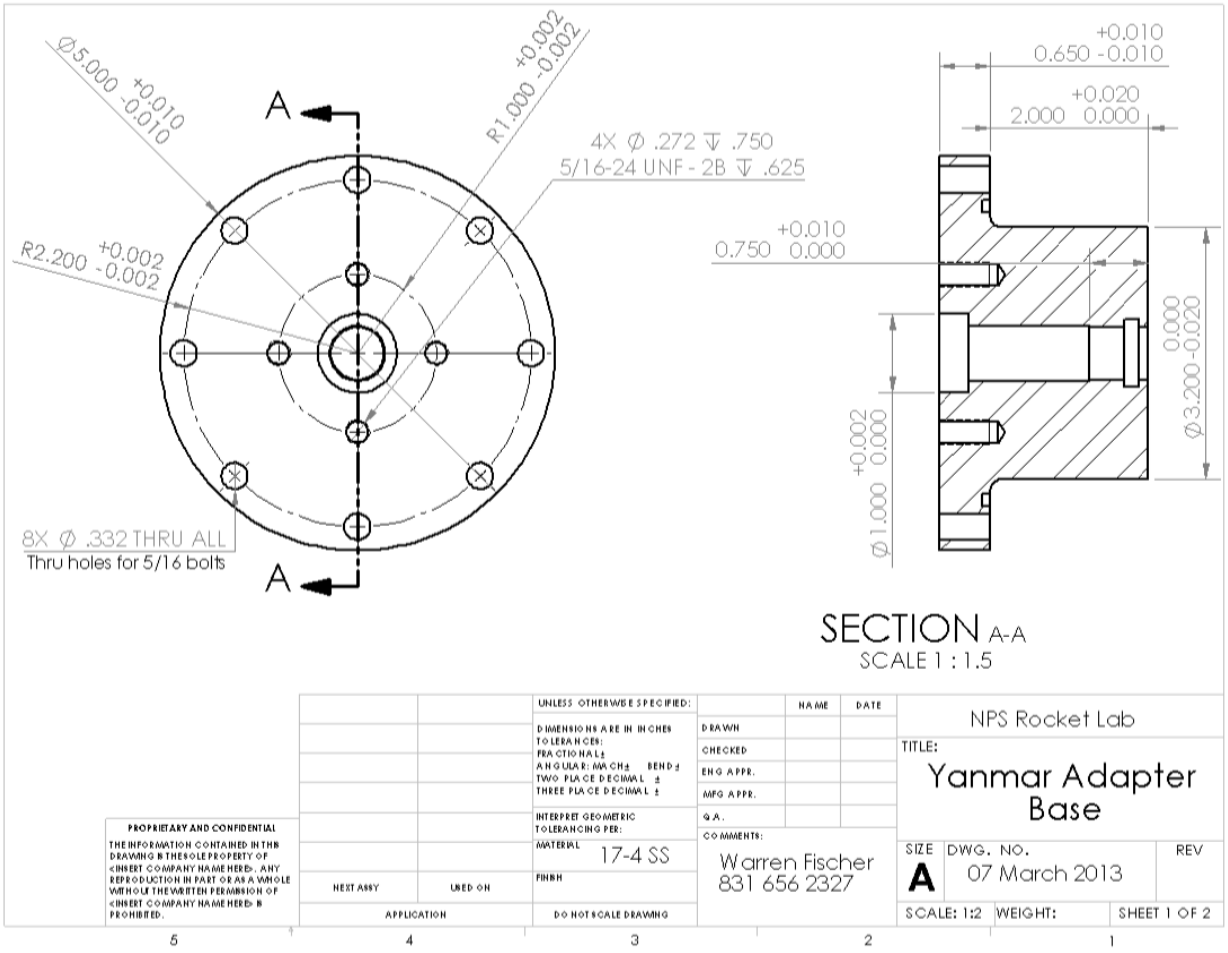

Figure 35. Yanmar Injector Adapter Fabrication Drawing (View 1 of 2)

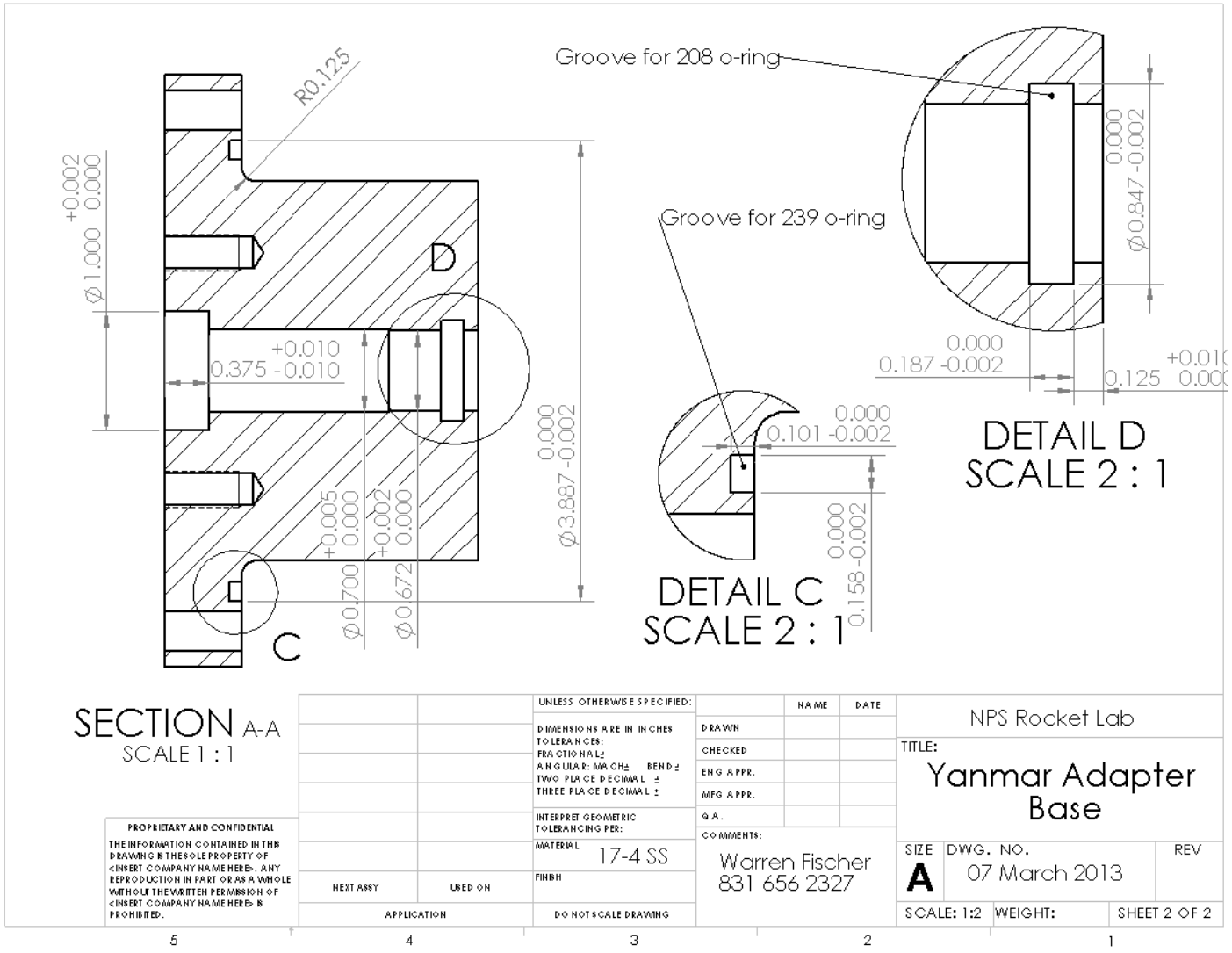

Figure 36. Yanmar Injector Adapter Fabrication Drawing (View 2 of 2)

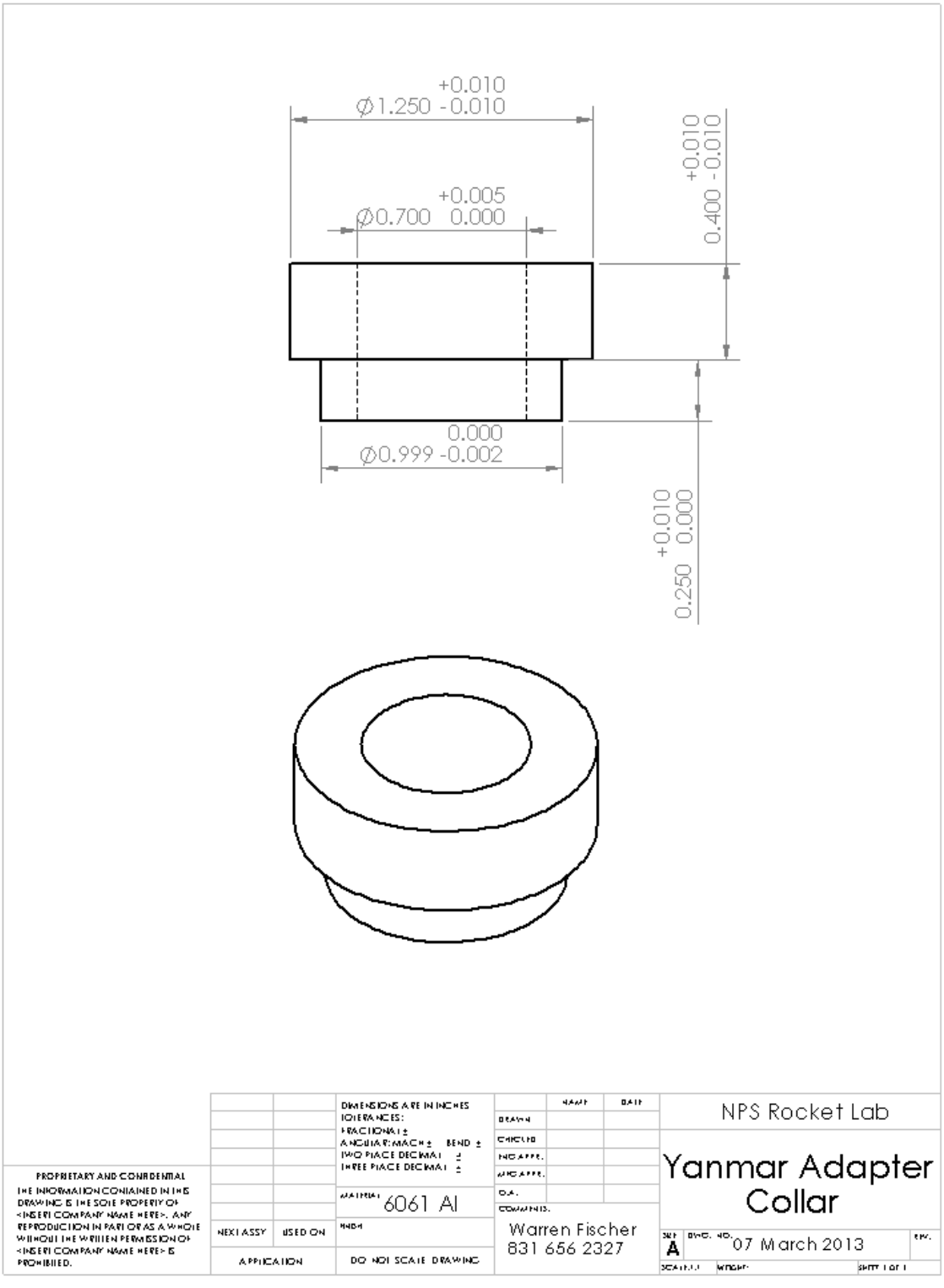

Figure 37. Yanmar Injector Adapter Collar Fabrication Drawing

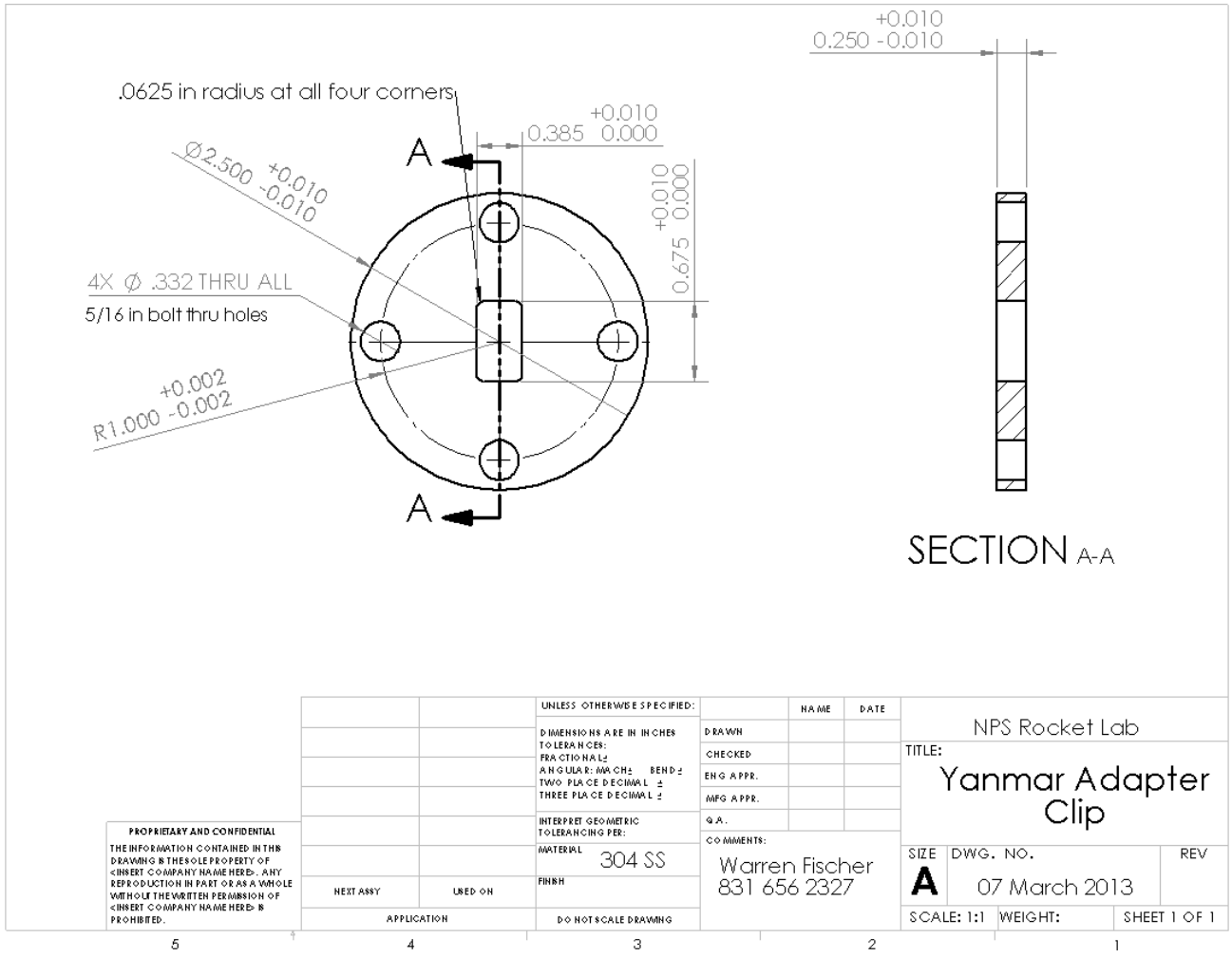

Figure 38. Yanmar Injector Adapter Clip Fabrication Drawing

H. EMD INJECTOR ADAPTER

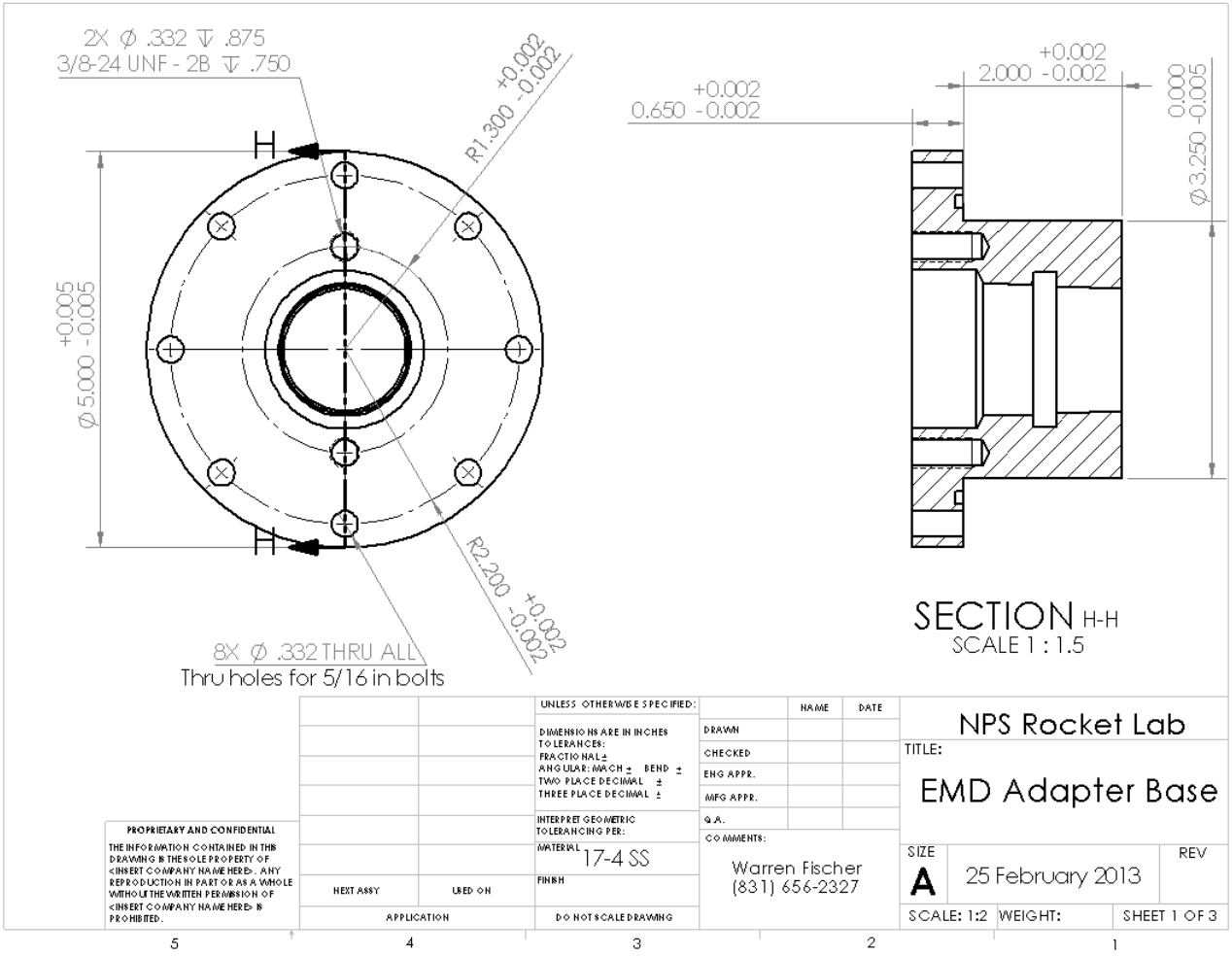

Figure 39. EMD Injector Adapter Fabrication Drawing (Page 1 of 3)

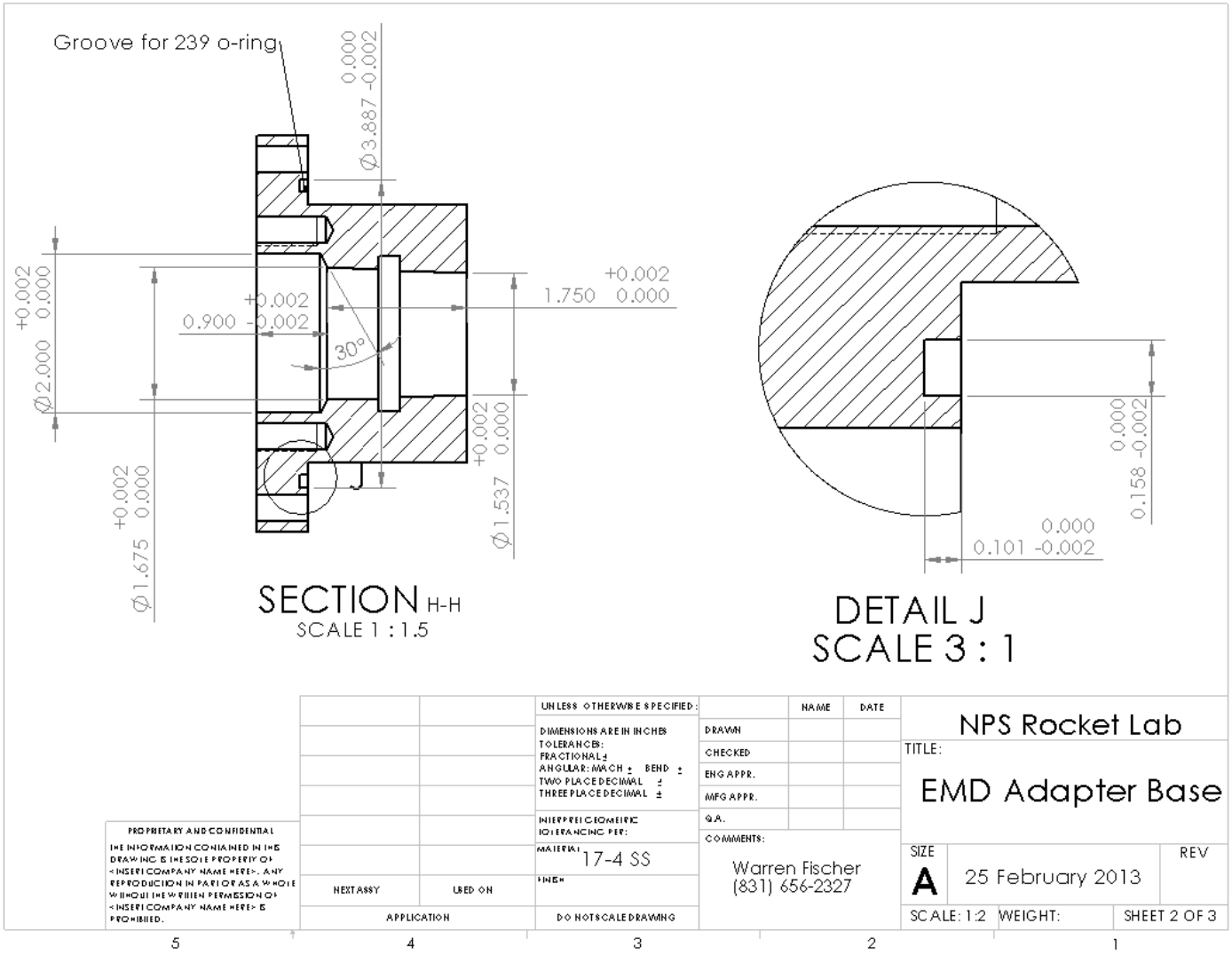

Figure 40. EMD Injector Adapter Fabrication Drawing (Page 2 of 3)

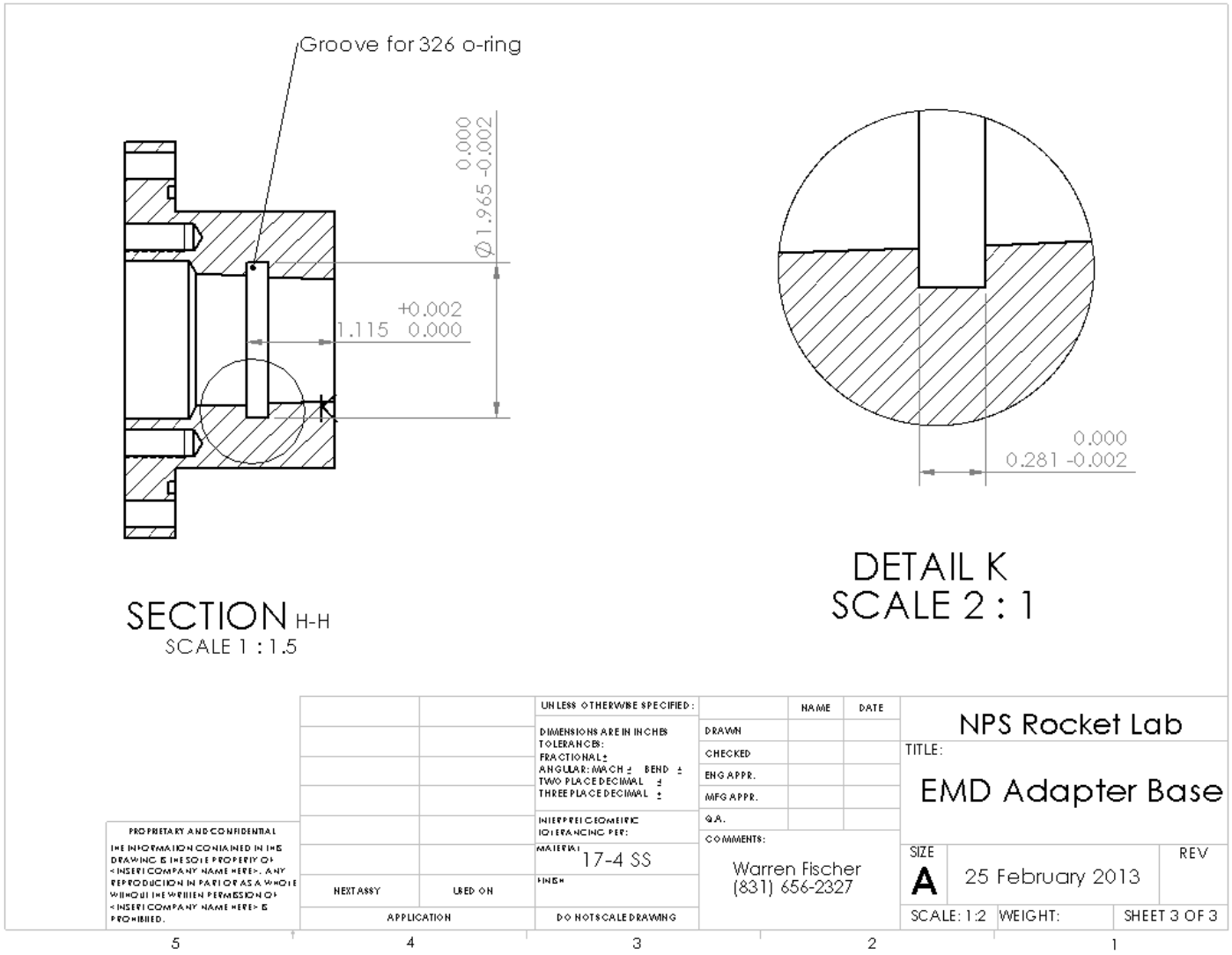

Figure 41. EMD Injector Adapter Fabrication Drawing (Page 3 of 3)

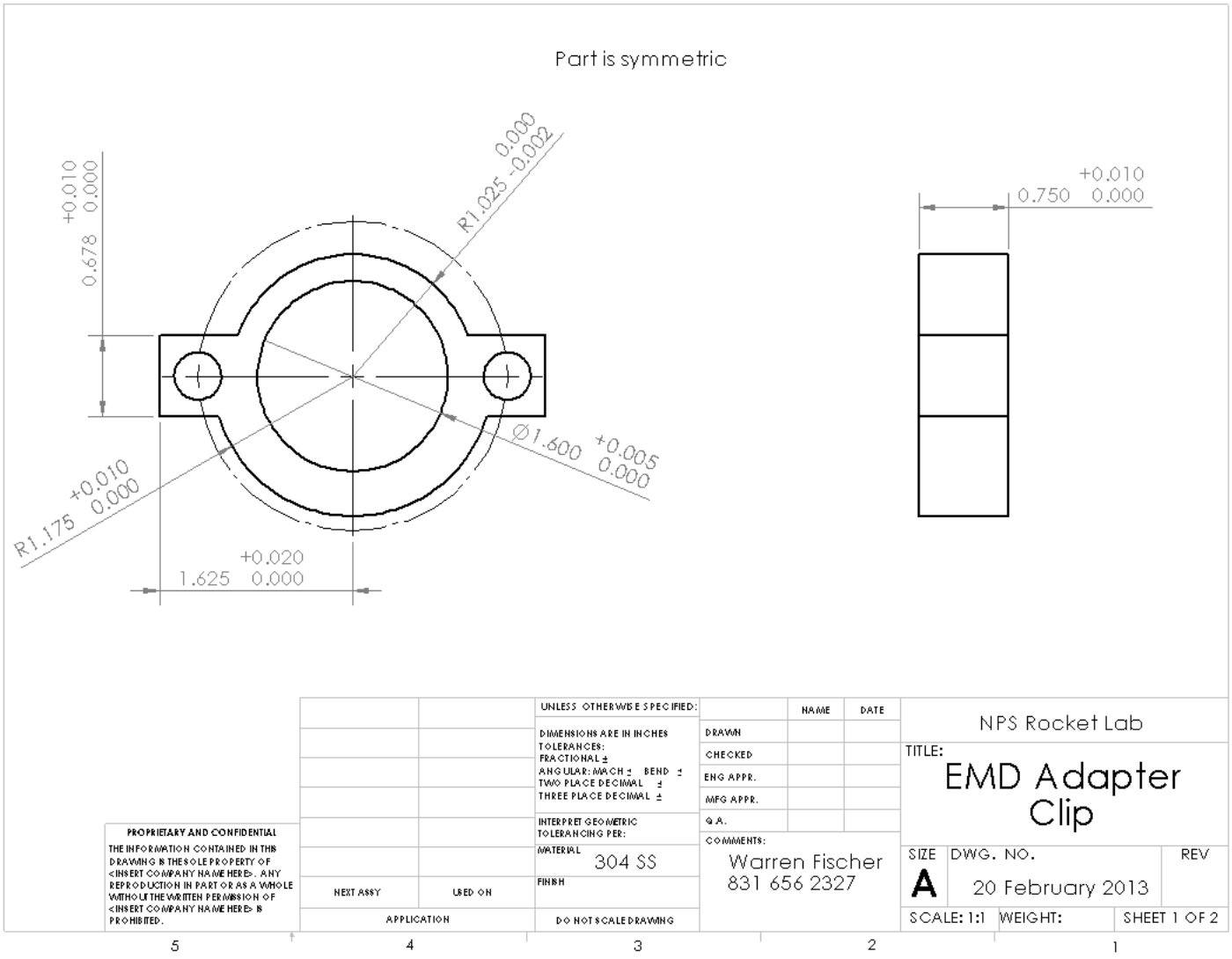

Figure 42. EMD Injector Adapter Clip Fabrication Drawing (View 1 of 2)

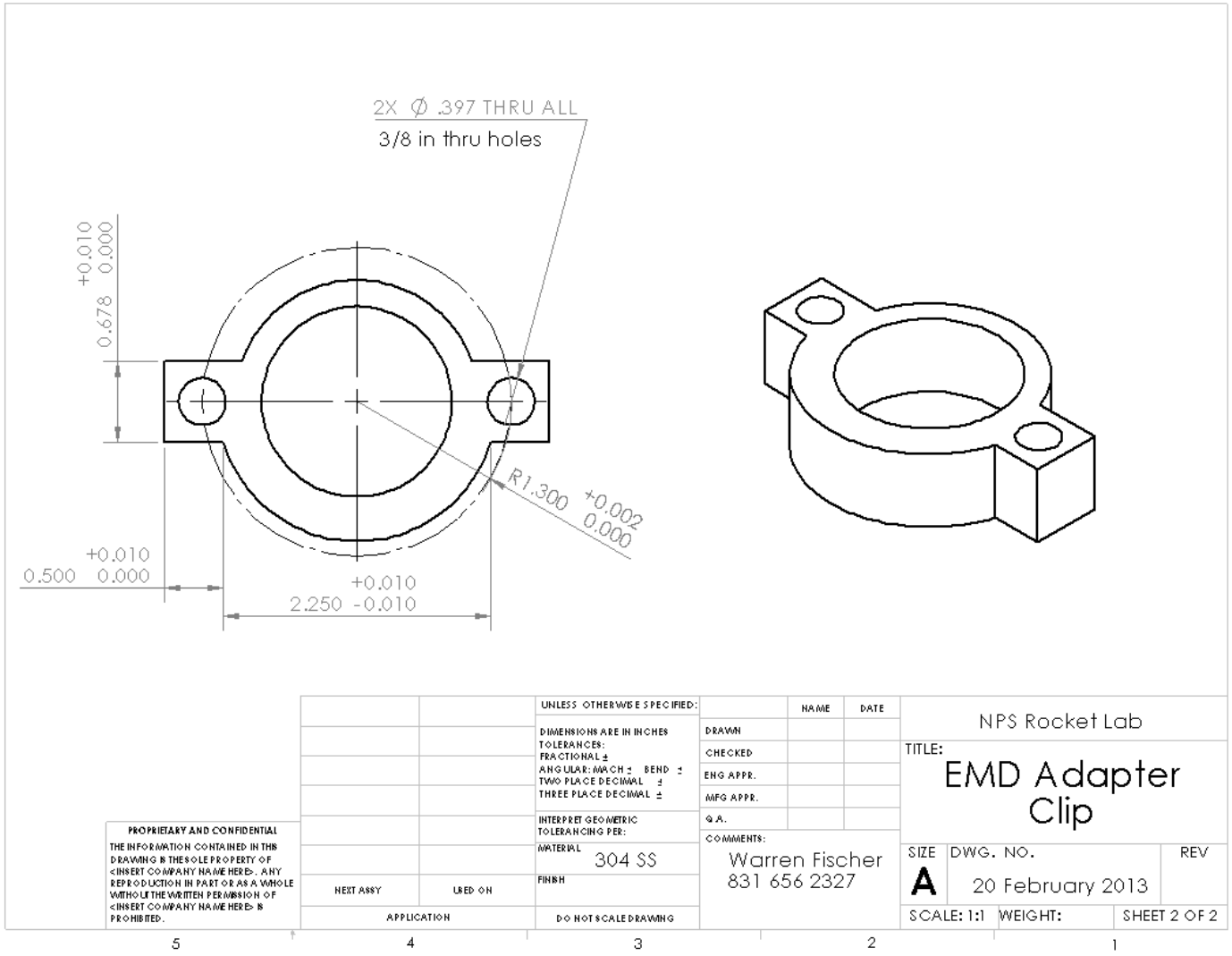

Figure 43. EMD Injector Adapter Clip Fabrication Drawing (View 2 of 2)

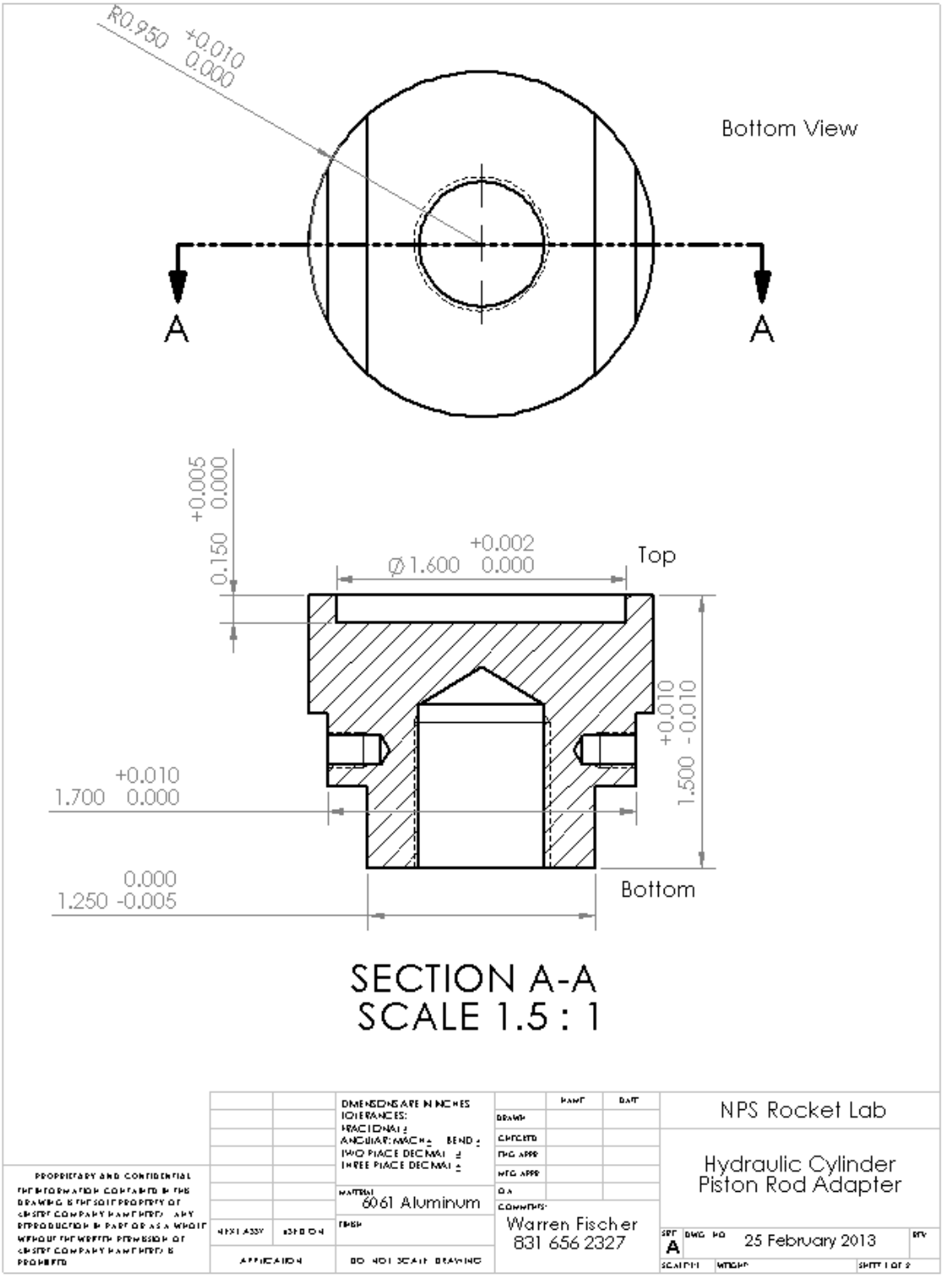

Figure 44. Fabrication Drawing for EMD Injector Adapter between Hydraulic Cylinder Output Rod and Injector Plunger (View 1 of 2)

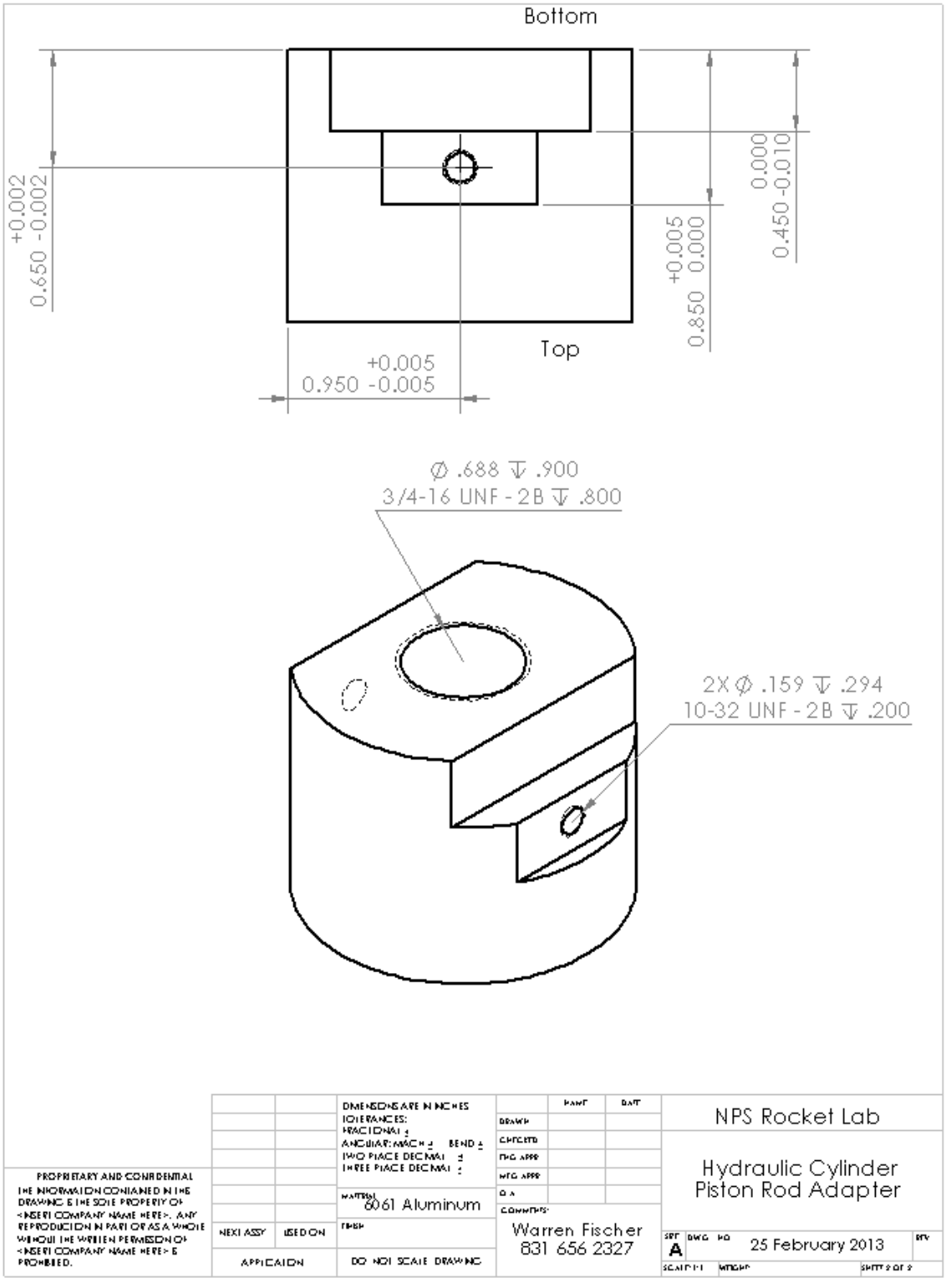

Figure 45. Fabrication Drawing for EMD Injector Adapter between Hydraulic Cylinder Output Rod and Injector Plunger (View 2 of 2)

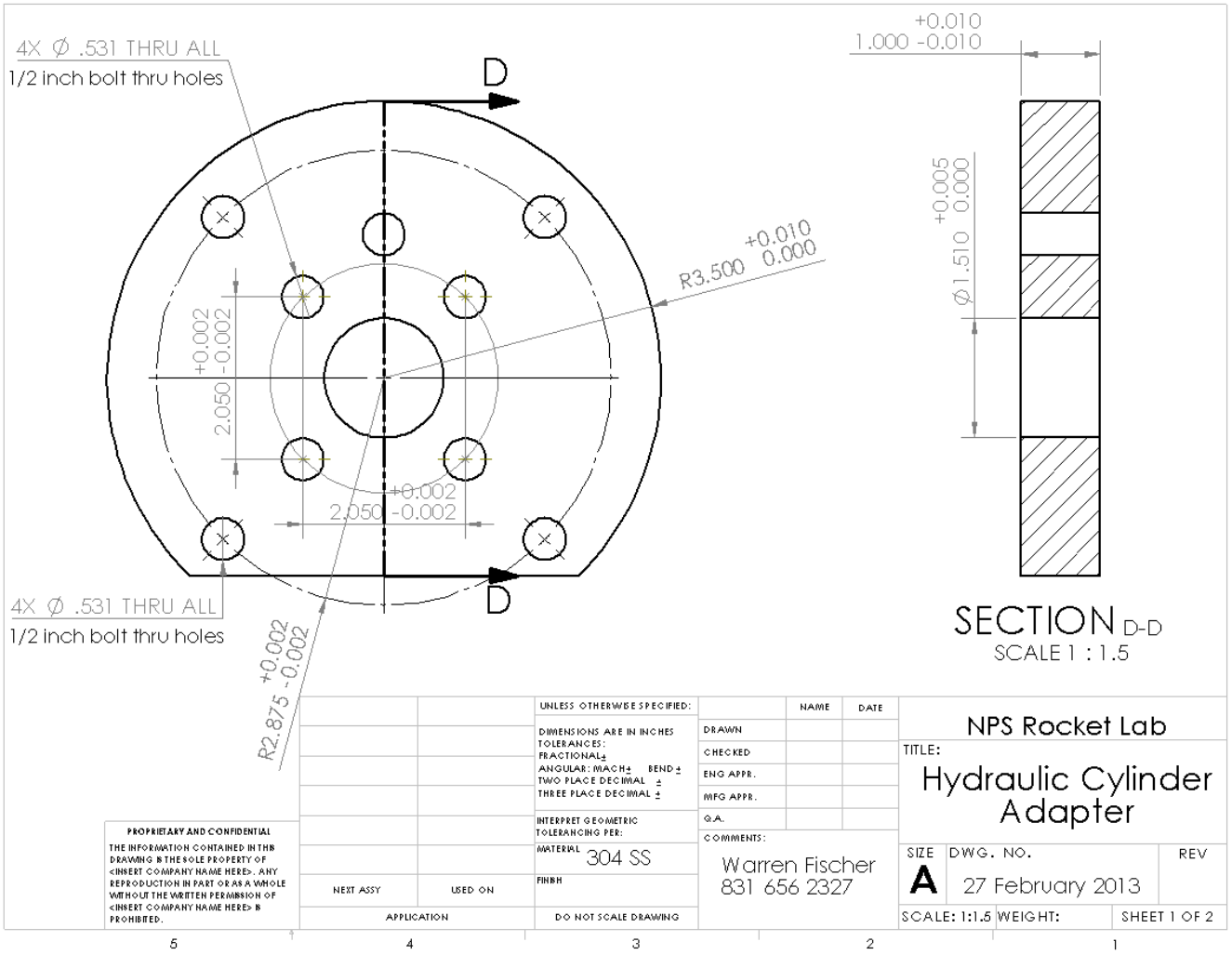

Figure 46. Fabrication Drawing for EMD Injector Adapter Hydraulic Cylinder Retaining Plate (View 1 of 2)

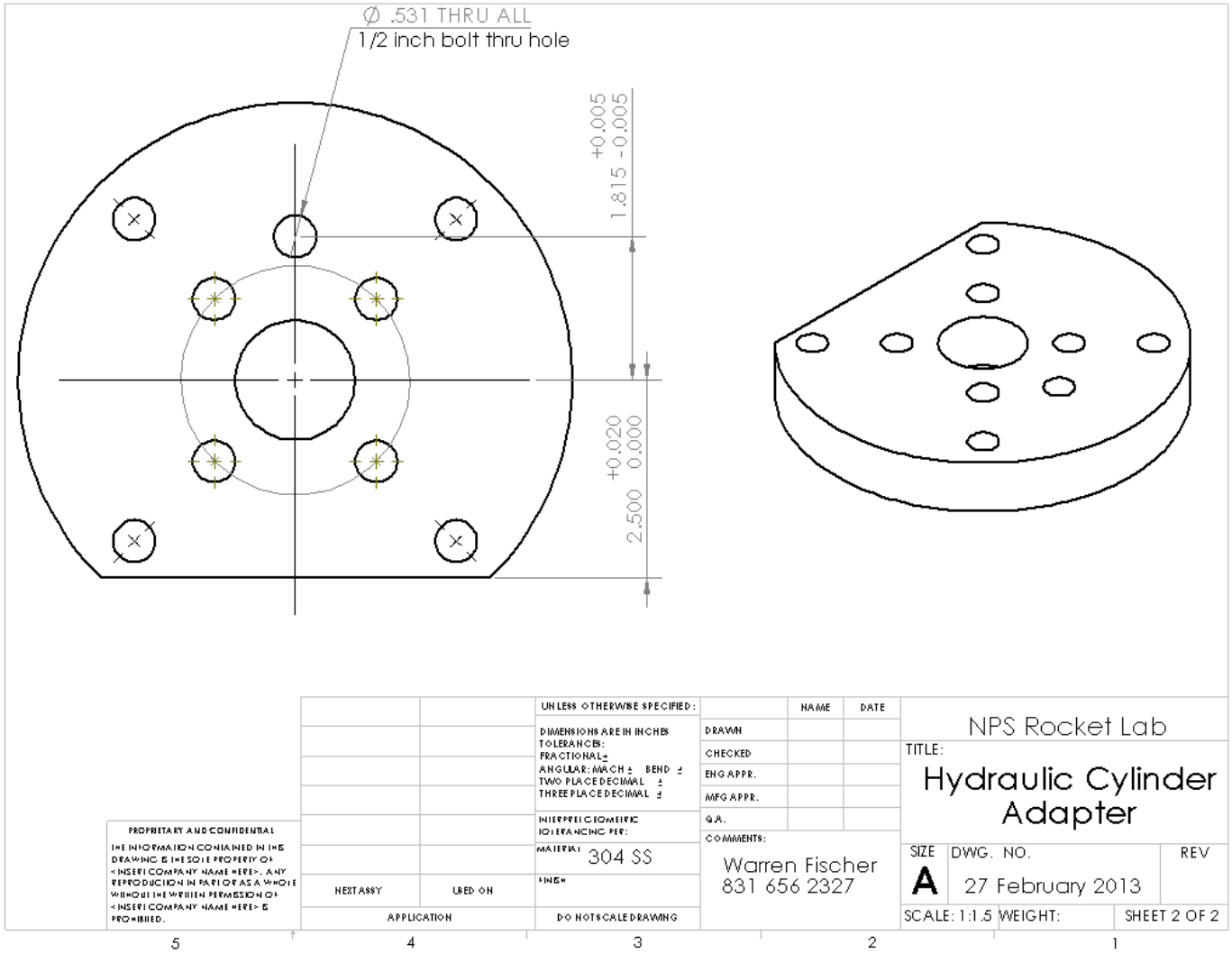

Figure 47. Fabrication Drawing for EMD Injector Adapter Hydraulic Cylinder Retaining Plate (View 2 of 2)

APPENDIX B. FABRICATION DRAWINGS FOR PARTICLE SIZING CHAMBER

A. ADAPTER PLATE FOR STURMAN AND EMD INJECTORS

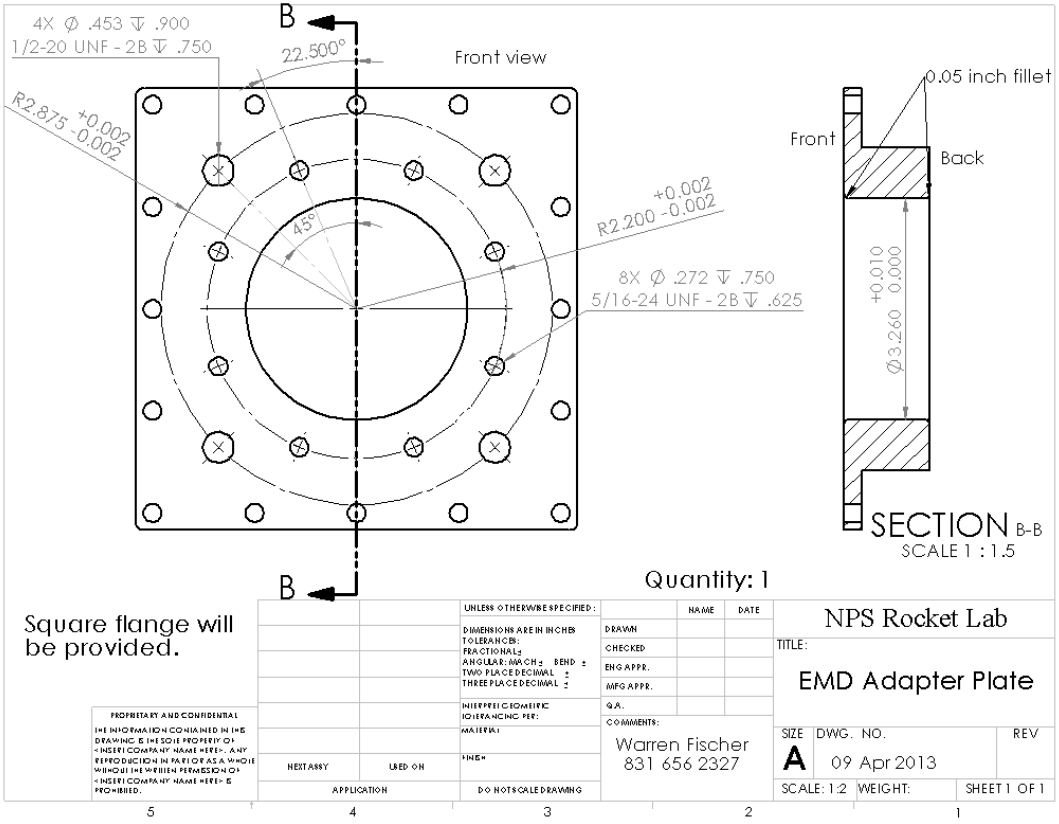

Figure 48. Fabrication Drawing for Sturman and EMD Injector Adapters

B. YANMAR INJECTOR ADAPTER PLATE

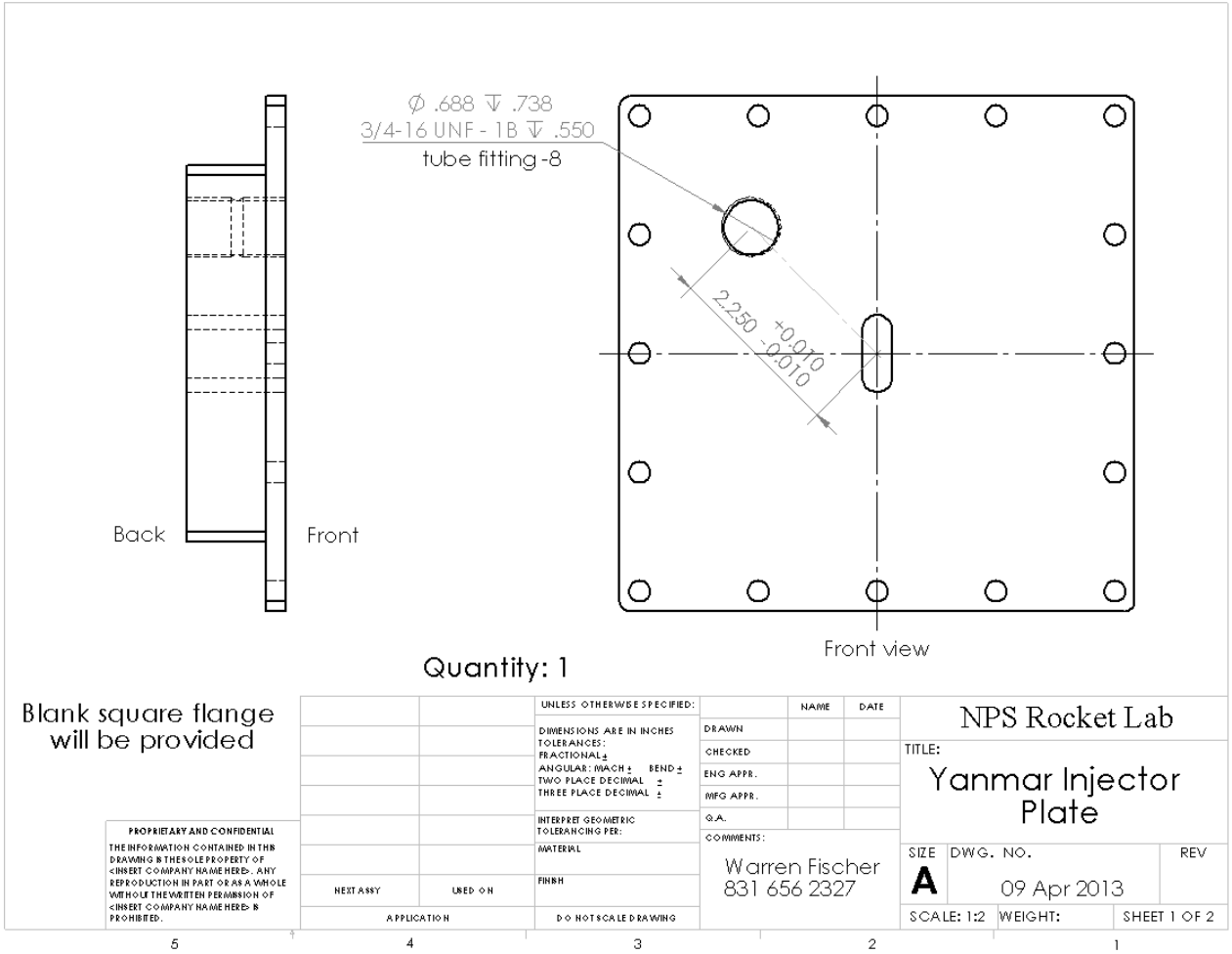

Figure 49. Yanmar Injector Adapter Plate Fabrication Drawing (View 1 of 2)

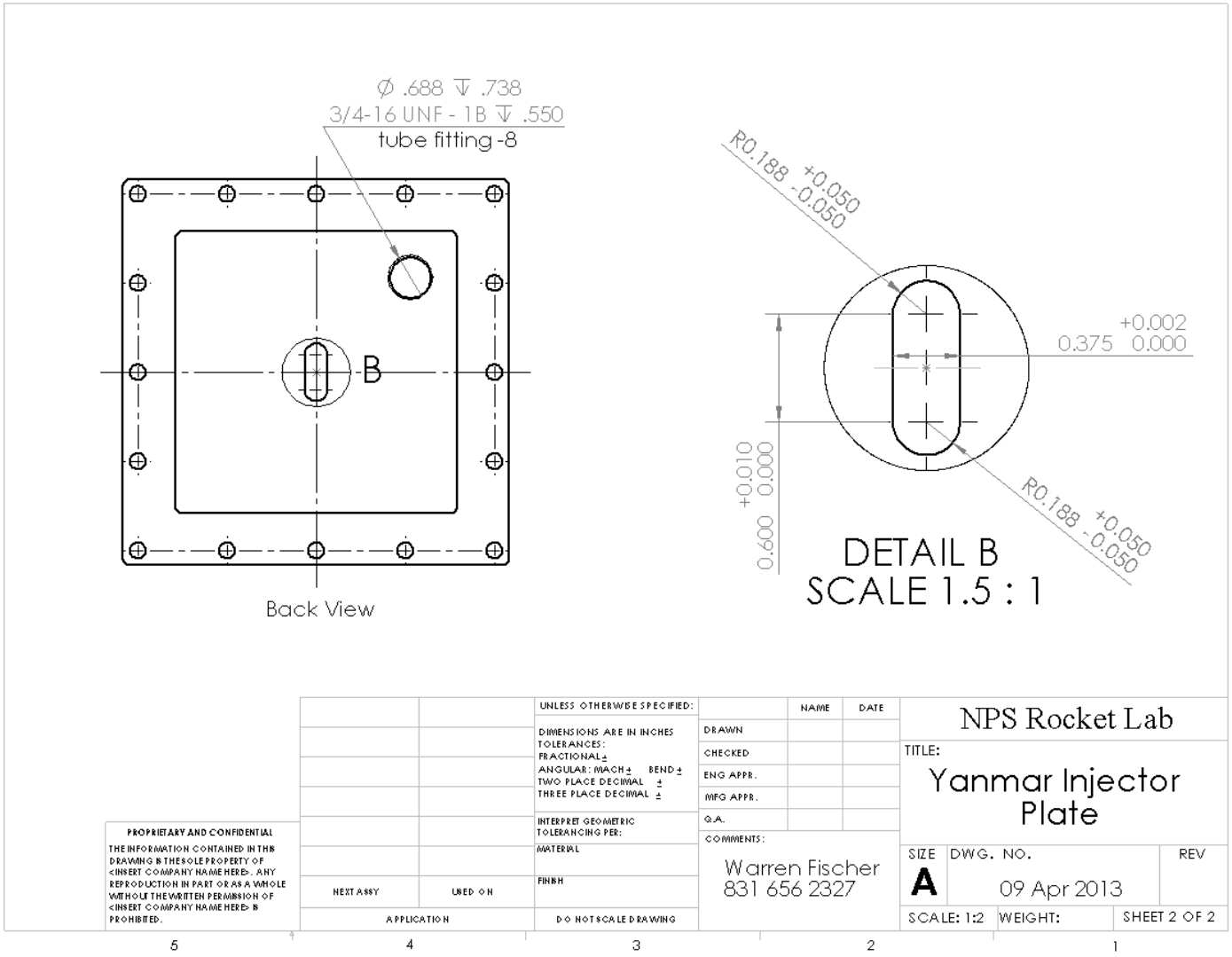

Figure 50. Yanmar Injector Adapter Plate Fabrication Drawing (View 2 of 2)

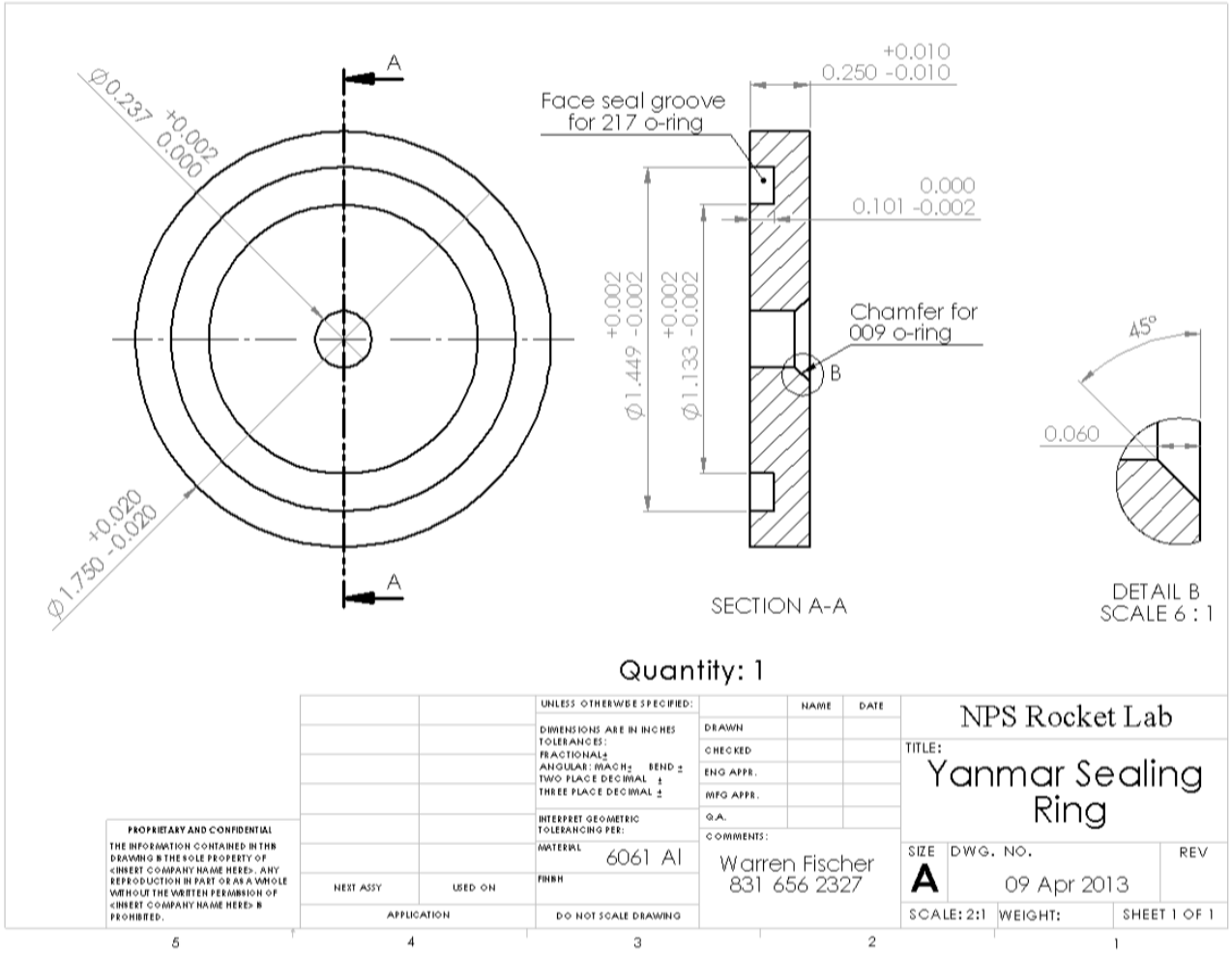

Figure 51. Yanmar Injector Adapter Sealing Ring Fabrication Drawing

APPENDIX C. MATLAB CODE USED TO ANALYZE PARTICLE SIZE DATA

```
%Code Authored by Mr. Dave Dausen, Lab Engineer, NPS Rocket Propulsion
Lab, modified by Warren Fischer

%Program to read from Dantec PDPA Exported Data textfiles...
%  Data file with the individual particles i.e.
SturmanInjParticles20MayRun10.txt

%Data Columns
%1.  Particle Number
%2.  AT (ms)
%3.  TT (micro sec)
%4.  LDA1 (m/s)
%5.  U12 (deg)
%6.  U13 (deg)
%7.  Diameter (micro meter)

clc
clear all
close all

%The Data is imported and sorted.  This is simple though has the
ability
%  to read in several datafiles and proccess the data.  Output is the
%  a histogram with diameters.

%  These are text and file inputs.
Location = 'F:\ParticleSizeProcessing';     %Update Drive
Folder = 'Results';
Filename = 'BioFuelParticles';
Inj = 'Sturman';
Fuel = 'HRD';
Setting = '1600';  %psi

%Multiple imports because there may be multiple data sets at a single
%pressure setting
BioParticleOrig1 = importdata('Data\SturmanInjParticles21MayRun9.txt',
'\t');  %Original for testing
%BioParticleOrig2 = importdata('Data\SturmanInjParticles21MayRun8.txt',
'\t');  %Importing multiple files
% BioParticleOrig3 =
importdata('Data\SturmanInjParticles20MayRun8.txt', '\t');
% BioParticleOrig4 =
importdata('Data\SturmanInjParticles20MayRun9.txt', '\t');
% BioParticleOrig5 =
importdata('Data\SturmanInjParticles20MayRun10.txt', '\t');
% BioParticleOrig6 =
importdata('Data\SturmanInjParticles20MayRun4.txt', '\t');
% BioParticleOrig7 =
importdata('Data\SturmanInjParticles20MayRun5.txt', '\t');
```

```
BioParticleRawData1 = BioParticleOrig1.data(:,7);
%BioParticleRawData2 = BioParticleOrig2.data(:,7);
% BioParticleRawData3 = BioParticleOrig3.data(:,7);
% BioParticleRawData4 = BioParticleOrig4.data(:,7);
% BioParticleRawData5 = BioParticleOrig5.data(:,7);
% BioParticleRawData6 = BioParticleOrig6.data(:,7);
% BioParticleRawData7 = BioParticleOrig7.data(:,7);

% BioParticleDiameterData = vertcat(BioParticleRawData1,
BioParticleRawData2,...
%     BioParticleRawData3, BioParticleRawData4, BioParticleRawData5,...
%     BioParticleRawData6, BioParticleRawData7);

%BioParticleDiameterData = vertcat(BioParticleRawData1,
BioParticleRawData2);

BioParticleDiameterData = BioParticleRawData1;     %Use if only one
data file

DataPoints = length(BioParticleDiameterData);
%This is to analyze the Particles in BioParticleDiameterData and plot
%  The maximum is interpolated from LDA and PDA manual, Page4-75, Table
A1.2
BioParticles = sort(BioParticleDiameterData);
MinD = 0.5;  %Minimum particle size micrometer
MaxD = 332;  %Maximum particle size using Mask A (PDPA detector),
micrometer

%Search for values 0.5 to 332 micron for Histogram
X1=1;
for R = 1 : DataPoints
    if BioParticles(R) <= MinD
        X1 = R;
    end
    if BioParticles(R) <= MaxD
        X2 = R;
    end
end

%Post Processing particles follwing (Average and StandardDev)
Diameter10Individual = BioParticles(X1:X2);


[NumPart,Bin] = hist(Diameter10Individual,50);
%Filters out bins with small counts
for R = 1 : length(Bin)
    if NumPart(R) <= 2
        NumPart(R) = 0;
    end
end
```

```
Diameter10=Bin(1:length(Bin));
%Calculate Average Diameter10 based on bin diameter and number of
counts in
%each bin
Diameter10Calc=0;
FinalNumPart=0;
for S=1:length(Bin);
Diameter10Calc=Diameter10Calc+Diameter10(S)*NumPart(S);
FinalNumPart=FinalNumPart+NumPart(S);
end
AverageD10=Diameter10Calc/FinalNumPart;

%Calculate Sauter Mean Diameter based on bin diameter and number of
counts
%in each bin
SMDTop = 0;
SMDBottom = 0;
for K = 1 : length(Diameter10)
    SMDTop = Diameter10(K)^3*NumPart(K) + SMDTop;
    SMDBottom = Diameter10(K)^2*NumPart(K) + SMDBottom;
end
SauterDiameter32 = (SMDTop/SMDBottom);



figure(1)
hold on
NumPartNorm = (NumPart / max(NumPart));
bar(Bin,NumPartNorm);

grid on
title([Inj,' Injector ',Fuel,' at ',Setting,' Psi:  Number of Particles
Vs. Size'],'fontsize',10,'fontweight','b');

text(120,0.95,['Average diameter d[1,0]: ',num2str(AverageD10),' \mu
m'],'FontSize',10,'fontweight','b','EdgeColor','k');
text(120,0.85,['Sauter Mean diameter d[3,2]:
',num2str(SauterDiameter32),' \mu
m'],'FontSize',10,'fontweight','b','EdgeColor','k');

xlabel('Particle size (\mu meters)','fontsize',10,'fontweight','b');
ylabel('Number of Particles
(Normalized)','fontsize',10,'fontweight','b');
axis([MinD MaxD 0 1.05]);

%Writing text and pictures to folder...
mkdir(Location,Folder);
warning off;

%Datafile is in the following format
%  1.  Bin numbers (Micrometer)(X-axis)
%  2.  Particle Data (Y-axis)
%  3.  Normalized Particle Data (Y-axis)
%  4.  Average D10 (Micrometers)
%  5.  Sauter D32 (Micrometers)
```

```
%  6.  Total number of Particles

dlmwrite([Location,'/',Folder,'/',Filename,Inj,Fuel,Setting,'Psi.txt'],
Bin, 'delimiter', '\t', ...
         'precision', '%3.1f','newline','pc');
dlmwrite([Location,'/',Folder,'/',Filename,Inj,Fuel,Setting,'Psi.txt'],
NumPart, 'delimiter', '\t', ...
         'precision', 3, '-append','newline','pc');
dlmwrite([Location,'/',Folder,'/',Filename,Inj,Fuel,Setting,'Psi.txt'],
NumPartNorm, 'delimiter', '\t', ...
         'precision', 3, '-append','newline','pc');
dlmwrite([Location,'/',Folder,'/',Filename,Inj,Fuel,Setting,'Psi.txt'],
AverageD10, 'delimiter', '\t', ...
         'precision', '%3.4f','-append','newline','pc');
dlmwrite([Location,'/',Folder,'/',Filename,Inj,Fuel,Setting,'Psi.txt'],
SauterDiameter32, 'delimiter', '\t', ...
         'precision', '%3.4f','-append','newline','pc');
dlmwrite([Location,'/',Folder,'/',Filename,Inj,Fuel,Setting,'Psi.txt'],
DataPoints, 'delimiter', '\t', ...
         'precision', '%3.0f','-append','newline','pc');

DataPlot = getframe(figure(1));
imwrite(DataPlot.cdata,[Location,'/',Folder,'/',Filename,Inj,Fuel,Setti
ng,'Plot.tiff'],'tiff');
```

LIST OF REFERENCES

[1] J. T. Bartis and L. V. Bibber, *Alternative Fuels for Military Applications*. Santa Monica, CA: Rand, 2011.

[2] P. Paige. (2009, October 16), *Navy Secretary announces ambitious energy goals* [Online]. Available: http://www.onr.navy.mil/Media-Center/Press-Releases/2009/naval-energy-forum-2009.aspx

[3] L. Wright, (2010, April 22). *Navy Tests Biofuel-Powered "Green Hornet,"* [Online]. Available: http://www.navy.mil/submit/display.asp?story_id=52768

[4] B. Sizemore, (2010, October 23). "Navy unveils its 'mean, green riverine machine' in Norfolk," *The Virginian Pilot* [Online]. Available: http://hamptonroads.com/2010/10/navy-unveils-its-mean-green-riverine-machine-norfolk?cid=ltst.

[5] P. A. Caton and J. S. Cowart, "Combustion and fuels," in *Piston Power*, ch. 5, pp. 127–163, unpublished.

[6] D. M. Leahey *et al.*, "Combustion of biodiesel- and ethanol-diesel mixtures with intake injection", SAE paper 2007-01-4011, SAE Fluid Systems and Powertrain Conference, Oct. 2007, Chicago.

[7] L. L. Anderson and D. A. Tillman, "Light liquids and chemicals from coal," in *Synthetic Fuels from Coal*, John Wiley, 1979, ch. 8, pp. 122-135.

[8] S. Mikkonen, "Second-generation renewable diesel offers advantages," *Hydrocarbon Processing*, vol. 87, pp. 63–66, Feb. 2008.

[9] H. Aatola *et al.*, "Hydrotreated vegetable oil (HVO) as a renewable diesel fuel: trade-off between NOx, particulate emission, and fuel consumption of a heavy duty engine," *SAE International Journal of Engines*, 2009, vol. 1, no. 1, pp. 1251–1262, doi: 10.4271/2008-01-2500.

[10] J. D. Kinder and T. Rahmes, "Evaluation of bio-derived synthetic paraffinic kerosene (Bio-SPK)," Boeing, Chicago, IL, Sustainable Biofuels Research & Technology Program, June 2009.

[11] P. Anbarasan *et al.*, "Integration of chemical catalysis with extractive fermentation to produce fuels," *Nature*, vol. 491, pp. 235–238, Nov. 2012.

[12] J. Cowart *et al.*, "Performance, efficiency and emissions comparison of diesel fuel and a Fischer-Tropsch synthetic fuel in a CFR single cylinder diesel engine during high load operation," SAE Technical Paper 2008-01-2382, 2008, doi: 10.4271/2008-01-2382.

[13] R. Reitz, *et al.*, “Office of Naval Research alternative fuels teleconference,” Office of Naval Research, University of Wisconsin Engine Research Center, Madison, WI, 2012, unpublished.

[14] K. Millsaps *et al*., “Alternative fuels teleconference,” Office of Naval Research, Naval Postgraduate School, Monterey, CA, Feb. 2013, unpublished.

[15] P. A. Caton, L. J. Hamilton, and J. S. Cowart, “Understanding ignition delay effects with pure component fuels in a single-cylinder diesel engine,” *Journal of Engineering for Gas Turbines and Power*, vol. 133, Mar. 2011.

[16] D. J. Luning Prak, D. W. O’Sullivan, “Seawater interactions with fuels: Fuel properties and water solubility,” U. S. Naval Academy, Annapolis, MD, Chemistry Department, July 2011, unpublished.

[17] D. J. Luning Prak, “Determination of the interfacial properties of alternative fuels and fluids that are of operational importance to the Navy,” U. S. Naval Academy, Annapolis, MD, Chemistry Department, Sept. 2009, unpublished.

[18] D. Guimond, private communication, Jan., 2013.

[19] P. Flynn *et al*., "Diesel combustion: an integrated view combining laser diagnostics, chemical kinetics, and empirical validation," SAE Technical Paper 1999-01-0509, 1999, doi:10.4271/1999-01-0509.

[20] R. D. Reitz, “Modeling atomization processes in high-pressure vaporizing sprays,” *Atomisation and Spray Technology*, 1987, vol. 3, no. 4, pp. 309–337.

[21] F. M. White, “Dimensional analysis and similarity,” in *Fluid Mechanics*, 6th ed. New York, McGraw-Hill, 2008, ch. 5, p. 311.

[22] R.D. Reitz, F.V. Bracco, ‘Mechanisms of breakup of round liquid jets,” in *The Encyclopedia of Fluid Mechanics*, vol. 3, N. Cheremisnoff, Ed., Houston, Gulf Publishing, 1986, ch. 10, pp. 233–249.

[23] R. Ochoterena *et al.*, “Optical studies of spray development and combustion characterization of oxygenated and Fischer-Tropsch fuels,” SAE Technical Paper 2008-01-1393, 2008, doi: 10.4271/2008-01-1393.

[24] L. Pickett, S. Kook, and T. Williams, “Visualization of diesel spray penetration, cool–flame ignition, high-temperature combustion, and soot formation using high-speed imaging,” *SAE International Journal of Engines*, 2009, vol. 2, no. 1, pp. 439–459, doi:10.4271/2009-01-0658.

[25] A. C. Eckbreth, “Survey of laser diagnostics,” in *Laser Diagnostics for Combustion Temperature and Species*, Cambridge, MA, Abacus Press, 1988, ch. 1, p. 14.

[26] *LDA and PDPA Reference Manual*, Dantec Dynamics, Skovlunde, Denmark, 2011, pp. 6–32.

THIS PAGE INTENTIONALLY LEFT BLANK

INITIAL DISTRIBUTION LIST

1. Defense Technical Information Center
   Ft. Belvoir, Virginia

2. Dudley Knox Library
   Naval Postgraduate School
   Monterey, California